Electrostatic anchoring of SNAP25 to the plasma membrane

Dissertation

zur

Erlangung des Doktorgrades (Dr. rer. nat.)

der

Mathematisch-Naturwissenschaftlichen Fakultät

der

Rheinischen Friedrich-Wilhelms-Universität Bonn

vorgelegt von

Pascal Weber

aus

Linz am Rhein

Bonn 2021

Angefertigt mit Genehmigung der Mathematisch-Naturwissenschaftlichen Fakultät der

Rheinischen Friedrich-Wilhelms-Universität Bonn

1. Gutachter: Prof. Dr. Thorsten Lang

2. Gutachter: Prof. Dr. Christoph Thiele

Promotionsdatum: 29.06.2021

Erscheinungsjahr: 2021

Declaration – *Erklärung*

Parts of this work were previously published:

Teile dieser Arbeit wurden bereits vorab veröffentlicht:

Weber P, Batoulis H, Rink KM, Dahlhoff S, Pinkwart K, Söllner TH, Lang T.
Electrostatic anchoring precedes stable membrane attachment of SNAP25/SNAP23 to the plasma membrane. eLife;6:e19394. (2017) DOI: https://doi.org/10.7554/eLife.19394, PMID:28240595

Table of contents

List of Figures

List of supplementary figures

List of tables

Abbreviations

Atto647N-DPPE	Atto647N-1,2-dipalmitoyl-*sn*-glycero-3-phosphoethanolamine
BCA	bicinchoninic acid assay
BHK	baby hamster kidney
BSA	bovine serum albumin
CCD	charge-coupled device
CLSM	confocal laser scanning microscope
CRR	cysteine-rich region
DAPI	4′,6-diamidino-2-phenylindole
DMEM	Dulbecco's Modified Eagle's Medium
DNA	deoxyribonucleic acid
DOPS	1,2-dioleoyl-*sn*-glycero-3-phosphoserine
DPBS	Dulbecco's Phosphate Buffered Saline
DTT	dithiothreitol
EDTA	ethylenediaminetetraacetic acid
EE	early endosomes
EGFP	enhanced green fluorescent protein
EGTA	ethylene glycol-bis(β-aminoethyl ether)-N,N,N′,N′-tetraacetic acid
EL	endosome like
EMCCD	electron multiplying charge-coupled device
MEM	minimal essential medium
FCS	fetal calf serum
FRAP	fluorescence recovery after photobleaching
GFP	green fluorescent protein
GSH	glutathione
GSL	glycosphingolipid

GST	glutathione S-transferases
HRP	horseradish peroxidase
IPTG	isopropyl-thiogalactoside
LE	late endosome
LUT	lookup table
MARCKS	myristoylated alanine-rich C-kinase substrate
mEGFP	monomeric variant of green fluorescent protein
NA	numerical aperture
NGF	nerve growth factor
P	pellet
PAT	Palmitoyl transferases
PBS	phosphate-buffered saline
PC	phosphatidylcholine
PCR	polymerase chain reaction
PE	phosphatidylethanolamine
PH	pleckstrin homology
PI	phosphatidylinositol
PIP	polyphosphoinositide
PIP_2	phosphatidylinositol 4,5-bisphosphate
PIP_3	phosphatidylinositol (3,4,5)-trisphosphate
PKC	protein kinase C
PLC	phospholipase C
PLL	poly-L-lysine
PM	plasma membrane
PMSF	phenylmethylsulfonyl fluoride
POPC	1-palmitoyl-2-oleoyl-*sn*-glycero-3-phosphocholine
POPE	1-hexadecanoyl-2-octadecenoyl-*sn*-glycero-3-phosphoethanolamine

PS	phosphatidylserine
RFP	red fluorescent protein
RIPA	radioimmunoprecipitation assay buffer
ROI	region of interest
RT	room temperature
S	supernatant
s.d.	standard deviation
s.e.m.	standard error of mean
SDS	sodium dodecyl sulfate
SDS-PAGE	sodium dodecyl sulfate-polyacrylamide gel electrophoresis
SM	sphingomyelin
SNAP23	synaptosomal-associated protein, 23 kDa
SNAP25	synaptosomal-associated protein, 25kDa
SNARE	soluble N-ethylmaleimide-sensitive factor attachment receptor
SRP	signal recognition particles
SV	synaptic vesicle
Syx1A	Syntaxin 1A
t1/2	half time
TBS	tris buffered saline
TBS-T	tris buffered saline Tween 20
TC	tissue culture
TMA-DPH	1-(4-trimethyl-ammoniumphenyl)-6-phenyl-1,3,5-hexatriene-p-toluolsulfonate
TRITC	tetramethylrhodamine
VAMP	vesicle-associated membrane protein

1 Summary

Neurotransmission is based on incredibly rapid membrane trafficking cycles, mediating the release of neurotransmitters. The fusion machinery of the well-studied SNARE[1] protein complex ensures the speed and precision of synaptic transmission. One critical part of this machinery is the initially cytosolic SNARE protein SNAP25[2], which needs to be in constant supply at the active zones of the plasma membrane.

The focus of this study lies on the investigation of the self-organizational principle underlying the plasma membrane targeting of SNAP25, an aspect that has not yet been extensively studied. Over the course of this study, the existence of an electrostatic anchoring mechanism is revealed, which mediates the initial contact of SNAP25 to the plasma membrane.

A small polybasic cluster present in the cysteine-rich region of SNAP25 is responsible for the electrostatic anchoring. To characterize this region, different SNAP25 mutant constructs are mainly analyzed via confocal laser scanning microscopy, to reveal differences in SNAP25's localization.

Although previous studies suggested similar anchoring mechanisms based on electrostatic interactions, the results presented show that the comparatively small cluster is sufficient to facilitate initial membrane contact in the case of the neuronal SNAP25 and its ubiquitously expressed homologue SNAP23[3].

[1] soluble N-ethylmaleimide-sensitive factor attachment receptor
[2] synaptosomal-associated protein, 25kDa
[3] synaptosomal-associated protein, 23 kDa

The study further identifies the potential lipid interaction partner PIP_2[4] as the most likely candidate for SNAP25's electrostatic anchoring mechanism.

This for SNAP25 newly discovered electrostatic anchoring mechanism, reliant on only a small polybasic cluster, represents an extension of previous theories of plasma membrane targeting via electrostatic interactions and could have potential generality, as other proteins might use a similar electrostatic anchor.

[4] phosphatidylinositol 4,5-bisphosphate

2 Introduction

The first section of this introduction is about the important fundamentals of the plasma membrane and the lipids and proteins involved. Section two gives an overview of the well-studied SNARE fusion machinery and describes in greater detail the main subject of this study, the membrane protein SNAP25. Finally in the third section, current scientific views and models dealing with membrane association of membrane proteins are introduced and current views about membrane targeting mechanisms for SNAP25 are compared.

2.1 The plasma membrane

The basis of all life not only requires the capability of reproduction, it needs a distinction between itself and the environment. Therefore all cells, which constitute the basic building blocks of life, are enclosed by a membrane. This cell membrane, also known as the plasma membrane (PM), is the border that separates a living cell from its surroundings. It acts as an insulating barrier, giving the cell the ability to store potential energy and compartmentalize its biochemical processes. However, after the term "cell" was first used by Robert Hooke in 1665 (Hooke, 1665), which was further developed into the cell theory by Matthias Jakob Schleiden and Theodor Schwann in 1839 (Schwann, 1839), the question what exactly separates cells became answered only decades later.

Today the plasma membrane is a well-studied structure with a tremendous variety of molecules involved in its composition and, due to its multitude of functions, it is considered a cell organelle itself. The most apparent purpose of the plasma membrane is to serve as a border separating molecules in the inner cytosolic part of the cell from the extracellular space. But another prominent key feature of any membrane is the selective permeability allowing certain molecules to pass through the membrane, whereas other

molecules are hindered or blocked off entirely. The difference in the ability of molecules to permeate a membrane is dependent on their partition coefficient between water and oil. This observation at the end of the 19th century led to Charles Ernest Overton's hypothesis that the outer border of cells has the basic properties of oil. It has hydrophobic / lipophilic components, meaning it does not mix with water but with other oils (Kleinzeller, 1999). Later the chemical analysis of isolated membranes of red blood cells revealed that the plasma membrane is indeed mainly composed of phospholipids. Lipids are mainly water-insoluble biomolecules that are highly soluble in organic solvents. The phospholipids are a subclass of lipids and have both a hydrophobic tail and a hydrophilic head. When dissolved in benzene and mixed in water, they form a membrane after the benzene evaporates, exposing only the hydrophilic heads to the water.

Based on this observation in 1925 E. Gorter and F. Grendel developed a simplistic model of the cell membrane being a phospholipid bilayer (Figure 1a), sheltering the hydrophobic lipid tails from, and exposing the hydrophilic heads to, water (Gorter & Grendel, 1925).

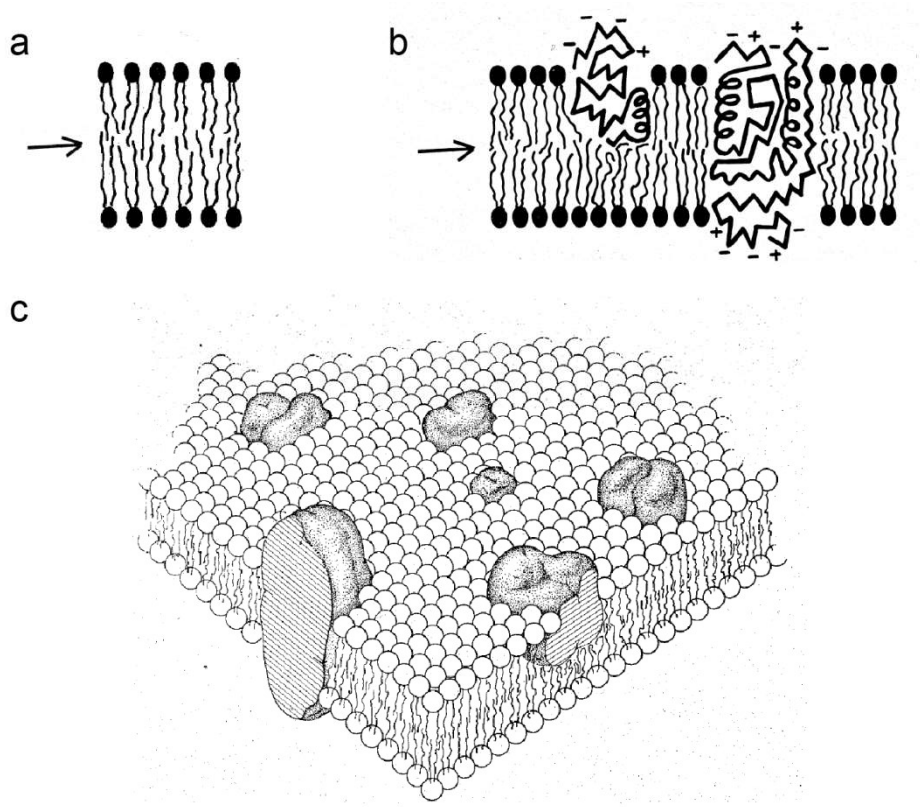

Figure 1: Sea of lipids - Singer and Nicolson's fluid mosaic model

(a) A first basic model depicting the phospholipids forming a hydrophobic core with their hydrophobic tails (arrow), while orienting their hydrophilic head groups (black dots) to the surrounding water surface. At first the proposed model for a biological membrane focused only on lipids, but it was later advanced by the inclusion of proteins **(b)**, which are integrated with their hydrophobic regions into the lipid bilayer while hydrophilic regions (including negatively or positively charged residues) are exposed to the surface. **(c)** S. J. Singer and G. Nicolson further developed this very basic model and postulated that proteins are not fixed in place but can diffuse across a fluid "sea of lipids" (modified from Singer & Nicolson, 1972).

Besides phospholipids, the analysis of the plasma membrane revealed that it consists of proteins too. At first, the proteins were supposed to envelope the lipid bilayer like a sandwich, which was proposed in 1935 in the Davson-Danielli-model. Only decades later in 1972 this model was updated by S.J. Singer and G. Nicolson, proposing the insertion of the proteins into the lipid bilayer (Figure 1b) and postulating the fluid-mosaic-model (Figure 1c). This membrane model emphasizes that the proteins are not fixed in place in a rigid layer of lipids but can move rather freely. Important evidence for

the fluidity of the membrane was the observation of a temperature-dependent intermixing of cell surface antigens after the formation of a mouse-human multinucleate cell (Frye & Edidin, 1970). The phospholipid bilayer is mainly kept together by fluctuating hydrophobic interactions, which are far weaker than covalent bonds, allowing for lateral diffusion of both lipids and proteins across the so called "sea of lipids" (Figure 1c).

The fluid mosaic model is updated constantly upon new insights about the basic building blocks involved and is still relevant for understanding the complex structure and dynamics of the plasma membrane. The mosaic characteristics become clearer in an updated modern version of the model (Figure 2) emphasizing the different constituents present in the membrane. Most noticeable is the increased compartmentalization of the membrane by the inclusion of the cytoskeleton and the underlying picket-fence model (Sheetz et al., 1989; Kusumi et al., 1993; Kusumi et al., 2005) and the addition of membrane domains enriched with different proteins or lipid species showing a more complex organizational structure (Simons & Gerl, 2010). The updated membrane model shows different types of interactions occurring with integral membrane proteins and glycoproteins, membrane lipids, and membrane-associated cytoskeletal systems and extracellular matrix components. Thus the plasma membrane is not just a simple border but can be seen as a major meeting point (Escribá et al., 2008) between lipids and proteins as many different entities meet to form different functional structures (Nicolson, 2014; Laude & Prior, 2004).

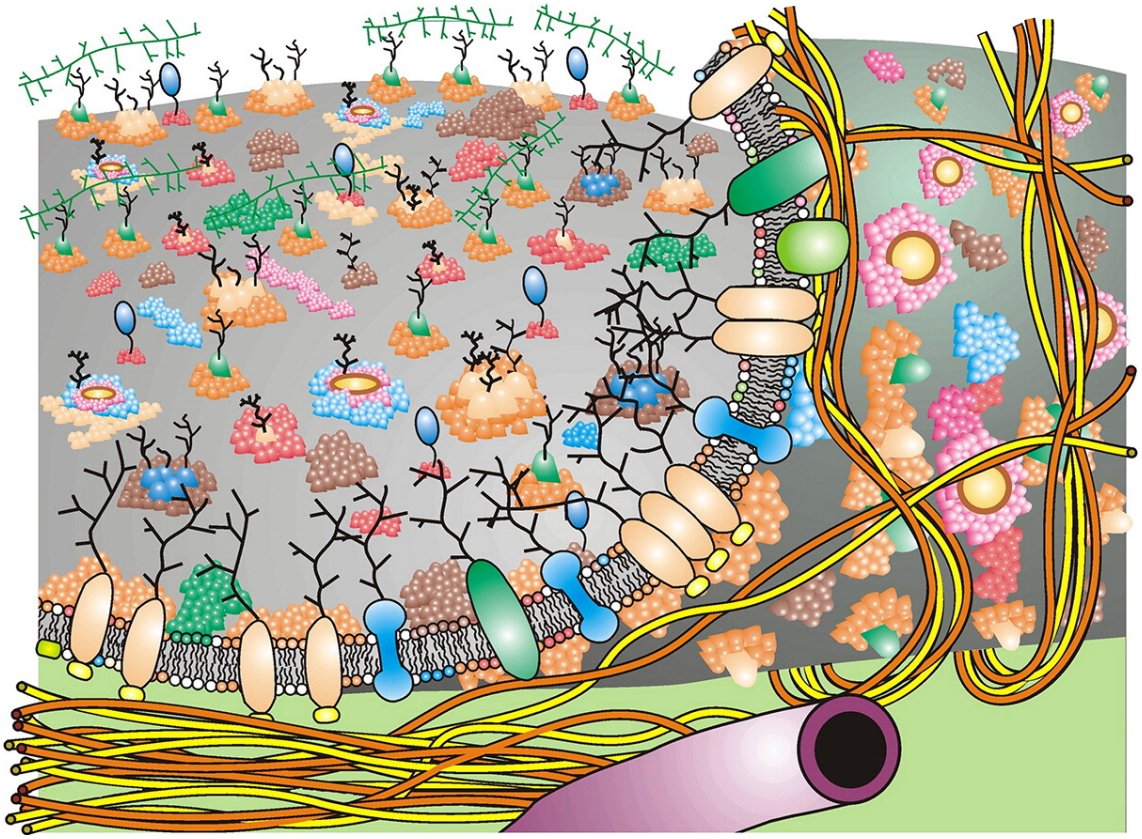

Figure 2: The meeting point - updated fluid-mosaic-membrane model

An updated modern version of the fluid-mosaic-membrane model includes membrane domain structures and membrane-associated cytoskeletal and extracellular structures that can restrict lateral diffusion. This "peeled-up" membrane model allowing a view on both the inner and outer membrane shows differences in lipid composition between both sides. Different proteins build homo- and heterogeneous clusters to interact with each other but also with the lipids surrounding them. Depicted are different kinds of lipid species (illustrated by different colors) forming small lipid islands which can interact with different proteins contributing to their specific roles and functions. This updated modern version of the plasma membrane more clearly shows that the membrane serves here as a central meeting point (Escribá et al., 2008) for proteins and lipids interacting with each other. Although many open questions remain; extensive studies continue to unravel more and more important interactions and functions of the molecules involved (Nicolson, 2014).

Despite being in the spotlight of attention for many years, unraveling the complex cellular processes executed by the numerous proteins of the plasma membrane remains challenging. Further it became clear that not solely proteins are accountable for important processes, but lipids themselves can regulate the location and activity of many

membrane proteins (Escribá et al., 2008) and thus a tight relationship between proteins and interacting lipids is required (Coskun & Simons, 2011). These interactions and their associated functions define the modern view and open questions about biological membranes today.

2.1.1 Types of membrane proteins

Although lipids are the main building blocks of biological membranes, key functions of signaling pathways or functions like exo- or endocytosis are mainly associated with the activities of membrane proteins. They can be divided into integral proteins, which span through the membrane, called transmembrane proteins, or proteins which are attached to only one side of the lipid bilayer (Figure 3). Both types intercalate into the hydrophobic core of the lipid bilayer with their own hydrophobic parts or by attachment of fatty acid chains that anchors the protein into the cytosolic monolayer. The so-called peripheral membrane proteins mostly adhere only temporarily by non-covalent interactions to other integral proteins. Transmembrane proteins function on both sides of the membrane, often acting as a receptor for signal transduction or as a transporter enabling the transport of molecules across the bilayer. During the process of translation they are directly inserted into the target membrane. In contrast many peripheral proteins function exclusively on the cytosolic side of the membrane, either binding another integral protein directly or are anchored with the help of other membrane proteins via lipid modifications like myristoylation or palmitoylation to its target membrane.

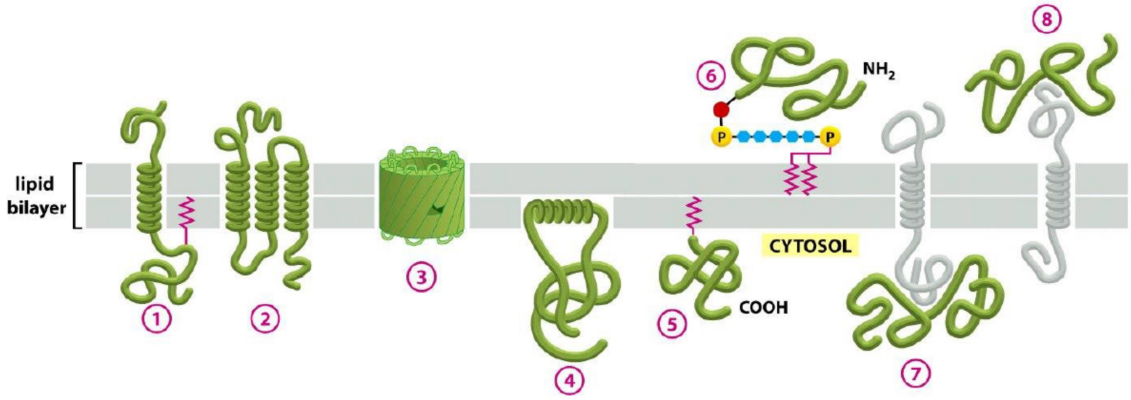

Figure 3: Different types of membrane proteins

Most of the transmembrane proteins are embedded as a single α-helix (1), multiple α-helices (2) or as a β-sheet (3). Some are only attached to the cytosolic side of the membrane by an amphipathic α -helix (4) or via lipid anchoring (5) and others are bound via polysaccharides, anchored to phosphatidylinositol, to the extracellular side (6). Some proteins are attached via non-covalent interactions to either intra- or extracellular domains (7 & 8) of other transmembrane-proteins (Alberts et al., 2008).

Once anchored to the membrane, the executed functions are often attributed to other defined regions or domains of the protein and comprise enzymatic activities. The domains are built up by different amino acids and their side chain characteristics are classified as charged, hydrophobic or polar and provide the protein with its different specific functions. For example a single amino acid, a proline, is critical for the host specificity of E-cadherin, a cell adhesion molecule (Lecuit et al. 1999). Another example is a single amino acid in the M1 protein responsible for different pathogenic potentials of the influenza virus H5N1 (Nao et al. 2015). These examples illustrate that a few or even a single amino acid can be responsible for a protein's function, its specificity or are critical for its localization, a perception which is investigated during this study.

2.1.2 Lipids of the cell membrane

Cells have thousands of lipid species, which are classified into several major categories. They show a very high degree of structural diversity, defined by their different fatty acid tail variations, biochemical modifications as well as sugar residue additions. Amongst many different classification systems, depending on their structural composition, lipids can be categorized into eight different major classes: fatty acyls, glycerolipids, glycerophospholipids, sphingolipids, sterol lipids, prenol lipids, saccharolipids, and polyketides (Fahy et al., 2005; Fahy et al., 2009; Fahy et al., 2011).

Almost all of the lipid molecules in cell membranes are amphipathic, meaning they have a hydrophilic polar headgroup and one or two hydrophobic hydrocarbon tails and will assemble in a bilayer in water to form micelles by themselves through hydrophobic interactions. A typical biological membrane contains several major lipid classes, needed for membrane associated processes such as vesicle fusion, membrane sorting and signal transduction.

The three major classes of lipids found in the plasma membrane are, glycerophospholipids, sphingolipids and sterols (Table 1). They were first mainly recognized for their structure-giving role, but advances in the field have revealed specific functions for numerous lipid species.

	Percentage of total lipids [%]
Phosphatidylcholine	45-55
Phosphatidylethanolamine	15-25
Phosphatidylinositol	10-15
Phosphatidylserine	5-10
Phosphatidic acid	1-2
Sphingomyelin	5-10
Cholesterol	10-20

Table 1: Membrane lipid composition of an average mammalian cell
The major structural lipids in membranes are phosphatidyl-choline, phosphatidylethanolamine, phosphatidylinositol, phosphatidylserine and phosphatidic acid. Sphingomyelin is the major sphingolipid and cholesterol the major sterol found in mammalian cells. Percentages of total lipids are averaged from several sources (modified from Vance, 2015).

Similarities in the structure of lipids lead to a number of different subclasses grouping different lipid species. The phospholipids such as phosphatidylethanolamine, phosphatidylserine (PS), phosphatidylcholine and sphingomyelin all contain a phosphate group and modifications of the headgroups define the physicochemical properties of the different lipid species (Figure 4).

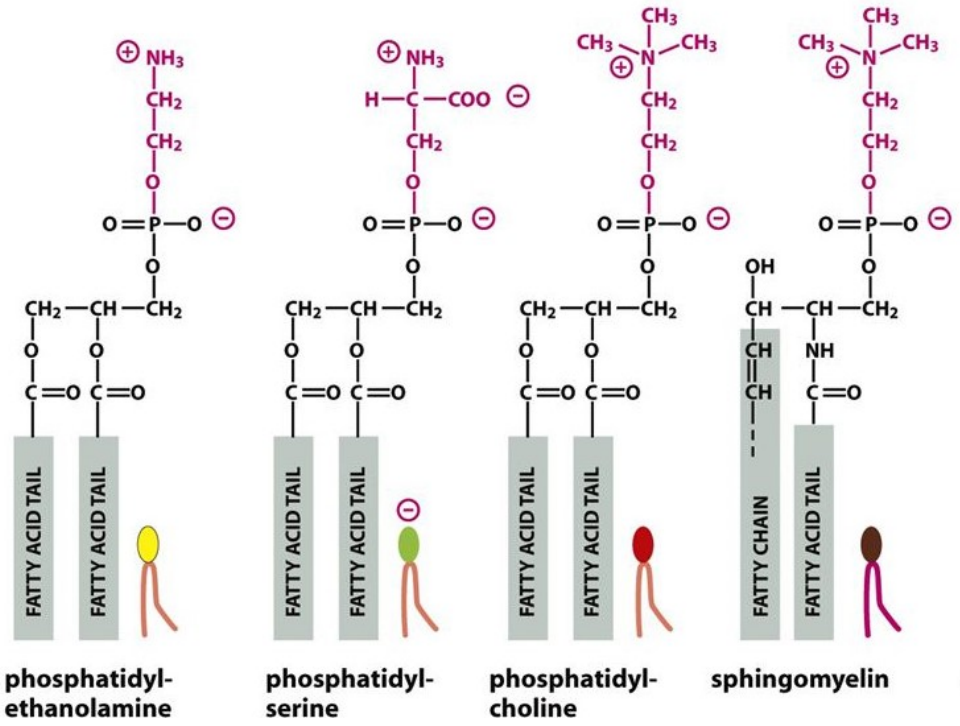

Figure 4: Major phospholipids of the plasma membrane

Depicted are the structural formulae of the different headgroups of phosphatidyl-ethanolamine (yellow), phosphatidylserine (green), phosphatidylcholine (red) and sphingomyelin (brown). All headgroups contain a phosphate and are linked either via glycerol or in the case of sphingomyelin via a sphingosine to the hydrophobic fatty acid tails. Note that the headgroup of phosphatidylserine (green) has a negative charge and contributes especially to the physicochemical characteristics and differences between the inner and outer leaflet of the plasma membrane (see also Figure 5) (Alberts et al., 2008).

The most abundant lipid, the phosphatidylcholine, accounts for more than 50 % of the cellular lipids and is found predominantly up to 77 % (Verkleij et al., 1973; van Meer et al., 1981) in the outer leaflet. Other lipid species such as phosphatidylethanolamine or phosphatidylserine are enriched or almost exclusively present in the inner leaflet. The asymmetric distribution of the different lipid species across the two leaflets of the plasma membrane forms the physicochemical basis of the intra- and extracellular side of the membrane.

How the partly very high asymmetry in the lipid distribution across the plasma membrane contributes to the plasma membrane organization is yet to be fully unraveled (van Meer et al., 2008; van Meer & de Kroon, 2011), but it has been shown to be important for many cytosolic proteins that bind to specific lipid headgroups. One important example is protein kinase C (PKC), which carries out a multiplicity of functions, for which the presence of phosphatidylserine is required (Dey et al., 2017).

In addition the asymmetric distribution (van Meer, 2011) of the negatively charged phosphatidylserine also results in a significant difference in the overall net charge between the inner and outer leaflet (Figure 5). Thus the inner leaflet is negatively charged and has a surface potential that attracts positively charged ions, proteins and peptide motifs, which can be important for the membrane localization of proteins (Yeung et al., 2008) (see chapter 2.3.3 Membrane association driven by electrostatics).

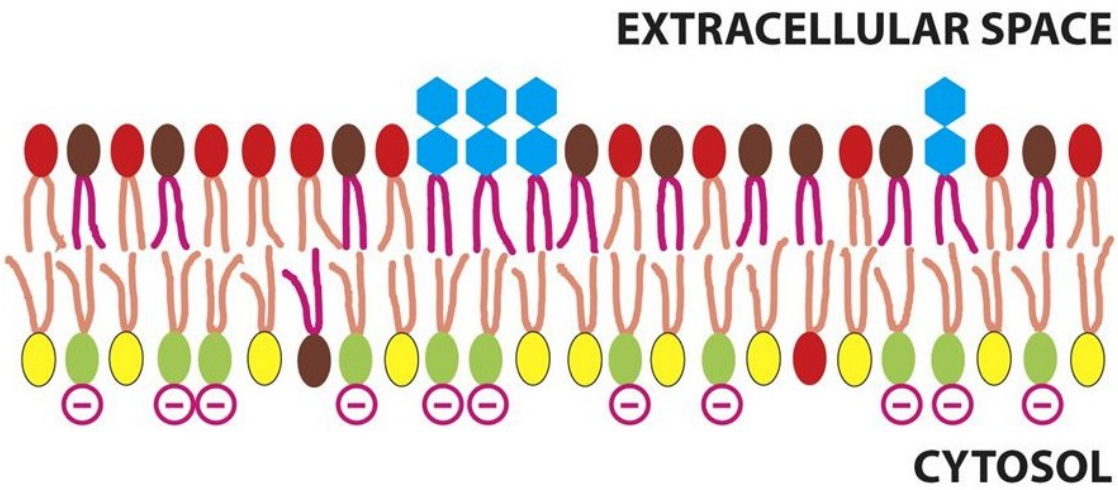

Figure 5: Negative net charge of the inner leaflet of the plasma membrane

Lipids are distributed asymmetrical across both outer and inner leaflet of the plasma membrane. Phosphatidylcholine (red headgroup), sphingomyelin (brown headgroup) as well as glycolipids (blue hexagon) are predominantly found in the outer leaflet. Phosphatidylethanolamine (yellow headgroup) and the negatively charged phosphatidylserine (green headgroup) are enriched in the cytosolic leaflet of the plasma membrane. This asymmetrical distribution of phosphatidylserine contributes greatly to a charge difference between both bilayers and to an overall negative net charge of the cytosolic part of the plasma membrane (Alberts et al., 2008).

Today more than 10,000 lipids (Fahy et al., 2009; Wenk, 2010) are known and the use of such a vast diversity of lipid species is still poorly understood but has continued to attract more attention in recent years (Shevchenko & Simons, 2010). So besides the prominent protein-protein interactions, the actual role of lipids has risen to be of increased interest in many fields of science. The study of lipids, lipidomics, employs large scale mass spectrometry analysis and the comprehensive analysis of lipids has revealed the crucial role they play in many physiological processes (Subramaniam et al., 2011). Analogous to the study of the proteome (Legrain et al., 2011), it involves the identification of thousands of lipid species and the characterization of the complete lipid profile, the lipidome, of an entire cell or organism. Evaluating whole cell lysates has revealed that, like the proteome and transcriptome, the cellular lipidome is subject to

changes under physiological conditions (Lydic and Goo 2018) and through various stimuli (García-Cañaveras et al. 2017).

In the past, several models tried to unravel possible interaction mechanisms between lipids and proteins. Since the lateral distribution of different lipid species across the plasma membrane is not evenly spread, one proposal includes the formation of micro- or nanodomains of lipids (Engelman, 2005), which build up small (10-200 nm) heterogeneously enriched, highly dynamic, transient membrane rafts, that compartmentalize cellular processes (Simons & Ikonen, 1997; Kusumi et al., 2005; Jacobson et al., 2007; Lingwood and Simons, 2010; Simons & Gerl, 2010).

In conclusion it has become more and more evident that many different lipids have not only structure-giving roles but they also have a major influence on biological processes. The most prominent example of this is the lipid phosphatidylinositol (PI) 4,5-bisphosphate (PIP_2), whose role as a second messenger was already identified at an early stage (Berridge, 1984; Berridge & Irvine 1984) and countless interactions have been identified since.

2.1.3 PIP_2's role in the plasma membrane

Phosphatidylinositol 4,5-bisphosphate (PIP_2) makes up less than one percent of the membrane phospholipids, but is represented and discussed in a large number of reviews awarding it a role in many different cellular processes (Figure 6), making it one of the most important signaling molecules of mammalian cells (Czech, 2000; Cockcroft & De Matteis, 2001; Cremona & De Camilli, 2001; Hilgemann et al., 2001; Hurley & Meyer, 2001; Irvine & Schell, 2001; Martin, 2001; Payrastre et al., 2001; Simonsen et al., 2001; Vanhaesebroeck et al., 2001; Toker, 1998).

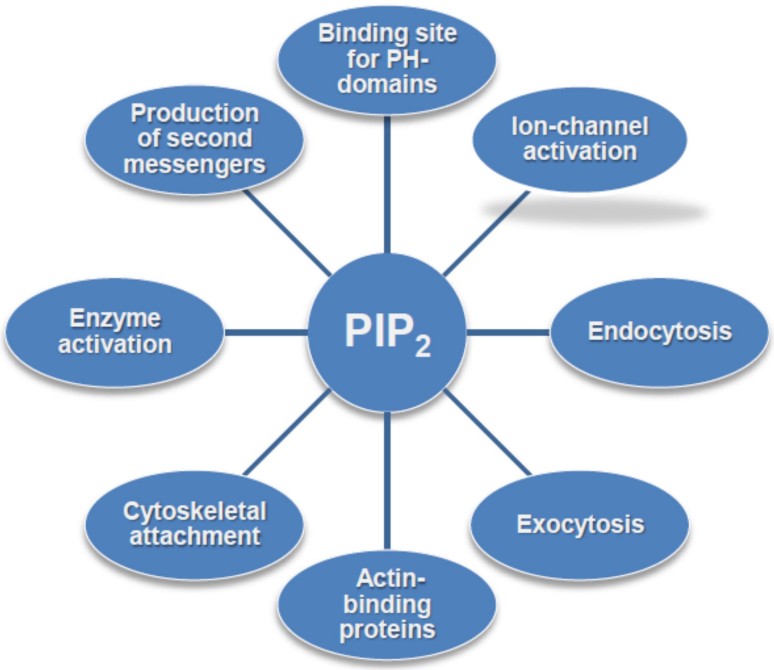

Figure 6: Diverse and numerous functions carried out by PIP_2

PIP_2 acts not only as a second messenger itself but can also be a precursor for inositol triphosphate and diacylglycerol. It is required for clathrin-mediated endocytosis (Höning et al., 2005) and plays a role in exocytosis (Simonsen et al., 2001). In addition it can activate different ion channels in the plasma membrane (Suh & Hille, 2005; Gianoli et al., 2017), acts as a cofactor in enzyme activation and is sensed by actin binding proteins (Papayannopoulos et al., 2005). Proteins containing the pleckstrin homology domain (PH domain) can be bound by PIP_2 which, in the case of the phospholipase C-delta 1, enhances its enzyme activity (Lomasney et al., 1996) (Modified from McLaughlin & Murray, 2005).

Earlier studies showed that PIP_2 acts as a precursor for second messengers like inositol trisphosphate and diacylglycerol (Berridge, 1984), but it can also serve as a second messenger on its own (Odorizzi et al., 2000; Raucher et al., 2000; Huang et al., 1998). It is required for neuronal exocytosis and PIP_2 levels at the plasma membrane determine the rates of sustained exocytosis in stimulated cells (Aoyagi et al., 2005; Wen et al., 2010; Bogaart et al., 2011). The apparent high diversity of functions of PIP_2 led to the

suggestion that it is non-uniformly distributed and concentrates in pools in the plasma membrane (Martin, 2001; Simonsen et al., 2001). One import role is the regulation of protein localization, often dependent on membrane binding domains (Hurley & Misra, 2000) like the PKC homology domains (Hurley et al., 1997; Nalefski & Falke, 1996) and the pleckstrin homology (PH) domain (Lomasney et al., 1996; Bottomley et al., 1998). PIP_2 is, like phosphatidylserine, concentrated at the inner leaflet of the plasma membrane (Figure 7). Here PIP_2 can act as a binding partner for several different proteins containing these binding domains, localizing them to the plasma membrane.

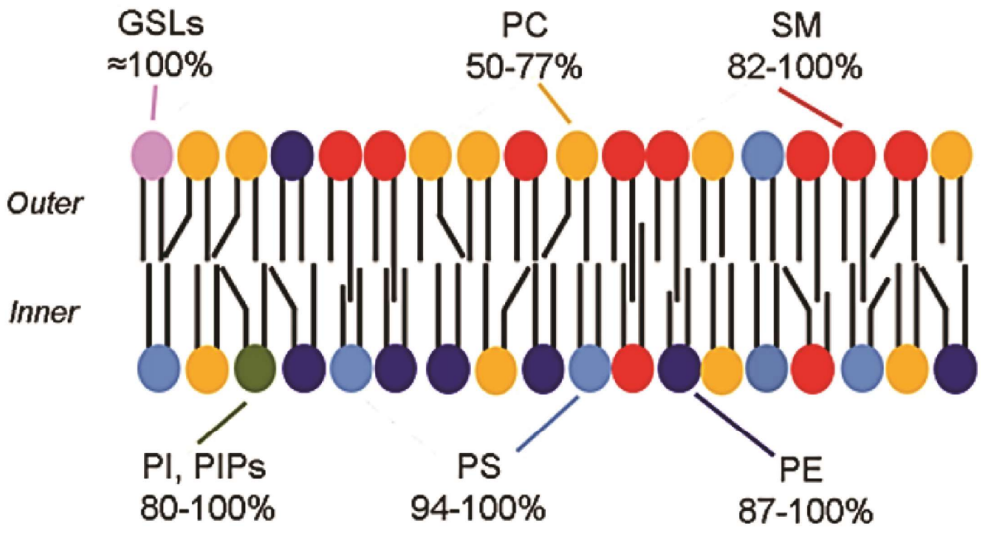

Figure 7: Lipid distribution across the inner and outer leaflet of the PM

Shown is a schematic model of the asymmetrical distribution of phospholipids and glycolipids in the plasma membrane with percentages corresponding to the approximate distribution between the outer and inner leaflet of the plasma membrane of erythrocytes. Phosphatidylcholine (PC, yellow) and sphingomyelin (SM, red) are most abundant in the outer leaflet, whereas glycosphingolipids (GSLs, pink) are believed to exist exclusively in the outer leaflet. The inner leaflet is enriched in phosphatidylethanolamine (PE, dark blue), phosphatidylinositols (PI, green), phosphatidylserine (PS, light blue), as well as different phosphorylated phosphatidylinositols like the prominent phosphatidylinositol 4,5-bisphosphate, also known simply as PIP_2 or PI(4,5)P2 (PIPs, green) (Fujimoto & Parmryd, 2017).

Unlike many other lipids, such as the highly abundant phosphatidylcholine (PC) or cholesterol, PIP_2 has a negative net charge (Figure 8a), which is dependent on the given circumstances like the local pH value or protein interactions (van Paridon et al., 1986; Toner et al., 1988) and the charge of PIP_2 can therefore range between -3, -4 and -5.

In addition the larger and negatively charged head group of PIP_2 (Figure 8b) protrudes further out into the aqueous phase then other lipid species. This opens up the possibility of interactions with clusters of basic residues, anchoring a peripheral protein to the plasma membrane (McLaughlin et al., 2002).

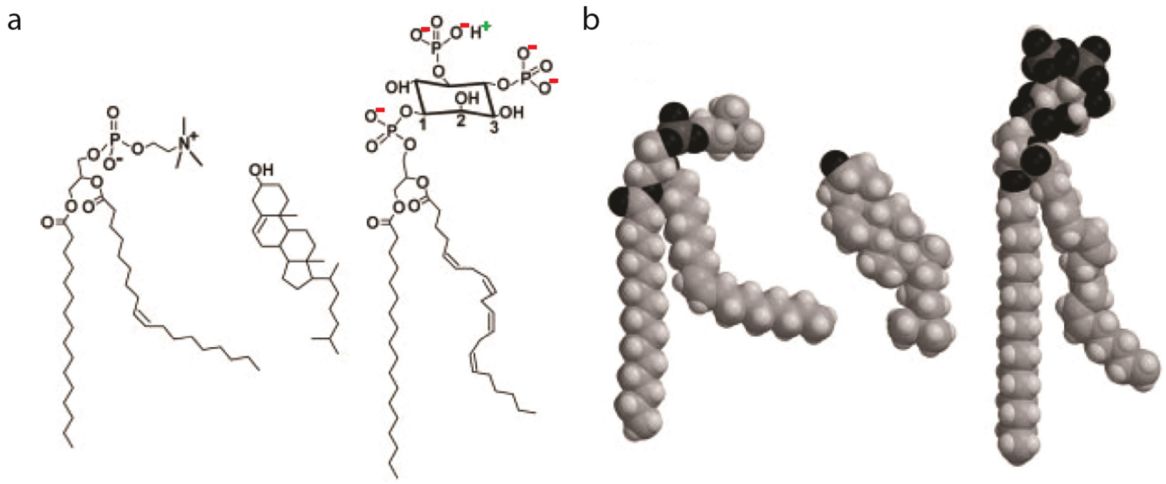

Figure 8: Structural formula and space filling models for PC, cholesterol and PIP_2

(a) From left to right are the chemical structures of PC, cholesterol and PIP_2. PC is a zwitterion and has a neutral net charge like cholesterol, whereas PIP_2 has a negative net charge of -3 to -5 dependent on protein binding or the local pH value. **(b)** Molecular models showing size estimations for the three lipids, allowing to assume that PIP_2 may protrude further into the liquid phase then other phospholipids, which could enhance possible protein-interactions (modified from McLaughlin et al. 2002).

Consequently PIP_2 can also be seen as a potential electrostatic membrane anchor helping proteins to find their preferred place of interaction as in the case of small

GTPases[5] (Heo et al., 2006) or the myristoylated alanine-rich C kinase substrate (MARCKS) (Wang et al., 2002; Gambhir et al., 2004). This mechanism is possibly enhanced by enrichment of PIP_2 in pools or nanodomains present in the plasma membrane (Kwiatkowska, 2010; Wang & Richards, 2012). The underlying general concept is described as a reduction of dimensionality or local concentration effect (McLaughlin et al., 2002), confining a protein's function to the surface phase, a few nanometer-sized region adjacent to the membrane (Aveyard & Haydon, 1973). The regulation of proteins can therefore be dependent on very basic physical interactions like electrostatic interactions (McLaughlin and Murray, 2005) with lipids (Czech, 2000; McLaughlin et al., 2002). This concept has also been described for the transmembrane protein Syntaxin 1A as "membrane protein sequestering" mediated by electrostatic interactions with PIP_2 (Bogaart et al., 2011).

The advances in the field of lipidomics also lead to the use of small lipid-based probes opening up the possibility of proteome-wide detection of lipid-protein interactions (Gubbens and de Kroon, 2010). Based on these advances, new approaches like the membrane-lipid therapy lead to additional possibilities in treatment of diseases like cancer, neurodegenerative disorders and other diseases (Escribá et al., 2008).

Utilizing the specificity of PH domains for binding selectively to PIP_2 or phosphatidylinositol (3,4,5)-trisphosphate (PIP_3) (Kavran et al., 1998), these binding domains can be used as tools to monitor changes in PIP_2 concentrations. Tagging the PH domain of phospholipase C delta 1 (PLC-delta 1) with green fluorescent protein (GFP) proved to be a viable tool for visualization of cellular phosphoinositide dynamics (Stauffer et al., 1998; Várnai & Balla, 1998; Holz et al., 2000; Watt et al., 2002; James et al., 2008).

[5] hydrolase enzymes binding nucleotide guanosine triphosphate (GTP)

With the help of this approach, the amount of PIP_2 enriched at the membrane fusion sites in PC12 cells, a cell line used for neurobiological and neurochemical studies, has been estimated to reach 3–6 % of the surface area (James et al., 2008).

Here PIP_2 is thought to sequester the SNARE protein Syntaxin 1A (van den Bogaart et al., 2011), leading to the enrichment of Syntaxin 1A in clusters (Lang et al., 2001) at the fusion sites, increasing the membrane fusion efficiency (van den Bogaart & Jahn, 2011) (see Figure 9). Syntaxin 1A and PIP_2 are thought to function as a molecular docking site and possibly facilitating the assembly of the complete SNARE fusion machinery (Jahn & Scheller, 2006; Aoyagi et al., 2005; van den Bogaart et al., 2011).

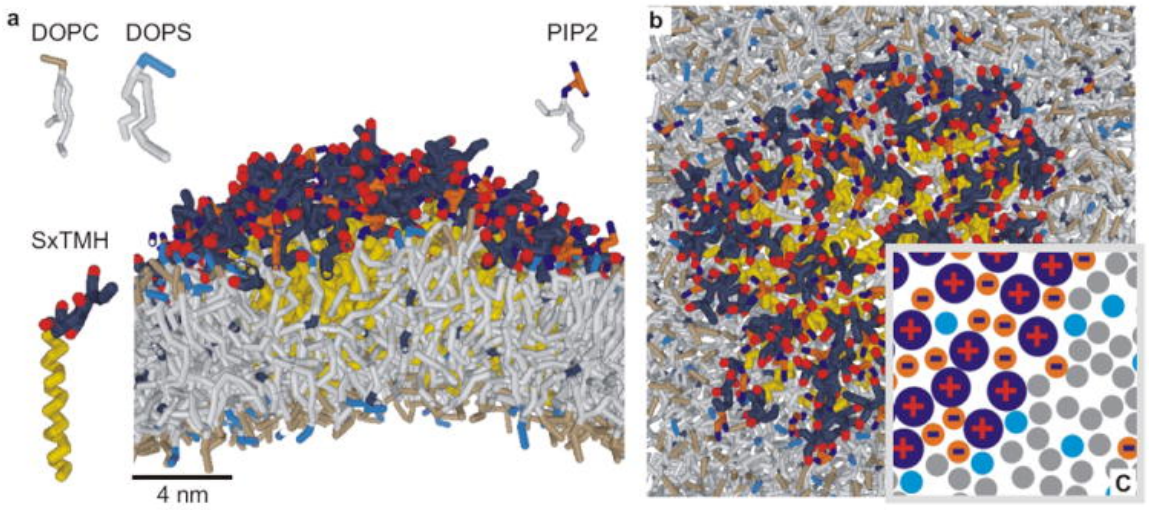

Figure 9: Molecular Dynamics simulation of the PIP_2-Syntaxin 1A microdomains
(a) Side and **(b)** top-view of a coarse-grained molecular dynamics simulation. The bilayer is composed of a 4:1 molar ratio of 1,2-dioleoyl-sn-glycero-3-PC (DOPC; grey) to 1,2-dioleoyl-*sn*-glycero-3-phosphatidylserine (DOPS; cyan). PIP_2 (Orange-blue) was only present in the membrane leaflet facing the N-terminus of Syntaxin 1A (yellow + blue-red). **(c)** Simplified scheme of the cluster (modified from van den Bogaart et al., 2011).

2.2 Membrane proteins working together

The human brain is one of the most complex structures known to mankind and its neuronal network comprises billions of neurons. Every single neuron can be connected to thousands of others via so called synapses, where the exchange of information, the neurotransmission, is based on a rapid and accurate interplay of dozens of molecules. Adopting fundamental knowledge about basic functional mechanisms is the key for developing a preferably complete understanding of this complicated process, involved not only in neurotransmission but generally in the fusion of vesicles.

A well characterized complex is build up by the soluble N-ethylmaleimide-sensitive factor attachment receptor proteins (SNARE). It is responsible for neuronal exocytosis during neurotransmission, taking place in billions of neurons at every point in time in the life of an organism.

2.2.1 The SNARE fusion machinery

Important for the transmission of information in neuronal networks is the release of neurotransmitters out of the active zone of the transmitting neuron into the synaptic cleft, where they bind receptors of the postsynaptic cell. Responsible for the release is a machinery build up by the SNARE complex, leading to the fusion of synaptic vesicles with the target plasma membrane (Söllner et al., 1993; Rothman, 1994; Jahn & Scheller, 2006). Simplified, this fusion machinery consists of the SNARE proteins Syntaxin 1A, synaptobrevin and SNAP25. These membrane proteins are localized at the plasma membrane (Syntaxin 1A and SNAP25) and the vesicular membrane (synaptobrevin) and stabilize in a complex, ultimately leading to the fusion of the two membranes.

For the discovery of this machinery (Figure 10) regulating the vesicle traffic the Nobel prize in physiology or medicine in 2013 was awarded jointly to James E. Rothman,

Randy W. Schekman and Thomas C. Südhof ("The Nobel Prize in Physiology or Medicine 2013" [6]).

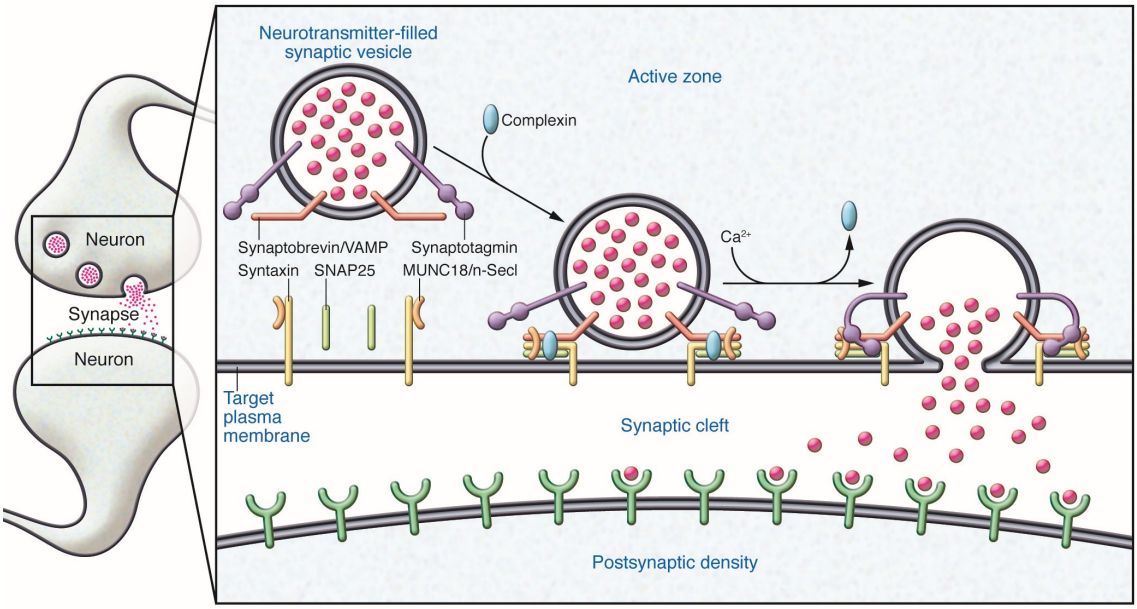

Figure 10: Fusion of a synaptic vesicle via the SNARE machinery

Neurotransmitter-filled synaptic vesicles in the active zone of a neuron dock to the target plasma membrane via the so-called SNARE machinery. The vesicular SNARE proteins synaptobrevin/VAMP bind to a primed complex of SNAP25, syntaxin and Munc18/n-Sec1 located at the plasma membrane. Complexin clamps the SNARE complex and prohibits SNARE fusion. Upon action potential-induced calcium influx, calcium binds to the vesicle-associated synaptotagmin, complexin dissociates and the SNARE's zipper together forming a cis-SNARE complex opening a fusion pore. The neurotransmitter is released into the synaptic cleft and binds to postsynaptic receptors completing the signal transmission from one neuron to another (Hurst, 2013).

The fusion can take place in vitro with artificial membranes with only the previously-mentioned three basic players present (Weber et al., 1998), but in vivo many different proteins are involved (Augustine et al., 1999; Brunger, 2001) in this major transport system. The role of fusion regulators such as synaptotagmin (Bhalla et al. 2006, Martens et al. 2007), Sec1/Munc18 (Shen et al. 2007) and complexin (Schaub et al. 2006) has

[6]NobelPrize.org. Nobel Media AB 2021. Mon. 22 Feb 2021. <https://www.nobelprize.org/prizes/medicine/2013/summary/>

been examined and discussed (McNew 2008), allowing a detailed picture to be made of the SNARE complex and its fusion mechanism. The complementary interactions of the SNARE proteins with Sec1/Munc18-like proteins (Südhof & Rothmann, 2009) and many other proteins show the complex nature of such critical processes, important not only for neurons but for exocytosis in all cells.

Ongoing research on the key players of the fusion machinery, underlying mechanisms like protein clustering (Sieber et al. 2007), concepts about the organization of the plasma membrane (Kusumi et al. 2011) and the inclusion of lipid-protein interactions (Honigmann et al. 2013) help to complete the picture of the regulation and processes of this machinery (Chapman 2008; Jahn & Fasshauer 2012).

2.2.2 SNAP25

One protein of the SNARE complex is SNAP25 (synaptosomal-associated protein of 25 kDa), a peripheral membrane protein of 25 kDa consisting of 206 amino acids. It has two SNARE motifs: one N-terminal motif required for the interaction with Syntaxin 1A (Halemani et al. 2010) and one C-terminal motif connected by a linker region. Both SNARE motifs contribute to the SNARE core complex formation (Rizo & Südhof, 1998; Sutton et al., 1998) together with the SNARE motifs of the transmembrane proteins Syntaxin 1A and synaptobrevin (VAMP) (Figure 11).

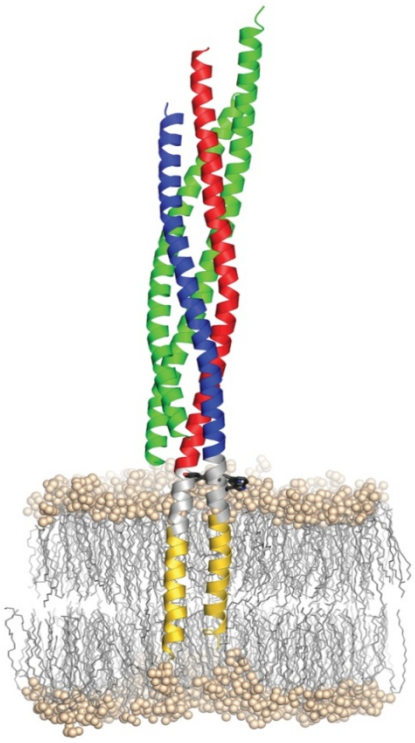

Figure 11: Model of the SNARE complex
Four α-helix bundles, one helix each contributed by Syntaxin 1A (red) and synaptobrevin / VAMP (blue) and two from SNAP25 (green), form the SNARE core complex (Stein et al. 2009).

Through alternative splicing (Puffer et al., 2001) two isoforms of SNAP25 (SNAP25a and SNAP25b) exist, which share high homology, with the exception of a different pattern in the cysteine-rich linker region. SNAP25b is the major isoform present in neurons and highly abundant in the synapse (Knowles et al., 2010; Jahn & Fasshauer, 2012; Wilhelm et al., 2014), while SNAP25a is mainly expressed during embryonic development. SNAP23 (synaptosome associated protein of 23 kDa), a homologue to SNAP25, is expressed ubiquitously and shows also a high degree of homology but has, besides minor alterations in its sequence, one additional cysteine present in the linker region (Chen et al. 1999; Vogel and Roche 1999).

SNAP25 is not only a presynaptic protein playing a role in vesicular exocytosis (Chen and Scheller 2001), but also plays a role in neurite outgrowth (Wu et al. 2011) and long-term potentiation (Jurado et al. 2013). SNAP25 has also been associated with brain

diseases, including Attention Deficit Hyperactivity Disorder (ADHD), schizophrenia and bipolar disorder, indicating that the protein may act as a shared biological substrate among different "synaptopathies" (Antonucci et al., 2016).

The linker region of SNAP25 contains four cysteins (C85, C88, C90 and C92) serving as palmitoylation sites (Hess et al., 1992; Bark & Wilson, 1994), binding SNAP25 to the plasma membrane via hydrophobic palmitoyl chains (Figure 12).

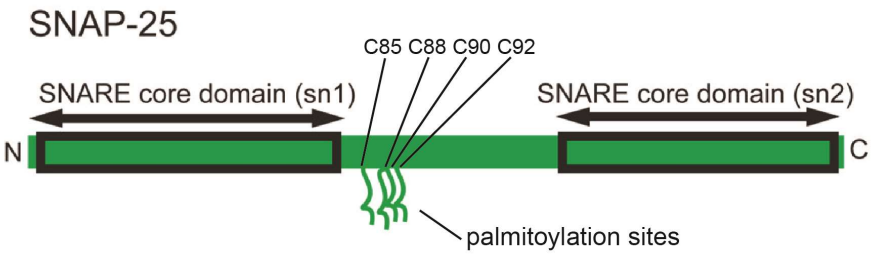

Figure 12: Palmitoylation sites of SNAP25

The linker region, connecting both SNARE domains, contains four cysteins (C85, C88, C90 and C92) that serve as palmitoylation sites, anchoring SNAP25 to the lipid bilayer of the plasma membrane (modified from Brunger et al., 2009).

SNAP25 has no transmembrane domain or a distinct membrane binding domain, but mutations within the linker region have been reported to block membrane association and targeting (Vogel et al., 2000; Washbourne et al., 2001). A stretch of thirty-six amino acids (85-120) seem to be responsible for targeting (Gonzalo et al., 1999) the membrane, as different disruptions within this area lead to mistargeting. SNAP25 can be found in 50–100 nm-sized clusters and co-localize with Syntaxin 1A and Munc18-1 in microdomains on the presynaptic plasma membrane of neurons (Pertsinidis et al., 2013).

2.3 Reaching the plasma membrane

One of the first and most important tasks of a protein in order to carry out its function is, of course, first finding its way to the place where it belongs, its "meeting point" (see chapter 2.1), where it can bind to a potential binding partner or carry out its function at the desired location. For integral membrane proteins this is achieved by a direct installation of the protein during translation into a membrane. This process is called co-translational translocation and uses signal peptides as "postal codes" in combination with signal recognition particles (SRP) during the translation of the protein, in order to transport itself to its target location (Nyathi et al., 2013). The Nobel Prize in Physiology or Medicine 1999 was awarded to Günter Blobel "for the discovery that proteins have intrinsic signals that govern their transport and localization in the cell".

2.3.1 Proteins utilizing specific binding domains

Initially cytosolic proteins that later localize to the plasma membrane usually have membrane binding domains. These can be protein domains that interact with other proteins but also lipid binding domains, like the PKC homology-1 domain (C1), occurring in over 200 different proteins (Hurley & Misra, 2000). Different types of PH domains bind to different phosphoinositides. As mentioned before (see chapter 2.1.3 PIP_2's role in the plasma membrane) the PH domain of PLC-delta binds with high affinity to PIP_2, anchoring it to the plasma membrane (Rebecchi & Pentyala, 2000). Since phosphoinositides are heterogeneously distributed in a cell (Figure 13), they can determine, or at least influence, at which location a protein is possibly enriched and active (De Matteis & Godi, 2004).

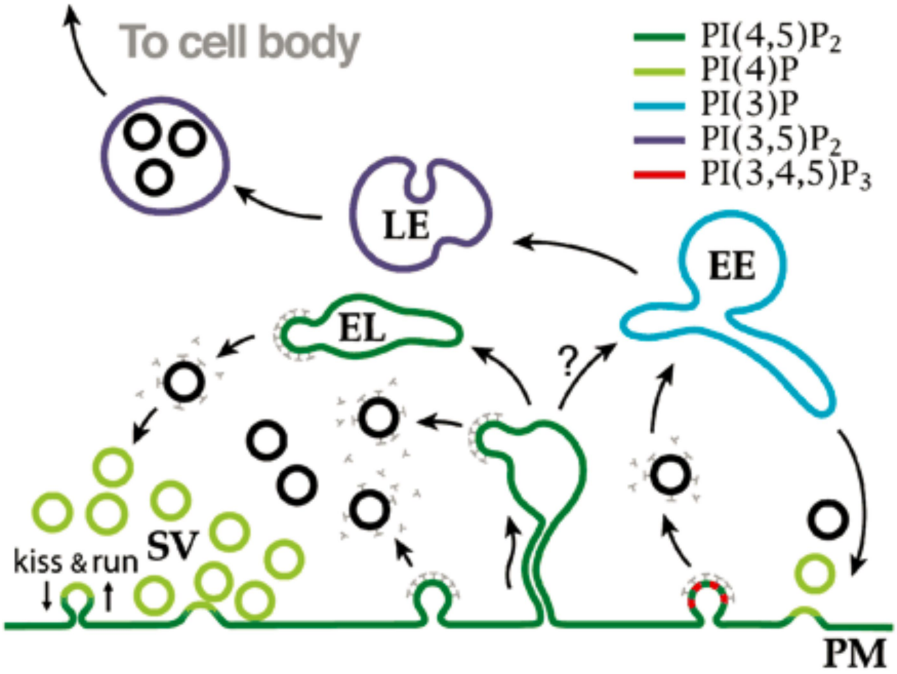

Figure 13: Distribution of phosphoinositides across different cellular membranes

PI(4)P is mainly detected on the Golgi apparatus as well as in synaptic vesicles (SV), PI(3)P on early endosomes (EE) and $PI(3,5)P_2$ on late endosomes (LE). The phosphoinositides $PI(3,4)P_2$, $PI(4,5)P_2$ and $PI(3,4,5)P_3$ are concentrated on the plasma membrane (PM). Deep invaginations of the PM and endosome-like (EL) structures generated from fissions before clathrin-mediated budding, contain $PI(4,5)P_2$ (Wenk & Camilli, 2004).

Again, one of the most prominent lipid examples of this principle is the phosphoinositide PIP_2, which acts as a membrane marker for several proteins (Lemmon, 2003). Its dynamic regulation can lead to a cycling of proteins between cytosol and membrane, which opens up a possible signal-dependent temporal activity-regulation of the protein (Hurley & Meyer, 2001).

2.3.2 Post-translational modifications

Many proteins are modified post-translationally, extending the repertoire of the twenty standard amino acid building blocks by modifying an existing functional group or introducing a new one. Phosphorylation (Turner et al., 1999) is one of the most common post-translational modifications and mainly a mechanism for regulating the activity of enzymes (Khoury et al., 2011). Glycosilation, the attachment of carbohydrate molecules, promotes the correct folding of the protein after translation, stabilizes the protein and serves as recognition targets for lectins - carbohydrate binding proteins.

The attachment of lipids, also known as lipidation (Schmidt & Schlesinger, 1979), often anchors the modified protein to the cell membrane. Thus an otherwise soluble cytosolic protein gets the ability to associate with membranes upon modification with hydrophobic lipid anchors (Baumann & Menon, 2002). Isoprenylation (Gelb, 1997; Zhang & Casey, 1996), glycophospholipid modifications (Glypidation) and acylation (Schlesinger & Magee 1982) are the main forms of lipidation. Acylation is either obtained by an N-amid bond, the myristoylation (Magee & Courtneidge, 1985; Towler et al., 1988) or by thioester linkage, the palmitoylation (*S*-acylation).

Palmitoylation is often used as a synonym for *S*-acylation, since the most common modification is with palmitic acid. The S-acylation happens via covalent addition of palmitic acid via thioester linkage to a thiol group of cystein residues (Schmidt et al., 1988). Usually other lipid modifications like myristoylation and isoprenylation are irreversible. The unique reversibility of palmitoylation (Linder & Deschenes, 2003; Smotrys & Linder, 2004; Bijlmakers & Marsh, 2003) however opens up the possibility of acting as an organizing system for peripheral membrane proteins (Rocks et al., 2010) or regulating the localization of a signaling protein to specific membrane subdomains (Mumby, 1997). It can have an influence on protein stability, protein-protein interactions and membrane trafficking as is proposed for directing the trafficking of the

enzyme glutamic acid decarboxylase (Kanaani et al., 2008) or the small GTPases of the Ras subfamily (Figure 14) (Salaun et al., 2010).

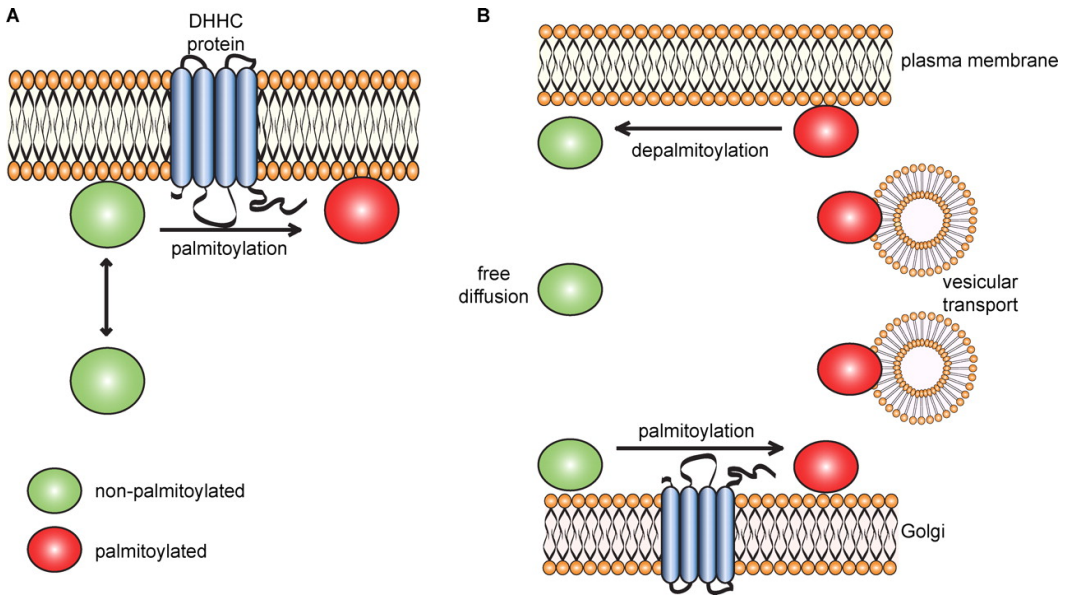

Figure 14: Palmitoylation regulating membrane trafficking of peripheral proteins

a) Peripheral proteins modified with a lipid anchor often show weak membrane affinity. Palmitoylation via a DHHC palmitoyl transferase attaches the protein to the plasma membrane. b) Small GTPases of the Ras subfamily are palmitoylated by Golgi localized DHHC proteins leading to plasma membrane localization via vesicular transport (Salaun et al., 2010).

Protein palmitoylation is thought to be an enzymatic reaction, mediated by palmitoyl transferases (PAT), carrying a so-called DHHC (Asp-His-His-Cys) motif (Varner et al., 2003). In mammals 24 of these proteins have been identified (Fukata et al., 2004) and, depending on the localization of the different palmitoyl transferases, a palmitoylation of proteins is possible at the endoplasmatic reticulum (Berger & Schmidt, 1985; Rizzolo & Kornfeld, 1988), the cis-Golgi network (Dunphy et al., 1981; Quinn et al., 1983) and the plasma membrane (Olson & Spizz, 1986).

The DHHC proteins have been predicted to have four to six transmembrane domains with the critical DHHC motif on the cytosolic side of the membrane (Politis et al.,

2005). Therefore any potential target protein need to be in close proximity to the cytosolic side of the membrane.

Palmitoylation often follows a myristoylation or a prenylation as a second step. After the myristoylated protein gets loosely attached to the plasma membrane, because of its enhanced hydrophobicity the palmitoylation anchors the protein stably to the membrane (Bhatnagar & Gordon, 1997; Alland et al., 1994, Deschens, 2013). This is the so called "kinetic membrane trapping model" (Dunphi & Linder, 1998; van´t Hof & Resh, 1997; Shahinian & Silvius, 1995; Hancock et al. 1990). But nonetheless, palmitoylation can also occur without any other premodification, as with the neuronal proteins SNAP25 (Veit et al., 1996), SNAP23 (Chen et al., 1999) or G-alpha subunits (Linder et al, 1993).

2.3.3 Membrane association driven by electrostatics

Although membrane association of many peripheral proteins is primarily due to the hydrophobic penetration into the membrane interior of a hydrophobic lipid anchor chain, recent studies have revealed that there is another basic mechanism driven by basic electrostatic interactions at work (McLaughlin & Murray, 2005).

The cytosolic side of the plasma membrane is predominantly populated by phosphatidylserine, leading to an overall negative surface charge of the inner leaflet. A higher polyphosphoinositide (PIP) content in the form of phosphatidylinositol-4,5-bisphosphate (PIP_2) and phosphatidylinositol-3,4,5-trisphosphate (PIP_3) also contributes to this effect. The negatively charged lipid headgroups can be targeted by proteins containing multiple polycationic motifs facilitating a membrane contact that is driven by electrostatics (Heo et al., 2006).

K-Ras, a molecular on/off switch controlling cell proliferation, uses myristoylation in combination with a polybasic cluster to target and retain itself at the plasma membrane (Cadwallader et al., 1994; Wright & Philips, 2006). Many small GTPases of the Ras, Rab, Arf and Rho subfamilies seem to use this kind of mechanism to target phosphatidylinositol-4,5-bisphosphate with two or three polybasic subclusters, each covering four to five amino acids with positively charged residues (Heo et al., 2006).

Another example is p21-Ras where not only palmitoylation but also a polybasic domain in combination with hydrophobicity through prenylation of a CAAX[7] motif is required for plasma membrane localization (Hancock, 1990).

The myristoylated alanine-rich C-kinase substrate (MARCKS) has, besides its lipid anchor at the N-terminus, a conserved basic effector domain of 13 basic residues in the middle of the protein, binding to three PIP_2 molecules (Figure 15) (Gambhir et al.,

[7] C is a cysteine, the two A residues are aliphatic amino acids and the X can be one of several amino acids

2004). Although MARCKS is overall highly negatively charged, with the help of this electrostatic interaction it can bind to the also negatively charged plasma membrane.

This interaction between MARCKS and PIP_2 is described as a mechanism to control the availability of sequestered PIP_2 and therefore regulate its influence on physiological processes.

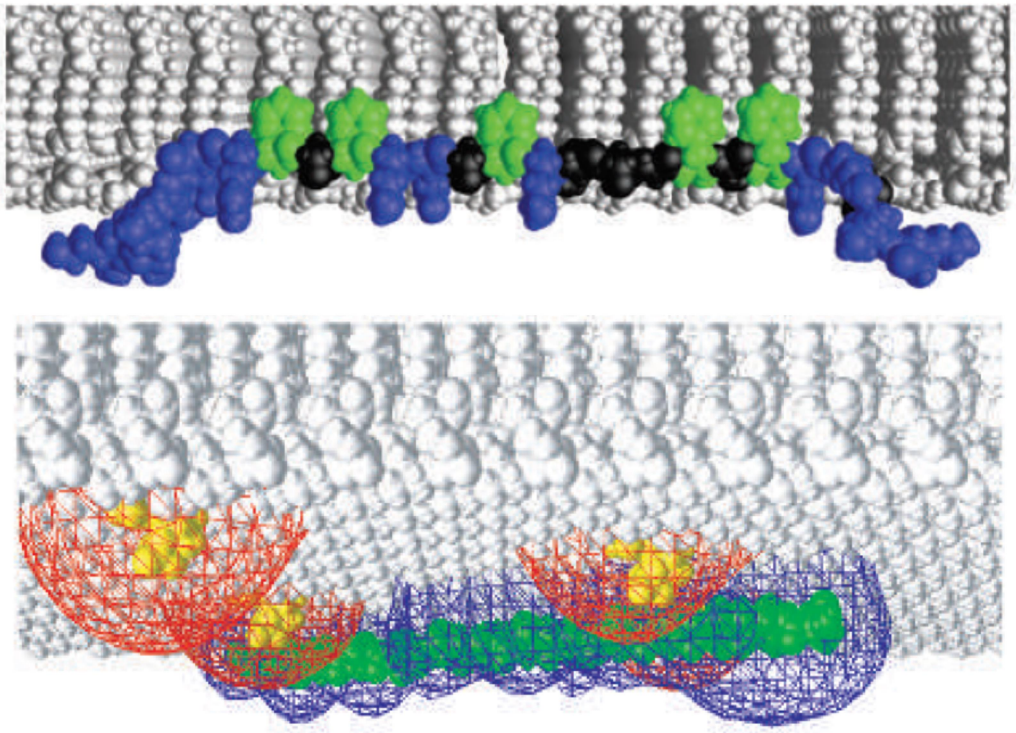

Figure 15: The effector domain of MARCKS

Shown are the five hydrophobic (green) and thirteen basic (blue) residues of the effector domain of MARCKS connecting to a lipid bilayer (white) in an atomic model (upper panel). Due to the basic residues the MARCKS peptide produces a local positive electrostatic potential (blue mesh) that acts as a basin of attraction for PIP_2 (yellow) with its negative electrostatic potential (red mesh) (lower panel) (modified after McLaughlin & Murray 2005).

In recent years it has become more and more clear that having multiple possible interaction mechanisms serving the same purpose and functioning together is crucial for some proteins. They are able to integrate multiple signals from each domain before

achieving its desired localization, which opens up the possibility of further regulation of its effective purpose (Strickfaden et al., 2007).

2.3.4 Membrane targeting of SNAP25

Different mechanisms for SNAP25 trafficking were discussed in recent years and the trafficking pathways and mechanisms by which the SNARE protein SNAP25 is targeted to specific membrane compartments are not well understood.

As previously discussed, the minimal region of SNAP25 that is critical for targeting the plasma membrane ranges from amino acid residues 85 to 120 (Gonzalo et al., 1999). This membrane-targeting domain represents two-thirds of the linker region that connects the N- and C-terminal SNARE domains of SNAP25 and includes the four cysteines acting as palmitoylation sites.

It is accepted that stable attachment of SNAP25 to the plasma membrane is achieved by palmitoylation of its cysteines in the cysteine rich region. Depending on how many and which cysteines are palmitoylated, different patterns of palmitoylation seem to affect the localization of SNAP25 at the plasma membrane and at the endosomes, supporting palmitoylation as the underlying critical factor for targeting of SNAP25 to the PM (Greaves & Chamberlain, 2011). The majority of SNAP25 resides at the plasma membrane but a pool of approximately 20 % is located in the endosome-trans-Golgi network (Aikawa et al., 2006). The half-life of the palmitoylation is estimated to be around three hours whereas the half-life of the entire SNAP25 protein was shown to be approximately eight to ten hours measured in PC12 cells (Lane und Liu, 1997).

Therefore a possible regulation of the SNAP25 trafficking through depalmitoylation and repalmitoylation cycles similar to the mechanism of small GTPases of the Ras subfamily has been discussed (Salaün et al., 2004).

However the localization of all DHHC proteins, which are firmly embedded into the lipid bilayer and responsible for the palmitoylation, is restricted to the plasma

membrane or other membranes of inner organelles and implies that SNAP25 requires a specific membrane-targeting mechanism to facilitate initial membrane interaction in order to get into the proximity of the DHHC proteins. The palmitoyl acyltransferase DHHC 2 is located at the plasma membrane and therefore is a likely candidate to execute the palmitoylation of SNAP25 at the plasma membrane (Greaves et al., 2010). Considering SNAP25 and the cytosolic leaflet of the PM are both dominantly negatively charged, SNAP25 should be mostly repellent to close contact with the PM. Since SNAP25 has no other lipid modifications or distinct membrane binding domains, it remains unclear how the crucial proximity to DHHC proteins is achieved.

In one case the establishing of initial contact with the membrane was speculated to involve hydrophobic forces from hydrophobic residues located in the vicinity of the cysteine-rich domain (Greaves et al., 2009). Another possible mechanism of SNAP25 membrane association is the proposal that SNAP25 localizes together with its SNARE interaction partner Syntaxin 1A to the plasma membrane (Figure 16) (Vogel et al., 2000; Washbourne et al., 2001).

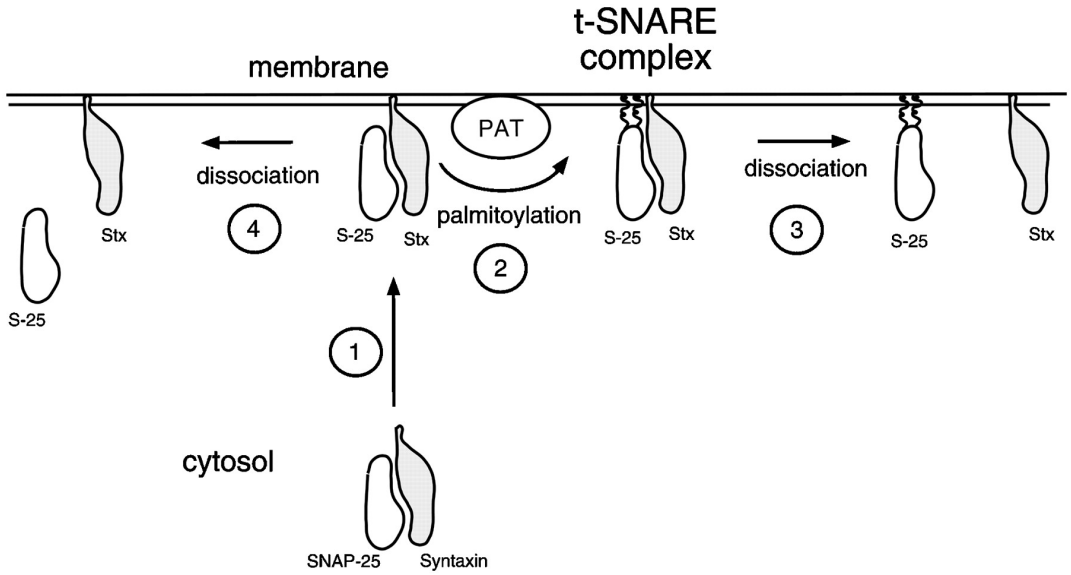

Figure 16: Co-trafficking of SNAP25 with syntaxin to the plasma membrane

A post-translationally assembled SNAP25-Syntaxin complex targets the plasma membrane with the help of Syntaxin 1A's transmembrane domain (1). Now SNAP25 can be palmitoylated at the plasma membrane (2) generating together with syntaxin a steady-state SNARE complex. Syntaxin 1A can dissociate from the complex leaving SNAP25 attached via its palmitoyl anchors to the membrane (3). SNAP25 that is not palmitoylated can dissociate from syntaxin and return to the cytosol (4) (Vogel et al., 2000).

Contrary to this model another study showed a syntaxin-independent mechanism for SNAP25 membrane targeting, suggesting the need for a neuronal co-factor (Gonzalo et al.,1999; Loranger & Linder, 2002).

In summary several possible mechanisms have been proposed for the membrane targeting of SNAP25. So far, however, the models are contradictory and therefore it is not sufficiently clarified how SNAP25 is targeted to the plasma membrane. The focus of previous studies relied mostly on the palmitoylation itself or possible interaction partners that help SNAP25 to be integrated at its designated localization.

Although having an overall negative net charge, the surroundings of the cysteine-rich region (CRR) show an overall excess of three positive charges after offsetting positive against negative charges. In comparison to other proposed electrostatic anchoring mechanisms, like in the case of MARCKS or K-Ras which utilize several polybasic

clusters or patches with an overall higher positive net charge, the small excess charge of three in the CRR of SNAP25 is very low. But particularly in the presence of multivalent lipids present in the membrane such as PIP_2, which could act as an electrostatic counterpart, this limited number of charged residues may be sufficient for facilitating an initial membrane contact and electrostatically anchor SNAP25 to the plasma membrane until being thoroughly bound via palmitoylation. Therefore PIP_2 might function as a molecular docking site similar to its protein-lipid interactions with Syntaxin 1A (.

This electrostatic anchoring mechanism could represent an underestimated mechanism playing a role in all kinds of cells. One example would be the lipid transfer proteins, where a lysine exchange leads to a loss of Osh4-mediated sterol transfer (Schulz.et al., 2009).

3 Aims of the study

Although the synaptosomal-associated protein of 25 kDa (SNAP25) is an important participant of the well described SNARE fusion machinery, its membrane targeting mechanism is still mostly unsolved. As is already described for other peripheral proteins like K-Ras (Cadwallader et al., 1994; Wright & Philips, 2006), interactions via a polybasic domain could play a pivotal role in the initial membrane association of SNAP25. Therefore the emphasis of this study is set upon the identification of a possible electrostatic anchoring mechanism as a precondition for the stable attachment of SNAP25 to the plasma membrane.

3.1 Characterization of the electrostatic anchoring of SNAP25

Primarily to characterize and approach the possible existence of an electrostatic anchoring mechanism, localization patterns of SNAP25 after protein mutagenesis in the targeting region changing the overall net charge were compared using life cell imaging in neuronal PC12 cells.

The ubiquitously-expressed homolog of SNAP25, SNAP23, was also investigated to see if this targeting mechanism might apply to SNAP23 as well. Western blot analysis of prepared membrane fractions were conducted to confirm the microscopic analysis and additionally with the help of unroofed cells, so called membrane sheets, the plasma membrane was investigated for bound SNAP25 variants in isolation from the rest of the cell.

Since past studies (Vogel et al., 2000; Washbourne et al., 2001) discussed a membrane targeting of SNAP25 coupled to syntaxin and to rule out a possible influence of the protein mutagenesis on the interaction with syntaxin, a fluorescence recovery after

photobleaching (FRAP) analysis was employed to study the interaction of SNAP25 and the SNAP25 mutants with syntaxin in the cell membrane.

In addition, the palmitoylation of SNAP25 was analyzed via click-labelling of a palmitate analogue with a fluorophore, in order to confirm a requirement of palmitoylation for membrane association of SNAP25 and to assess the palmitoylation status of the mutated SNAP25 variants introduced during this study.

3.2 Identifying the electrostatic anchoring partner in the plasma membrane

Secondly the nature of the negatively charged lipids embedded in the plasma membrane, that might play a role in targeting, was elucidated. In order to identify the most likely candidate PIP_2 as a possible partner for the electrostatic anchoring of SNAP25, competition experiments with the PH domain of phospholipase C-delta in addition to binding studies of reconstituted liposomes containing distinct lipid compositions were conducted.

4 Materials and Methods

4.1 Materials

All standard chemicals, reagents and consumables were purchased from the companies Carl Roth GmbH & Co. KG (Karlsruhe, Germany), Sigma-Aldrich Chemie GmbH (München, Germany), Bio-Rad Laboratories, Inc. (Hercules, USA), Merck KGaA (Darmstadt, Germany) or New England Biolabs Inc. (Ipswich, USA). Materials for cell culture work were purchased from Sarstedt (Nümbrecht, Germany).

4.1.1 Plasmids

plasmid	source	vector backbone
Syntaxin 1A-mGFP	described in Sieber et al., 2006	pEGFP-N1
mEGFP[8]-SNAP25B [wt-SNAP25 *(+3)*]	described in Halemani et al., 2010	pEGFP-C1
SNAP25-GST[9] [GST-wt-SNAP25 *(+3)*]	kindly provided by Helena Batoulis; described in Batoulis et al., 2016	pGEX-6P1
pEGFP-C1	GenBank accession No.: U55763, Clontech, Mountain View, CA	pEGFP-C1
pEGFP-N1	GenBank accession No. U55762, Clontech, Mountain View, CA	pEGFP-N1
pGEM®-T Easy	#A1360, Promega, Mannheim, Germany	pGEM®-T Easy
pGEX-6P1	GE Healthcare, Solingen, Germany	pGEX-6P1
PH-GFP	Addgene, No.:21179, Stauffer et al. 1998	pEGFP-C1

Table 2: Plasmids (not self-created)

[8] monomeric variant of green fluorescent protein
[9] glutathione S-transferase

4.1.2 Kits used for DNA purification

DNA-purification kits were used according to the manufacturer's instructions.

Kit	Manufacturer	Catalogue Nr.
NucleoSpin Plasmid	Macherey und Nagel, Düren, Germany	REF 740588.50
NucleoSpin Gel and PCR clean-up	Macherey und Nagel, Düren, Germany	REF 740609.50
NucleoBond Xtra Midi	Macherey und Nagel, Düren, Germany	REF 740410.50
NucleoBond PC500	Macherey und Nagel, Düren, Germany	REF 740574.50

Table 3: DNA Purification kits

4.1.2 Cell lines

PC12

PC12 cells (gift from Rolf Heumann, Bochum, Germany; similar to clone 251; Heumann et al., 1983) are derived from the pheochromocytoma of a rat (*rattus norvegicus*) adrenal medulla. The PC12 cells showed the characteristic changes in morphology (neurite varicosities) as the typical response to treatment with nerve growth factor (NGF).

HepG2

The HepG2 cell line (CLS, Eppelheim, Germany; # 300198) originally stems from a hepatoblastoma (*homo sapiens*). The cells grow adherently and in a single layer in small cell clusters.

BHK

The Baby Hamster Kidney (BHK) cell line is an adherent non-neuronal fibroblast cell line that lacks any endogenous Syntaxin 1A (Sieber et al. 2006)

4.1.3 Cell Culture media

PC12 cell culture media

Dulbecco's Modified Eagle's Medium (DMEM) with high (4.5 g/l) glucose (PAN biotech) supplemented with 10 % (v/v) horse serum (Biochrom AG), 5 % (v/v) fetal calf serum (FCS) (Biochrom AG) and 100 U/ml penicillin, 100 ng/ml streptomycin (PAN biotech).

HepG2 culture media

MEM Eagle (PAN Biotech, # P04-08509) supplemented with 10 % (v/v) FCS (Biochrom), 2mm stable glutamine (PAN Biotech) and 100 U/ml penicillin, 100 ng/ml streptomycin (PAN biotech).

BHK culture media

DMEM supplemented with high (4.5 g/l) glucose, 10 % tryptose phosphate (Gibco, Paisley, UK), 5 % FCS, 2 mM L-Glutamine and 100 U/ml penicillin, 100 ng/ml streptomycin (PAN biotech).

PBS for cell culture

Dulbecco's Phosphate Buffered Saline (DPBS) without Ca^{2+} and Mg^{2+}; KCl 200 mg/l, KH_2PO_4 200 mg/l, NaCl 8 g/l, Na_2HPO_4 1.15 g/l; pH 7.2 (PAN Biotech, #P04-36500).

Trypsin/ ethylenediaminetetraacetic acid (EDTA)

Trypsin 0.05 %/EDTA 0.02 % in phosphate-buffered saline (PBS), w/o: Ca and Mg, w: Phenol red (PAN Biotech;#P10-0231SP).

4.1.4 Bacteria & bacteriological culture

Escherichia coli

Rosetta (DE3)pLysS, (Merck, Darmstadt, Germany) is optimized for eukaryotic protein expression and was used for expression of glutathione S-transferases (GST)-SNAP25 constructs.

E. coli XL-10 Gold® Ultracompetent Cells (Stratagene, La Jolla, CA) used for amplification of plasmid DNA.

LB medium

LB Broth (Lennox), 10 g/L tryptone, 5 g/L yeast extract, 5 g/L NaCl; pH 7 (Carl Roth (Karlsruhe, Germany) in ddH_2O.

Bacteria cultures were mixed with 30 % (v/v) glycerol and stored at –80 °C for long-term storage.

4.1.5 Buffers & solutions

Buffers and solutions were prepared using autoclaved deionized water (ddH_2O).

Buffer	Composition; pH
Phosphate buffered saline (PBS)	137mM NaCl, 2.7mM KCl, 10mM Na2HPO4, 1.76mM KH2PO4; pH 7.4
Tris buffered saline (TBS)	50 mM Tris, 150 mM NaCl; pH 7.4
PBS +Tween20 (PBS-T)	PBS with 0.05 % (v/v) Tween 20
TBS+Tween20 (TBS-T)	TBS with 0.05 % (v/v) Tween 20
Poly-L-lysine (PLL) (20x stock solution)	2 mg/ml PLL (Sigma-Aldrich; #P1524) in ddH_2O (stored at -20 °C)
Sonication buffer	120 mM KGlu, 20 mM KAc, 20 mM HEPES-KOH, 10 mM EGTA[10]; pH 7.2.
Ringer solution	130 mM NaCl, 4 mM KCl, 1 mM $CaCl_2$, 1 mM $MgCl_2$, 48 mM D(+)αglucose ,10 mM HEPES; pH 7.4.
Homogenization buffer	300 mM sucrose, 5 mM Tris-HCl, 0.1 mM EDTA, 1 mM PMSF[11] (freshly added); pH 7.4. Buffer was kept on ice and used ice-cold.
4x Laemmli buffer	250 mM Tris, 30 % [v/v] glycerol, 6 % [w/v] SDS, 0.04 % [w/v] bromophenol blue; pH 6.8.
Odyssey® Blocking Buffer	#402-467-0700, LI-COR Biosciences GmbH, Bad Homburg, Deutschland
RIPA lysis buffer	RIPA lysis buffer system; sc-24948, SantaCruz Biotechnology, USA
Click buffer	100 mM HEPES; pH 7.2, containing 500 mM tetrakis(acetonitrile)-copper(I)tetrafluoroborate (Sigma-Aldrich Chemie GmbH, München, Germany)

Table 4: Buffers & solutions

[10] ethylene glycol-bis(β-aminoethyl ether)-N,N,N′,N′-tetraacetic acid

[11] phenylmethylsulfonyl fluoride

In addition two different lysis buffers were used:

Lysis buffer I (for assessment of SNAP25 palmitoylation / Western Blot)

150 mM NaCl, 5 mM $MgCl_2$ 25mM HEPES; pH 7,2; 1 % [v/v] TritonX-100, 1 mM PMSF, 1 tablet Complete® EDTA free per 100 ml buffer (#05056489001, Roche, Mannheim, Germany), 100 µg/ml lysozyme;

Lysis buffer II (for liposome-binding studies)

150 mM NaCl, 50 mM Tris-HCl, 1mM EDTA; pH 7.4 - containing Roche cOmplete protease inhibitor, 1 mM dithiothreitol (DTT), 100 mg/ml lysozyme and two units/ml DNAse I.

4.1.6 Staining solutions

TMA-DPH staining solution

The supernatant after centrifugation of a saturated solution of 1-(4-tri-methyl-ammonium-phenyl)-6-phenyl-1,3,5-hexatriene-p-toluenesulfonate (TMA-DPH); (ThermoFisher, Waltham, USA) was added (10 %) to either Ringer solution (for cells) or sonication buffer (for membrane sheets). TMA-DPH solution was centrifuged at 17,000 x g for 3 min and the supernatant was transferred to a new reaction tube and centrifuged a second time. The second supernatant was used for microscopy.

Western Blotting Luminol Reagent

Luminol Reagent (# sc-2048,Santa Cruz Biotechnology, USA). Luminol reagent was used for Western blotting enhanced chemiluminescence using horseradish peroxidase (HRP) conjugated secondary antibodies.

4.1.7 Antibodies

Primary antibodies	Specifications
Anti GFP	rabbit polyclonal IgG; RRID: AB_303395; #ab-290 (abcam, Cambridge, UK) diluted 1:1000 in blocking solution (PBS-T, 5 % milk)
Secondary antibodies	
HRP goat-anti-rabbit	HRP goat-anti-rabbit; RRID:AB_631747, t# sc-2030, Santa Cruz Biotechnology, USA; diluted 1:5,000 in blocking solution (PBS-T 5 % milk)
IRDye 800CW-coupled	IRDye 800CW-coupled goat-anti-rabbit (LI-COR, #9263221); diluted 1:10,000 in Odyssey blocking solution containing 0.1 % Tween20.

Table 5: Primary & secondary antibodies

4.1.8 Technical instruments

Spectrophotometer

NanoDrop2000™ (Thermo Fisher Scientific, Waltham, USA) was used for DNA / plasmid concentration measurement.

Fluorescence, absorbance, luminescence plate reader

Infinite® 200 PRO multimode plate reader (Tecan, Maennedorf, Switzerland) was used for bicinchoninic acid assay (BCA) based protein concentration measurements.

Ultrasonic homogenizers

Sonopuls HD 2070, 70 W (Bandelin, Berlin, Germany)

SDS-PAGE and agarose gel electrophoresis equipment

Mini-PROTEAN Tetra Cell, Mini Trans-Blot® module, PowerPac HC Power Supply and Trans-Blot® SD Semi-Dry Electrophoretic Transfer Cell (Bio-Rad, Hercules, CA, USA), electrophoresis chambers and accessories for agarose gel electrophoresis (biostep, Jahnsdorf, Germany).

Membrane scanner

Odyssey® CLx Imaging System (LI-COR Inc., Lincoln, USA) was used for western blot detection and kindly provided by the Kolanus' laboratory (LIMES-Institute, University of Bonn).

Neon™ Transfection System

The Neon™ transfection system was used with the Neon™ Transfection System 100 µL Kit (MPK10096, Thermo Fisher Scientific Waltham, USA) according to the manufacturer's guidelines.

4.1.9 Microscopes

Confocal laser scanning microscopy (CLSM)

For confocal microscopy, the Olympus FluoView™ FV1000 laser scanning microscope (Olympus, Hamburg, Germany) with an UPlanSApo 60x NA 1.35 objective was used. The microscope features a 488 nm laser as well as 543 nm laser and a climate chamber (set to 37 °C) The Olympus Fluoview 3.0 software was used to operate the microscope (located at AG Kolanus, LIMES Institute, University of Bonn, Germany).

Epifluorescence microscopy

The Axio Observer D1 epifluorescence microscope (Zeiss, Jena, Germany) with an N XBO 75 Watt Xenon arc lamp was used. The microscope was equipped with a Plan-Apochromat 100x/NA 1.4 oil immersion objective and a 12 bit charge-coupled device (CCD) camera (1376 1040 pixel), yielding a pixel size of 64.5 nm x 64.5 nm. The following filter sets from AHF Analysentechnik were used for imaging: UV filter (F11-000) set for TMA-DPH staining of the PM, enhanced green fluorescent protein (EGFP) HC filter set (F36-525) for GFP fluorescence and TRITC HC filter set (F36-525) for mCherry fluorescence. The CamWare (3.01) software was used to operate the microscope (located at AG Lang, LIMES Institute, University of Bonn, Germany).

Olympus IX81 microscope equipped with an Olympus UPlanApo 10x/0.40 objective and an electron multiplying charge-coupled device (EMCCD) camera (ImagEM C9100-13, Hamamatsu Photonics, Hamamatsu, Japan) was used with the filter sets (AHF Analysentechnik) DAPI[12] HC (#F36-500), TRITC HC (#F36-503) and EGFP HC (#F36-525).

[12] 4′,6-diamidino-2-phenylindole

4.1.10 Software

Sequence Alignment

For the sequence alignments of SNAP25 the software Clustal Omega Version 1.2.2 (Sievers et al., 2011) was used.

Image analysis

ImageJ 1.50c W. (Rasband, National Institute of Health, USA). Western Blot fluorescent bands were quantified using ImageJ's Gel Analyser.

Data Plots

Sigma Plot 11.0 (Systat Software, San Jose, CA)

FRAP Curve Fits

OriginPro 8.0951 (OriginLab Corporation, Northampton,MA)

4.2 Methods

If not stated otherwise, experiments were carried out at room temperature (RT).

4.2.1 Cloning

All cloning work for all constructs was performed following standard methods and guidelines for cloning described by Sambrook and Russell (Sambrook and Russell, 2006). DNA-purification kits were used according to the manufacturer's instructions. All resulting cloning constructs were sequenced by GATC (Konstanz, Germany) and verified. Manually designed primers and oligonucleotides used for cloning were ordered from Eurofins Genomics (former MWG Operon) (Ebersberg, Germany).

All SNAP25 and SNAP23 plasmids for transient overexpression under the CMV promoter are based on the expression vector pEGFP-C. The plasmid DNA for wt-SNAP25*(+3)* (Halemani et al., 2010) and wt-SNAP23*(+3)* contains a monomeric variant of monomeric variant of green fluorescent protein (mEGFP) fused via a linker of five amino acids (RSRAL) N-terminally to the sequence of full-length rat SNAP25B (NP_112253.1) or SNAP23 (NP_073180). Oligonucleotides containing the desired mutations were inserted into the coding sequence via overlap extension or fusion polymerase chain reaction (PCR). The resulting fusion PCR products were cloned into the SacI and BamHI restriction sites, or in the case of SNAP25$_{(C\text{-}to\text{-}G)}$, the XhoI and KpnI restriction sites.

The resulting constructs were the following:

name	mutations
wt-SNAP25(+*3*)	[mEGFP + SNAP25B (1-206 -full length)]
SNAP25-*5*	[mEGFP + SNAP25B (1-206; K69A, K72A, K76A, K83A, K94A, K96A, K102A and K103A)]
SNAP25-$5_{hydrophob}$	[mEGFP + SNAP25B (1-206; K69L, K72L, K76L, K83L, K94L, K96L, K102L and K103L)]
SNAP25+*10*	[mEGFP + SNAP25B (1-206; E73K, N77K, D80K and D99K)]
SNAP25+*7*	[mEGFP + SNAP25B (1-206; D70A, E73A, E75A and D80A)]
SNAP25-1_{distal}	[mEGFP + SNAP25B (1-206; K69A, K72A, K102A and K103A)]
SNAP25-$1_{proximal}$	[mEGFP + SNAP25B (1-206; K76A, K83A, K94A and K96A)]
$SNAP25_{(C\text{-}to\text{-}G)}$	[mEGFP + SNAP25B (1-206; C85G, C88G, C90G and C92G)]
$SNAP25_{R191A/R198A/K201A}$	[mEGFP +SNAP25B (1-206; R191A, R198A and K201A)]

Table 6: SNAP25 constructs

SNAP23 constructs were created with the help of Stefan Dahlhoff:

name	mutations
wt-SNAP23 *(+3)*	[mEGFP + SNAP23 (1-210 -full length; wildtype)]
SNAP23-*3*	[mEGFP + SNAP23 (1-210; K64A, K71A, K78A, K91A, K97A, K100A)]
SNAP23+*10*	[mEGFP + SNAP23 (1-210; E70K, T72K, E75K, E94K)]
SNAP23+*11a*	[mEGFP + SNAP23 (1-210; D65K, E68K, E75K, E94K)]
SNAP23+*11b*	[mEGFP + SNAP23 (1-210; D65K, E70K. E75K, E94K)]
SNAP23+*16*	[mEGFP + SNAP23 (1-210; D65K, E68K, E70K, L73K, E75K, T90K, E94K, N98K)]
$SNAP23_{(C\text{-}to\text{-}G)}$	[mEGFP + SNAP23 (1-210; C79G, C80G, C83G, C85G, C87G)]

Table 7: SNAP23 constructs

The pEGFP-N1 vector served as the basis for the C-terminally red fluorescent protein (RFP)-tagged rat Syntaxin 1A created for this work. Syntaxin-RFP is inserted using the XhoI and the NotI restriction sites. A 12 amino acid linker (LVPRARDPPVAT) connects Syntaxin 1A (NP_446240) to a monomeric RFP (Campbell et al., 2002) lacking the first amino acid.

The plasmid for expression of mCherry-C1-PLCδ-PH is based on GFP-C1-PLCδ-PH (a gift from Tobias Moser, Addgene, plasmid 21179; (Stauffer et al., 1998), inserting mCherry into the vector using the AgeI and XhoI restriction sites.

The mCherry-C1-PLCδ-PH-K32A-W36N-R38K mutant, which is incapable of binding to PIP_2, (Flesch et al., 2005) was generated via fusion PCR followed by re-insertion into the vector using the restriction sites BamHI and XbaI.

For the expression of GST-tagged SNAP25 constructs (GST-SNAP25+*10* and GST-SNAP25-*5)*, they were N-terminally fused to a glutathione S-transferase (GST) tag. The GST-wt-SNAP25 *(+3)* construct was a kind gift from Helena Batoulis (Batoulis et al., 2016). The coding sequences for SNAP25-*5* and SNAP25+*10* were amplified with primers with an overhang containing restriction sites for BamHI (forward primer) and EcoRI (reverse primer). First, the sequences carrying the restriction sites were subcloned into the pGEM-T easy vector system via TA cloning. In a second step they were subcloned into the expression vector pGEX-6P1 via the BamHI and EcoRI restriction sites.

4.2.2 Cell Culture

All cell lines used during this study were cultured under sterile conditions and tested negative for mycoplasmic infections (GATC Biotech, Konstanz, Germany). Cells were maintained at 37 °C / 5 % CO_2 in culture flasks (TC Flask T75 ; #83.3911.002, Sarstedt, Nümbrecht, Germany) or on poly-L-lysine (PLL)-coated coverslips (25 mm diameter; Marienfeld (Lauda-Königshofen, Germany)) which were placed in six-well plates (TC Plate 6 Well; #83.3920, Sarstedt, Nümbrecht, Germany). Every 48 – 62 h, the cell culture medium was aspirated and replaced with fresh medium to remove dead cells and depending on the cell type and confluence passaging was performed every 2 - 4 days. For long-term storage cell suspensions were stored in liquid nitrogen. When they were needed the cells were defrosted for up to 3 minutes in a 37 °C water bath until only a small portion of the suspension was frozen. The suspension was transferred into the respective culture medium, centrifuged for 2.5 min at 200 x g, resuspended and placed in culture flasks.

PC12

PC12 cells were maintained at 37 °C and 5 % CO_2 in culture medium DMEM with high (4.5 g/l) glucose (PAN biotech, Aidenbach, Germany) supplemented with 10 % horse serum (Biochrom, Berlin, Germany), 5 % FCS (Biochrom) and 100 U/ml penicillin/100ng/ml streptomycin (PAN biotech).

HepG2

HepG2 cells were cultured in MEM (Pan biotech) supplemented with 10 % FCS and 100 U/ml penicillin/100ng/ml streptomycin. The cells were maintained at 37°C and 5% CO2 in a sterile incubator

BHK

For BHK cells essentially the same protocol was used for cell culture except that the growth media, DMEM was supplemented with high (4.5 g/l) glucose, 10 % tryptose phosphate broth (Gibco, Paisley, UK), 5 % FCS 2 mM L-Glutamine and 60 U/ml penicillin and 60 µg/ml streptomycin. The cells were grown at 37°C, 5% CO_2 in sterile incubators.

Harvesting of cells

Cells were detached by treatment with trypsin (0.05% Trypsin and 0.02% EDTA in PBS, PAN Biotech, cat# P10-0231SP) for 2 min. Trypsin was inactivated by adding the respective culture medium. Afterwards the cells were pelleted by centrifugation at 1000 x g at room temperature for 3 min and the pellet was washed with PBS.

4.2.3 PLL-coating of glass coverslips

The glass coverslips (Menzel Gläser, Braunschweig, Germany) were cleaned in absolute ethanol and sterilized by brief flaming. A volume of 500 µl of a 100 µg/ml poly-L-lysine (PLL; # P1524, Sigma Aldrich) dissolved in ddH_2O was placed onto each coverslip and incubated for 30 min at RT. Afterwards the coverslips were washed thoroughly with ddH_2O for 30 min and air-dried at RT.

4.2.4 Transfection of cells

For the transfection of cells the Neon® Transfection System (Thermo Fisher Scientific) was used according to the manufacturer's guidelines. Cells were harvested and resuspended in 125 µl buffer R (provided by the kit) before mixing with the plasmid DNA. The Neon® transfection tips (100 µl) were loaded with the cell suspension, mixed with 10 µg of plasmid DNA of the respective construct. For the co-transfections with Syntaxin-RFP 5 µg of each plasmid DNA was used and for the co-transfections with the

PH domain, 3.3 µg for SNAP25 constructs and 10 µg of PLC-δPH/PH_{mut} DNA was used. PC12 cells transfected applying a pulse at 1410 V and 30 ms pulse width, and HepG2 cells were transfected at 1200 V and 50 ms pulse width. Cells were plated onto PLL-coated coverslips and maintained for at least 48 hours (unless stated otherwise; e.g. Figure 22) before microscopic imaging or harvesting for SDS-PAGE and western blot analysis.

4.2.5 Generation of membrane sheets

For the generation of membrane sheets an ultrasonic homogenizer (Sonopuls HD 2070; Bandelin, Berlin, Germany) was used. PC12 cells on PLL-coated coverslips were subjected to a brief ultrasound pulse in ice-cold sonication buffer (120 mM KGlu, 20 mM KAc, 20 mM HEPES-KOH, 10 mM EGTA; pH 7.2) with a distance of 0.5 cm to the sonication tip. The pulse intensity was optimized for each cell type so that after ultrasound treatment mainly unroofed cells (with only the basal membranes left), the so-called membrane sheets, were present (see Figure 17). These freshly prepared membrane sheets were stained with TMA-DPH and imaged directly in sonication buffer for up to 35 min.

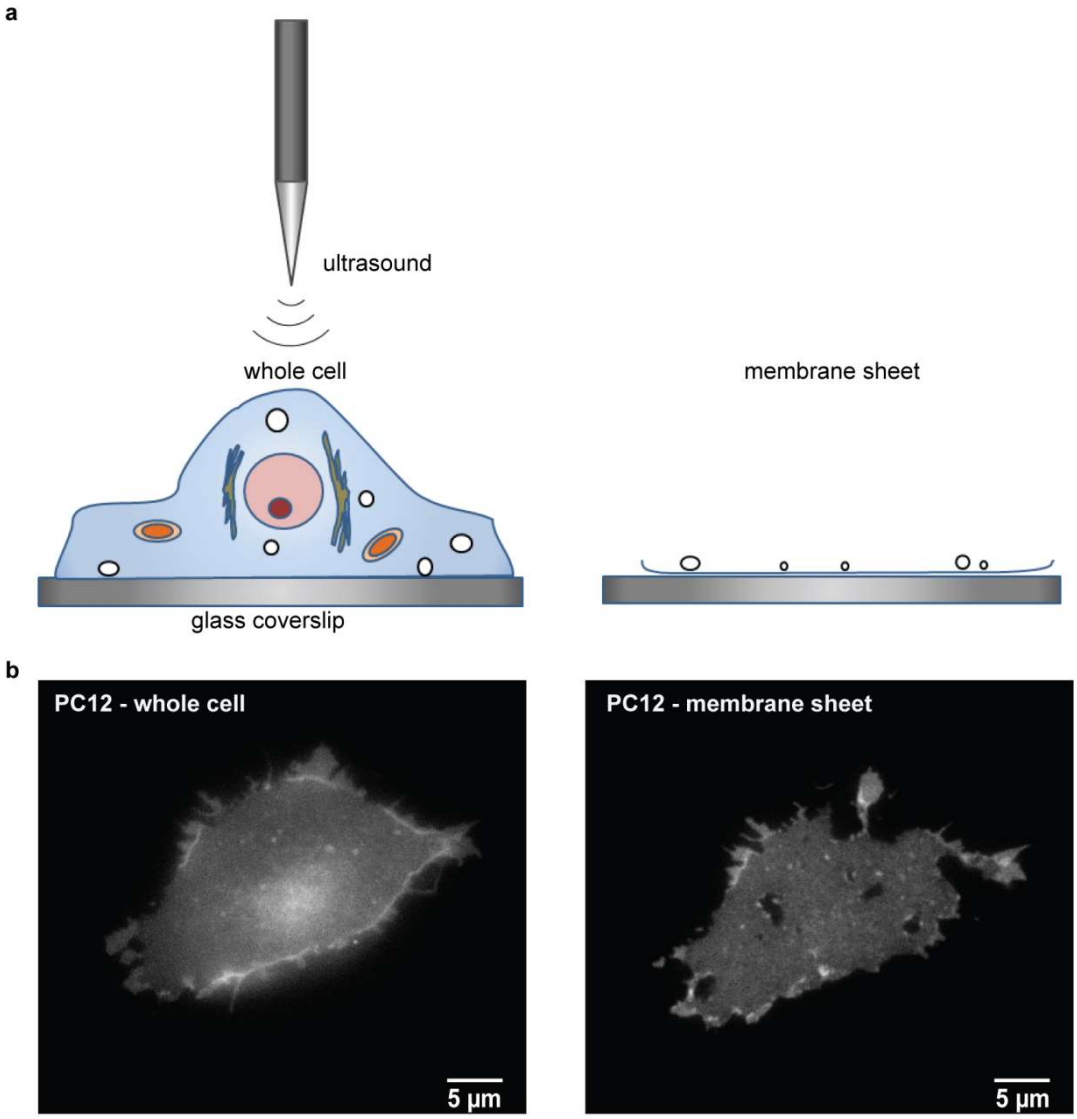

Figure 17: Generation of membrane sheets

(a) Illustration showing the generation of membrane sheets with the help of a short sonication pulse (own illustration). After the living adherent cells on PLL-coated glass coverslips are treated with the sonication pulse, only the basal membrane is left behind. This opens up the possibility of microscopy of the membrane with low signal-to-noise since the cytosolic background is no longer there. **(b)** Images of a PC12 cell (left) before and the remaining membrane sheet (right) after sonication. The fluorescent probe TMA-DPH is used for visualization of the membrane.

4.2.6 Epi fluorescence microscopy

For measuring the association of SNAP25 constructs with the plasma membrane on membrane sheets, a Zeiss Axio Observer D1 (see section 4.1.9 Microscopes) epifluorescence microscope was used. The pixel size for the captured images was 64.5 nm x 64.5 nm. Freshly prepared membrane sheets were stained with TMA-DPH and imaged in sonication buffer for up to 35 min. The TMA-DPH staining was applied for the visualization of the shape and integrity of the membrane sheets. Pictures were taken using filter sets F11-000 (AHF Analysentechnik, Tübingen, Germany) for TMA-DPH (blue channel), F36-525 (AHF Analysentechnik, Tübingen, Germany) for GFP (green channel), and F36-503 (AHF Analysentechnik, Tübingen, Germany) for mCherry. From the individual membrane sheets, the fluorescence intensity was measured in a region of interest (ROI) of 30 pixel x 30 pixel (PC12 membrane sheets) or 50 pixel x 50 pixel (HepG2 membrane sheets). The background fluorescence was measured in a second ROI and subtracted.

For assessing the co-transfection efficiency of intact HepG2 cells (48h after transfection, the cells were fixed in 4 % PFA (paraformaldehyde; Carl Roth) in PBS and imaged in PBS containing TMA-DPH. For image acquisition an Olympus IX81 microscope (see section 4.1.9 Microscopes) was used. With the help of the ImageJ software individual cells were outlined and their fluorescence intensity in the GFP- and mCherry-channel quantified. For each experiment and construct, a range of 21–96 membrane sheets were measured.

4.2.7 Confocal microscopy and analysis

For the linescan analysis of PC12 cells the FluoView1000 confocal laser scanning microscope (CLSM) was used (see section 4.1.9 Microscopes). The living cells were

imaged at 37°C in Ringer solution and by, focusing on the glass-cell interface, cells were checked for proper morphology and adherence to the coverslip in order to exclude dead or dying detached cells. For the linescan analysis a cross-section spanning across the plasma membrane including background outside the cell for background correction and spanning further into the cytosol is needed. Therefore clumps of cells were mostly avoided to ensure a proper section for analysis. In order to get a cross-section at the equatorial area of the cell, the focal plane of the microscope was adjusted and the scanning field was rotated to ensure a horizontal (90° angle to the cell membrane) linescan analysis is possible. The scanning field covered an area of 256 pixel x 256 pixel with a pixel size of 137 nm.

For the linescan analysis a horizontal ROI of 100 pixel length and 5 pixel width, was placed across the plasma membrane. The fluorescence intensities were averaged across the 5 pixels and recorded along the 100 pixel cross-section. Fluorescence intensities were background corrected and normalized to the peak intensity at the plasma membrane in order to compare cells with various fluorescence intensities of one experiment day. The linescans were aligned with reference to the peak intensity at the plasma membrane and the cytosolic fluorescence level was averaged over 5 pixels starting at a 10 pixel distance from the peak intensity at the plasma membrane. Finally, calculations of the ratios between the cytosolic level and the peak intensity at the PM were carried out. A range of 14-40 cells imaged per experiment/day were used per construct and several experiments/days as is indicated in the respective figure legends were averaged.

4.2.8 FRAP

For the FRAP measurements the CLSM FluoView1000 (see section 4.1.9 Microscopes) was used. The scanning speed was set to 40 µs per pixel and image sequences were recorded at 1.2 Hz for 113 seconds. Laser intensities for both 488 nm laser (for GFP) and 543 nm (for RFP) were reduced to a minimum to avoid bleaching during the recording of the image sequence.

Life membrane sheets were analyzed shortly after generation and imaged up to 35 min. Recordings of a scanning area of 100 pixel x 100 pixel with a pixel size of 0.414 µm started with a pre-bleaching phase of 3 images, followed by a 500 ms bleaching step and recording of the recovery phase. For the bleaching step a smaller ROI with a size of 7 pixels x 7 pixels (2.9 µm x 2.9 µm) was scanned at maximum intensity for the 488 nm laser in combination with a 405 nm laser.

For analysis the recovery traces were recorded in the bleached ROI (7 pixels x 7 pixels) and background-subtracted with a second ROI (7 pixels x 7 pixels) placed in the background. Afterwards the values were normalized to the average of the pre-bleach values. For one experiment, 7 – 15 membrane sheets per condition were measured and the normalized recovery traces were averaged. A hyperbolic curve $y(t) = \text{offset} + \text{maximal recovery} \times t/(t + t_{1/2})$ was fitted to the averaged recovery trace yielding the half time ($t_{1/2}$) of recovery and the maximal recovery.

4.2.9 Membrane Fractionation and Western Blot

The protein biochemistry experiments were performed following standard methods as described in (Kyhse-Andersen, 1984; Laemmli, 1970; Towbin et al., 1979) and for the homogenization and cell fractionation as described in (Rehm & Letzel, 2010).

After harvesting the cells (4.2.2 Cell Culture), the cells were centrifuged a second time and pellets were resuspended in 750 µl ice-cold homogenization buffer. For homogenization a Potter-Elvehjem homogenizer was used. The cells were kept on ice in a volume of 0.75 ml and homogenized by applying 100 strokes. The homogenate was centrifuged for 8 min at 800 x g at 4°C, yielding pellet P1 (containing non-homogenized cell debris) and supernatant S1. S1 was transferred into a new tube for a second centrifugation for 120 min at 20,000 x g and 4°C yielding pellet P2, containing the enriched membrane fraction which was resuspended in 750 µl homogenization buffer and the supernatant S2 with the cytosolic fraction.

The protein concentrations of P2 and S2 were determined using the BCA Protein Assay following the manufacture's protocol. Using the microplate reader Infinite® F200pro the absorbance at 595 nm was measured in 96-well-plates and the protein concentrations were determined referring to a BSA standard curve.

In order to load the same protein amounts for western blot analysis of the different SNAP25 constructs, the protein concentrations of P2 and S2 were adjusted to lowest concentrations of P2 and S2, respectively. Samples were boiled at 95°C for 10 minutes in 4x Laemmli buffer and 10 µg per lane were loaded for SDS-PAGE analysis.

Proteins were separated on 12 % gels and transferred onto nitrocellulose membranes (Carl Roth, Germany) by semi-dry blotting. The nitrocellulose membranes were blocked for one hour with blocking solution (PBS-T containing 5% milk powder). Afterwards the membranes were immunostained with a rabbit primary antibody against GFP diluted 1:1000 in blocking solution overnight at 4°C. After immunostaining the membranes were washed three times with PBS-T for 20 min.

The second antibody, goat-anti-rabbit, tagged with HRP was applied for 1 hour. After washing three times with PBS-T the membranes were developed on autoradiography films and the chemiluminescence was detected with Luminol Reagent. The developed

films were scanned and from the digital images band intensities were quantified using ImageJ's Gel Analyzer.

To analyse the expression levels of HepG2 cells of the same batch of co-transfected cells used for microscopy western blot analysis was performed (Supplementary Figure 4), following in principal the same protocol but with a different lysis buffer. Ten million HepG2 Cells were lysed after 48h in RIPA lysis buffer and centrifuged for 6 min at 10,000 x g. Samples were boiled in respective amounts of 4x Laemmli at 95°C for 10 min. Lysates were analysed by western blot, detecting the GFP with the anti GFP antibody. Band signal intensities were corrected for the amount of the lysate protein concentration determined with a BCA assay.

4.2.10 Assessment of palmitoylation by click chemistry and western blot

Using small lipid-based probes opens up the possibility of the identification of a protein modification in a considered protein. Click chemistry (see figure 18) uses the formation of a covalent bond between a chemically reactive group of a small target molecule and a fluorophore, which can be used for measuring different protein modifications like myristoylation (Martin et al., 2008) or palmitoylation (Martin & Cravatt, 2009, Yount et al., 2010).

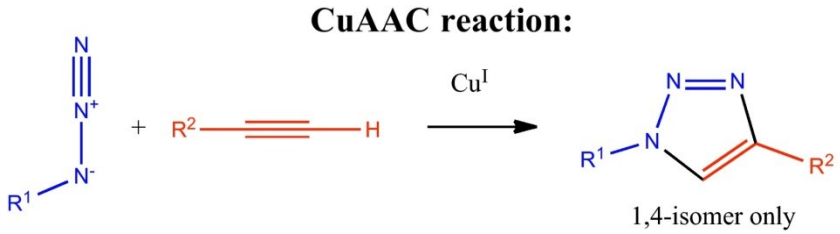

Figure 18: Click reaction

The picture shows the copper(I)-catalyzed azide-alkyne cycloaddition (CuAAC). The reaction can be used to bind a desired marker (R_1) labeled with an azide group to an alkyne group present on the target molecule (R_2) (modified after Liang & Astruc, 2011).

Approximately ten million PC12 cells were transfected using the Neon™ Transfection System. The cells were transfected with 15 µg plasmid DNA for the GFP fusion constructs: wt-SNAP25 *(+3)*, SNAP25-*5*, SNAP25+*10* or SNAP25$_{(C\text{-}to\text{-}G)}$. One hour after transfection, the medium was replaced with DMEM containing 15 % delipidized FCS (PAN biotech, Aidenbach, Germany) and 100 µM palmitate-alkyne (a kind gift from the Thiele lab, LIMES Institute, Bonn). After 15 h of incubation, feeding the cells with palmitate-alkyne, the cells were treated with trypsin and scraped off. After harvesting the cells were washed with PBS and after centrifugation resuspended in lysis buffer I. The lysis was promoted by vortexing and mild sonication followed by centrifugation for 10 min at 14,000 x g. For immunoprecipitation of the SNAP25-GFP fusion constructs

the supernatant was bound by GFP-trap beads (#gta-20, Chromotek, Martinsried, Germany) and incubated for 2 h at 4°C. After several washing, samples were taken up in click buffer where the incorporated palmitate alkyne was clicked to a Cy5-labelled azide (c_{final} = 100 µM). After incubation for 1 h at 37°C the samples were washed to remove non-bound Cy5-labelled azide. Immunoprecipitation samples were eluted by boiling in Laemmli buffer under non-reducing conditions for 10 min at 95 °C. The proteins were separated by SDS-PAGE and the samples were wet blotted to a nitrocellulose membrane, which was blocked with a 1:1 mixture of Odyssey blocking buffer and PBS. The detection was done with a rabbit anti-GFP primary antibody, followed by washing and incubation with an IRDye 800CW-coupled goat-anti rabbit secondary antibody. Finally the Cy5 fluorescence of the clicked palmitate and the IRDye 800CW fluorescence of the immunostained GFP were visualized using the Odyssey® CLx Imaging System (kindly provided by AG Kolanus, LIMES, University of Bonn, Germany). The fluorescent bands were quantified using ImageJ's Gel Analyser.

4.2.11 Liposome preparation

The liposome preparation was done by Kerstin M. Rink (Heidelberg University Biochemistry Center, Heidelberg, Germany) and the following protocol on the methodology was provided by her and is taken from *Weber et al. 2017*:

Atto647N-1,2-dipalmitoyl-*sn*-glycero-3-phosphoethanolamine (Atto647N-DPPE) was purchased from Atto-Tec. All other lipids were from Avanti Polar Lipids. The complex lipid mixture (5 µmol total amount of lipid) contains 34.5 mol % 1-palmitoyl-2-oleoyl-*sn*-glycero-3-phosphocholine (POPC), 15 mol % 1,2-dioleoyl-*sn*-glycero-3-phosphoserine (DOPS), 20 mol % 1-hexadecanoyl-2-octadecenoyl-*sn*-glycero-3-phosphoethanolamine (POPE), 25 mol % cholesterol (from ovine wool), 5 mol % liver L-α-phosphatidylinositol (from liver) and 0.5 mol % Atto647N-DPPE. For the lipid mixes containing brain L-α-phosphatidylinositol-4,5-bisphosphate ($PI(4,5)P_2$) or 1-

stearoyl-2-arachidonoyl-*sn*-glycero-3-phospho-(1'-myo-inositol-3',4',5'-trisphosphate) ($PI(3,4,5)P_3$) the amount of PI was reduced accordingly. The lipids were dissolved in chloroform or chloroform/methanol (3:1 ratio, for $PI(4,5)P_2$ and $PI(3,4,5)P_3$), mixed and dried under a flow of nitrogen. The remaining chloroform was removed by vacuum for 4 hours. The lipids were dissolved in 1 ml reconstitution buffer (25 mM HEPES/KOH pH 7.4, 200 mM KCl, 1 % (w/v) OG (n-Octyl-β-D glucopyranoside), 1 mM DTT (1,4-dithiothreitol) by 30 minutes shaking. To form liposomes, OG was diluted below the critical micelle concentration by the addition of 2 ml buffer (25 mM HEPES/KOH; pH 7.4, 200 mM KCl, 1 mM DTT). The residual OG was removed by flow dialyses with 4 L 25 mM HEPES/KOH pH 7.4, 135 mM KCl, 1 mM DTT overnight. Subsequently, a Nycodenz gradient centrifugation was performed to isolate the liposomes. Therefore, the dialyzed samples were mixed with an equal volume of 80% (w/v) Nycodenz and transferred into two SW60-tubes (Beckman Coulter). Layers of 750 µl 35% (w/v) Nycodenz, 150 µl 11.6 % (w/v) Nycodenz and 100 µl fusion buffer were added on top of the 40% (w/v) Nycodenz/liposome solution. The gradient was spun at 55000 rpm for 3 h 40 min at 4 °C. The liposomes were isolated, followed by a buffer exchange (25 mM HEPES/KOH pH 7.4, 135 mM KCl, 1 mM DTT, 0.1 mM EGTA, 0.5 mM $MgCl_2$, 1 mM DDT) using a PD MiniTrap G-25 (GE Healthcare Life Sciences). The amounts of lipids were quantified by measurement of Atto647N fluorescence (excitation: 639 nm, emission: 669 nm) in a Fluoroskan Ascent FL Microplate Fluorometer (Thermo Scientific).

4.2.12 Liposome binding studies

As preparation for the liposome binding studies the GST-wt-SNAP25 *(+3)*, GST-SNAP25-*5* and GST-SNAP25+*10* pGEX-6P1 constructs were transformed into *E. coli* (Rosetta (DE3)pLysS). The expression of the GST fusion proteins was induced with 1 mM isopropyl-thiogalactoside (IPTG) at 18 °C over night. After harvesting the bacteria

by centrifugation, they were lysed for 60 min at 4°C in lysis buffer II (150 mM NaCl, 50 mM Tris-HCl; pH 7.4 and 1 mM EDTA containing Roche cOmplete protease inhibitor, 1 mM DTT, 100 µg/ml lysozyme and 2 units/ml DNAse I). The lysate was mildly sonicated and centrifuged for 30 min at 20,000 x g. The supernatant was frozen in liquid nitrogen and thawed after transport for binding of the constructs directly to glutathione beads. An SDS-PAGE gels loaded with samples from each step of the purification process for both SNAP25-*5* and SNAP25+*10* GST-tagged constructs was carried out (see Figure 19).

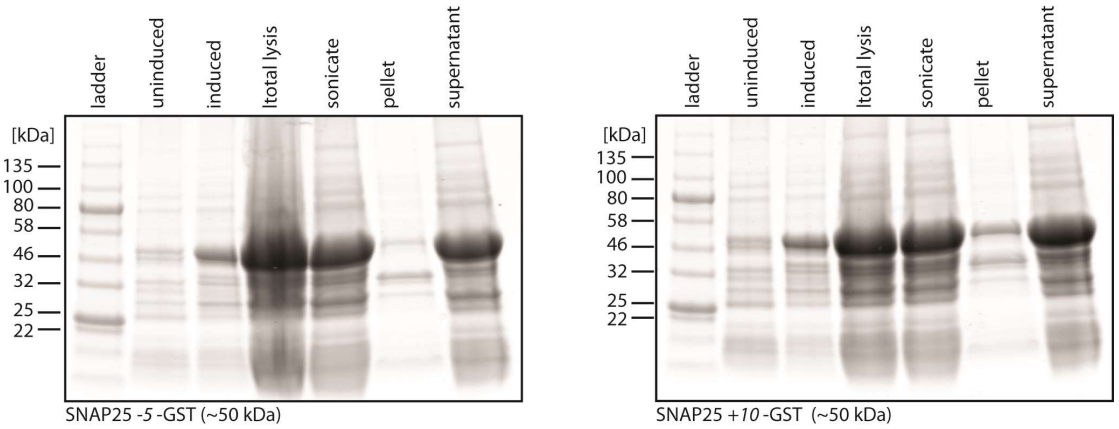

Figure 19: SDS-PAGE with samples from each step of the SNAP25 purification

Shown are coomassie-stained (Coomassie Brilliant Blue G-250; ThermoScientific, Waltham, USA) SDS-PAGE gels loaded with samples from each step of the purification process for both SNAP25-*5* and SNAP25+*10* GST-tagged constructs. The constructs with a weight of ~50 kDa were expressed and purified from *E. coli (*Rosetta (DE3)pLysS). After harvesting the bacteria were resuspended in lysis buffer II and mildly sonicated. Leaving behind any insoluble components via centrifugation the supernatant was frozen immediately in liquid nitrogen and stored for later usage.

The monitoring of SNAP25 interactions with the prepared liposomes was done by Kerstin M. Rink (Heidelberg University Biochemistry Center, Heidelberg, Germany) and the following protocol on the methodology was provided by her and is taken from *Weber et al. 2017*:

To monitor SNAP25 interaction with liposomes, 42 µg GST-SNAP25 constructs or a equimolar amount of GST were bound to 20 µl GSH sepharose 4 fast flow beads (GE Healthcare Life Sciences) prewashed 3 x with ddH_2O and 3 x with fusion buffer (25 mM HEPES/KOH pH 7.4, 135 mM KCl, 1 mM DTT, 0.1 mM EGTA, 0.5 mM $MgCl_2$, 1 mM DDT). 160 nmol liposomes in fusion buffer were added to the beads and incubated 1 h at 4°C on a rotation wheel. The beads were washed once with 1 ml fusion buffer and resuspended in 80 µl fusion buffer. The bound liposomes were detected by measuring the Atto647N fluorescence. The amounts of liposomes specifically bound to the different GST-SNAP25 constructs were calculated by subtracting the values derived from the GST controls.

I would like to thank Kerstin M. Rink and Thomas H. Söllner for the collaboration and help with the liposome binding studies.

5. Results

5.1 Analysis of the polybasic cluster-dependent membrane targeting

The first aim of this study is to identify a possible role for the polybasic cluster, a small accumulation of positive charges, located in the linker region of SNAP25, which may work as an electrostatic anchor for SNAP25 membrane targeting.

After considering the conserved amino acid sequence of the linker region of SNAP25 across different species, several different lysine residues are mutated to eradicate or partially eradicate the polybasic cluster. Furthermore several different protein mutagenesis are introduced to decrease or increase the net charge around the cysteine-rich region. The SNAP25 constructs are all tagged with GFP and expressed in PC12 cells, a cell line derived from a pheochromozytoma of the rat adrenal medulla and used for neurobiological studies. The different SNAP25 constructs are analyzed upon their membranous and cellular localization via confocal laser scanning microscopy.

5.1.1 Characterization of the CRR of SNAP25 in different species

As a starting point for the characterization of the targeting region of SNAP25, an evaluation of the highly conserved CRR of SNAP25 was conducted across different species. A closer look at the linker region of SNAP25 shows a highly conserved sequence of amino acids and an overall surplus of three positive charges in the delimited area of the CRR which is preserved across many different species (Figure 20).

Therefore the overall positive net charge in the CRR is not only found in SNAP25B from *Rattus norvegicus* (rat), which is the main subject of this study. The same net charge is also found in its isoform SNAP25A which has one out of the four cysteines in a different position. Other mammals like *Mus musculus* (mouse) and *Bos taurus* (bovine) and

higher mammals like *Macaca mulatta* (rhesus macaque), *Pongo abelii* (Sumatran orangutan), *Pan troglodytes* (chimpanzee) and *Homo sapiens* (human) show without exception a highly conserved CRR with a surplus of three positive charges. In addition the same level of similarity and the overall net charge is also conserved for *Gallus gallus* (chicken). This conserved net charge is formed by eight positive charges stemming solely from lysine residues and five negative charges from two glutamic acid and three aspartic acid residues. The ubiquitously expressed isoform SNAP25A from *Rattus norvegicus* (see Figure 20; P60881-2) shows a slightly altered amino acid sequence with a different position for one of the lysines, but the overall net charge remains the same.

A high similarity is also found in different fish species, but here the isoform SNAP25A carries a surplus of three charges, whereas SNAP25B has a surplus of one positive charge. An exception to the so far overall positive net charge of the CRR can be found in the less conserved sequence of *Drosophila melanogaster* (common fruit fly) with an overall negative net charge of -2 (see Figure 20;P36975).

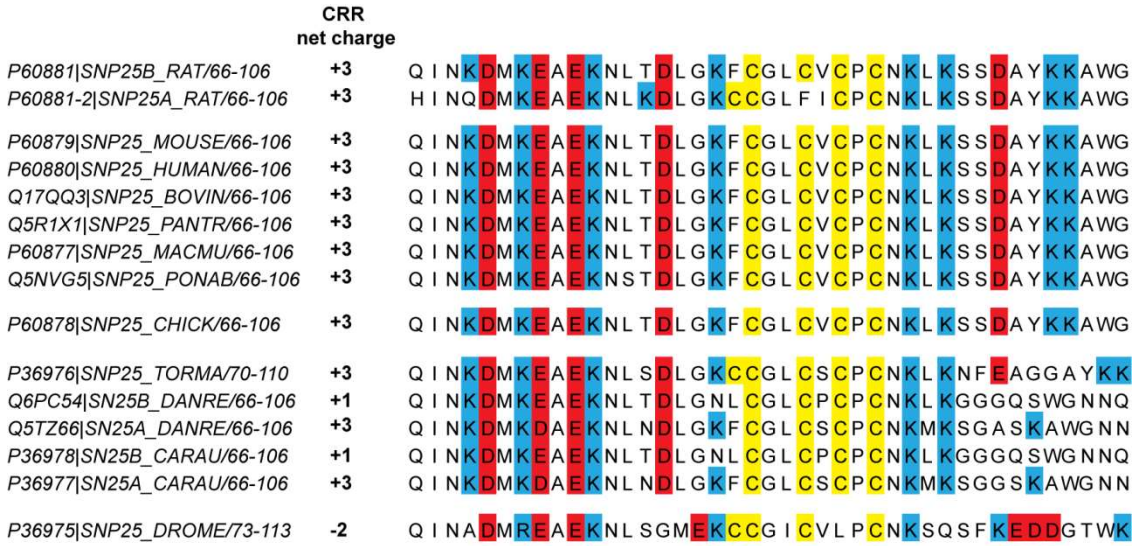

Figure 20: Conserved cysteine-rich region of SNAP25
Overview of the amino acid sequence variants for the SNAP25 gene from different species and, where available, the isoforms as found in the UniProtKB/*Swiss*-Prot-data bank with their respective entry identifiers (e.g. P60881 for SNAP25B). Depicted is a region ranging from amino acids 66 to 106 and, for a better comparison in the case of *Drosophila melanogaster,* a range between amino acids 73 to 113. The Species include *Rattus norvegicus* (RAT), *Mus musculus* (MOUSE), *Homo sapiens* (HUMAN), *Bos taurus* (BOVIN), *Pan troglodytes* (PANTR), *Macaca mulatta* (MACMU), *Pongo abelii* (PONAB), *Gallus gallus* (CHICK), *Torpedo marmorata* (TORMA), *Danio rerio* (DANRE), *Carassius auratus* (CARAU), and *Drosophila melanogaster* (DROME). Alignments were prepared with Clustal Omega Version 1.2.2 (Sievers et al., 2011) and colorized as follows: Cysteines are depicted in yellow, amino acids with positively charged residues in blue and negatively charged residues in red. The overall net charge for the CRR is shown for each gene variant. Though also found in the UniProtKB/*Swiss*-Prot-data bank, a fragment of rabbit SNAP25 lacking a cysteine-rich region is not included (Weber et al., 2017).

In conclusion all eight lysines responsible for the positive charges present in the CRR are highly conserved and serve as a possible target for mutagenesis.

5.1.2 Basic lysine residues in the CRR are crucial for efficient SNAP25 membrane targeting

In order to characterize the possible role of the positive charges present in the CRR several mutant constructs of rat SNAP25B containing a series of different mutations were generated and all constructs have a fluorescent monomeric GFP-tag at the N-terminus to visualize the subcellular distribution in living cells (Figure 21a).

At first, to test whether a disruption of the whole cluster of positive charges in the CRR would be crucial to membrane targeting, a construct was designed in which all eight lysines (K69, K72, K76, K83, K94, K96, K102 and K103) found in the CRR were substituted by alanines. Thus the resulting mutant SNAP25 has no lysines left in the CRR and a possible electrostatic interaction with negatively charged lipids in the plasma membrane is prevented. The overall net charge for SNAP25 in the CRR was thereby converted from a positive surplus (+3) in the wildtype SNAP25 (wt-SNAP25 *(+3)*) to an accumulation of negative charges. Since the overall negative charge excess is -5, the mutant construct was therefore termed SNAP25-*5* (Figure 21b).

To investigate the subcellular distribution of SNAP25-*5* in comparison to wildtype SNAP25, equatorial optical cross-sections of transfected neuroendocrine PC12 cells were imaged at a CLSM. A linescan analysis (see red box; Figure 21c) reflects the distribution of SNAP25 across the cell's profile and reveals a clear increased concentration at the plasma membrane compared to the cytosol for wt-SNAP25 *(+3)*. Comparing SNAP25-*5* with wt-SNAP25 *(+3)* shows the lack of the previously predominantly membrane-localized SNAP25 and hence a chiefly cytosolic distribution (Figure 21d).

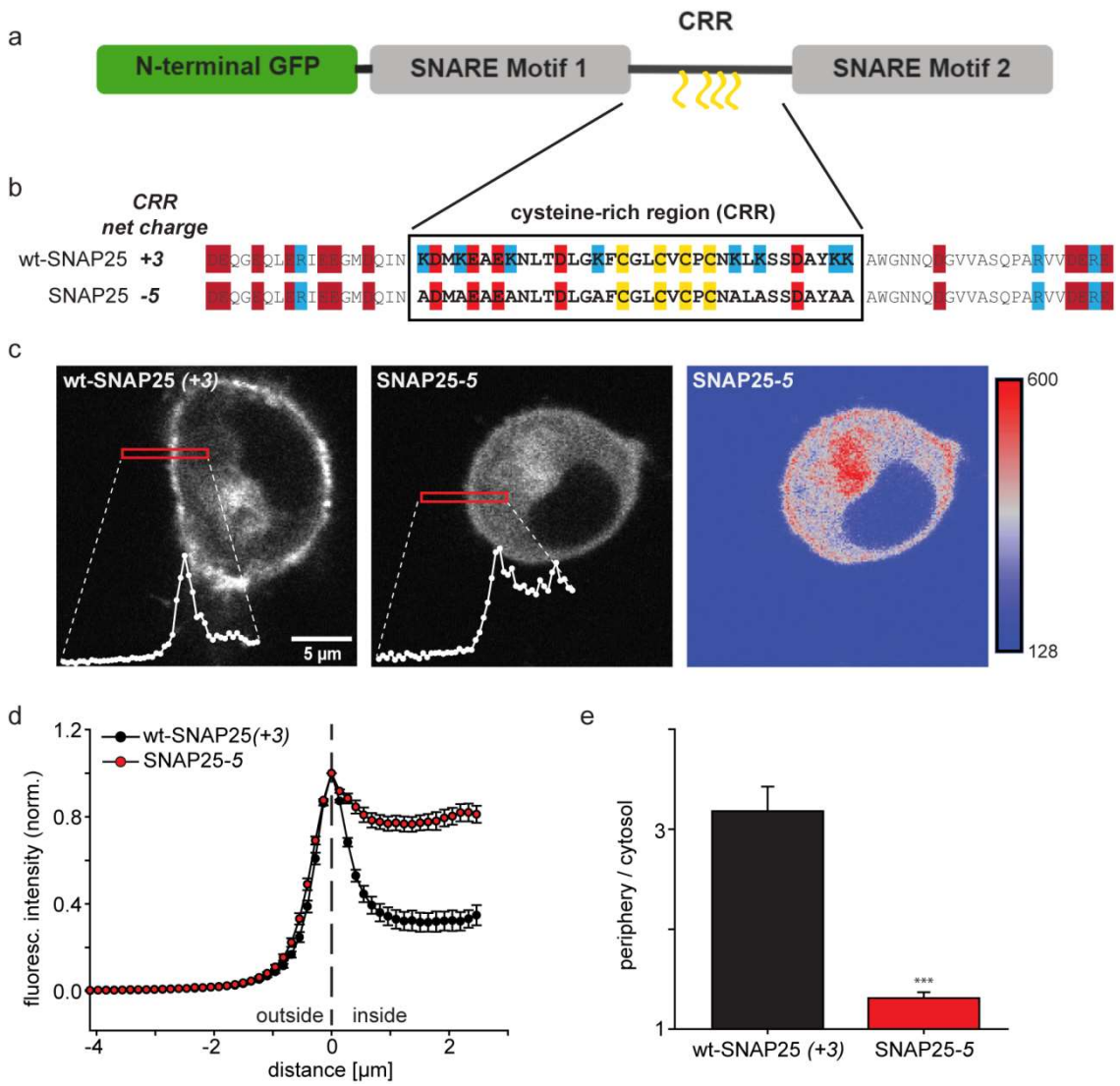

Figure 21: SNAP25 membrane targeting dependent on the polybasic cluster of the CRR

(a) SNAP25 was tagged with a monomeric variant of mEGFP fused N-terminally to the sequence of full-length rat SNAP25B. All fusion proteins contain a bridge of five amino acids between mEGFP and the N-terminus of SNAP25. The linker region of SNAP25B contains the CRR where the protein is palmitoylated (yellow chains). **(b)** Comparison of the amino acid sequence from position 51 to 125 for wt-SNAP25 *(+3)* and a construct with a decreased (SNAP25-*5*) net charge of the CRR (box). Cysteines (yellow) and amino acids with negatively charged (red) or positively charged (blue) side chains are colorized accordingly. (**c)** Confocal micrographs from live PC12 cells 48 hours after transfection, expressing wt-SNAP25 *(+3)* (left), SNAP25-*5* (middle) and a pseudo-colored image (with indicated arbitrary units) of SNAP25-*5* (right) for better visualization of the SNAP25

concentration at the membrane. Red elongated boxes mark the regions of interest (ROIs) in which the fluorescence distribution at the cell periphery was analysed by linescans. White graphs illustrate the corresponding fluorescence intensity traces for the respective cell. **(d)** The intensity traces were normalized to the membrane (dashed middle line) and averaged (n=16-40 ± s.e.m.) for wt-SNAP25 *(+3)* (black circles) and SNAP25-*5* (red circles). **(e)** Ratios of periphery and cytosol were averaged from several days (n=6 ± s.e.m.; t-test *p<0.05, **p<0.01, ***p<0.001) (modified from Weber et al., 2017).

Although the SNAP25-*5* construct shows a mainly cytosolic distribution, SNAP25 is not completely absent from the plasma membrane as a small fraction is still present in the periphery (Figure 21c; right panel). SNAP25-*5* is also still located in the perinuclear recycling endosome-trans-Golgi network, which is usually observed for wildtype SNAP25 (Aikawa et al., 2006).

For further quantification and since the expression levels of SNAP25 vary between cells the cytosol to periphery ratio is considered, which indicates the presence of a higher plasma membrane concentration in comparison to the inner cell for values above one. The periphery of the cell is representing mostly, but due to technical resolution not solely, membrane fluorescence. The cytosol / periphery ratios obtain a value very close to 1 if there is absolutely no increased concentration of fluorescence present at the membrane. The calculated average cytosol / periphery ratios confirm the observations from the linescans and show for the SNAP25-*5* construct a decreased average ratio of 1.31 compared to 3.15 for wt-SNAP25 *(+3)* (Figure 21e). This difference in the membrane association is observed 48 h after transfection but a trend already seems to start to develop directly after gene expression.

Two to four hours after transfection for both wt-SNAP25 *(+3)* and SNAP25-*5* a predominantly cytosolic expression is observed (**Figure** 22a). However, a more pronounced increase in membrane association can already be seen for wt-SNAP25 *(+3)* at this early stage when compared to SNAP25-*5* as the periphery to cytosol ratios are

1.81 for wt-SNAP25 *(+3)* and 1.25 for SNAP25-*5* (**Figure** 22c). The periphery to cytosol ratios show high variations in this early stage but nonetheless the basic trend indicates that the association of wt-SNAP25 *(+3)* is a process and an increased SNAP25 concentration at the plasma membrane develops over time. In contrast the targeting for SNAP25-*5* is hindered and only a very small increase in membrane-bound SNAP25 can be observed for a shorter time span after the start of gene expression.

In conclusion, the lysines forming the polybasic cluster present in the CRR are indeed crucial for efficient targeting of SNAP25 to the plasma membrane. Despite the lack of the electrostatic anchoring through the small positively charged cluster, a comparatively small amount of SNAP25 can still bind to the plasma membrane, which likely represents the still functional anchoring by palmitoylation.

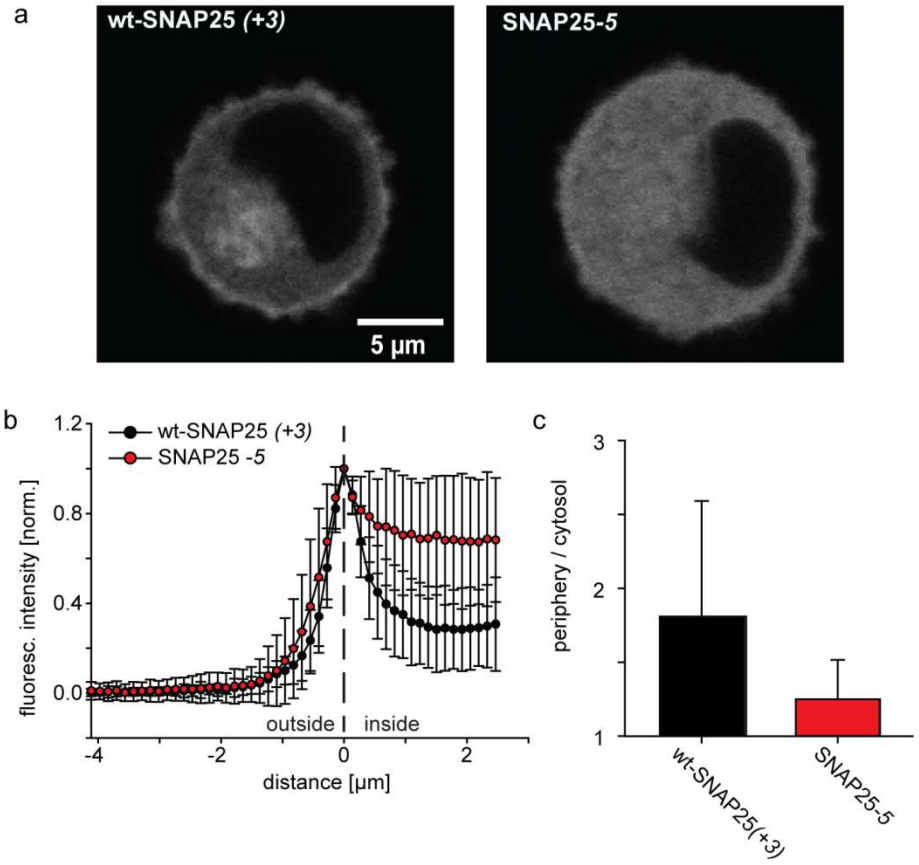

Figure 22: SNAP25 plasma membrane targeting 2-4 h after transfection
(a) Confocal micrographs from live PC12 cells expressing wt-SNAP25 *(+3)* (left) and SNAP25-*5* (right) two to four hours after transfection. **(b)** Intensity traces of individual cells were normalized to the membrane and averages (n=33-36 ± s.e.m.) for wt-SNAP25 *(+3)* (black circles) and SNAP25-*5* (red circles) are shown. **(c)** Ratios of periphery and cytosol were averaged from individual cells (n= 33-36 ± s.e.m).

If indeed the lack of electrostatic interactions of the lysines with the plasma membrane is responsible for the diminished membrane targeting, a reduced effect should be observed when only deleting a part of the polybasic cluster. Also a possible influence on the palmitoylation status of the cysteines located proximal to the lysines might be observed. Therefore and to further test whether the proximity of the lysines to the cysteines is crucial for the termination of membrane localization, two additional constructs were designed in order to reduce the amount of replaced lysines. The

construct termed SNAP25-*1 proximal* with the four lysines closest to the cysteins substituted is compared to a construct (SNAP25-*1 distal*) with substituted lysines further away from the cysteins (Figure 23).

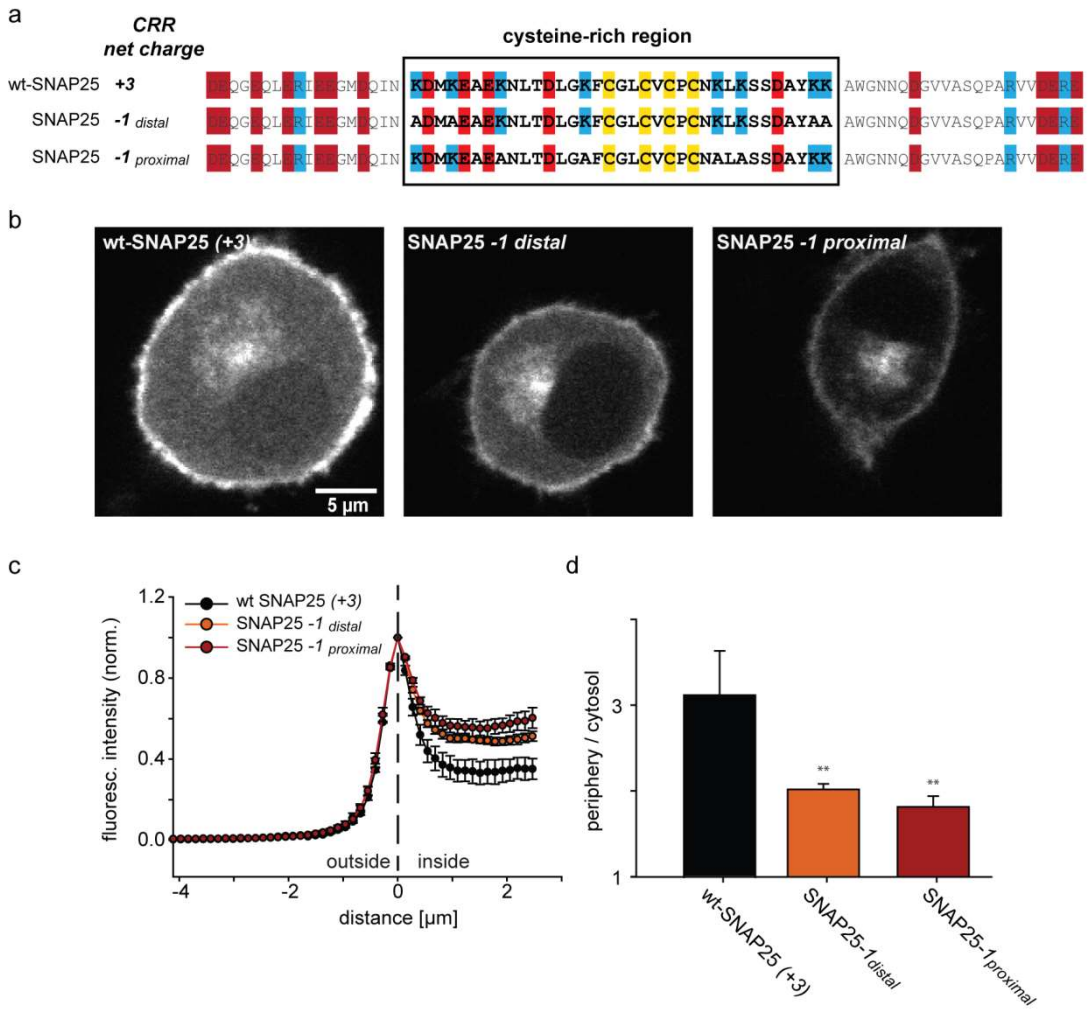

Figure 23: Disruption of the SNAP25 plasma membrane targeting for distal and proximal lysine substitutions

(a) Amino acid sequence of two constructs in which four different lysine residues were removed, proximal (K76A, K83A, K94A and K96A) or distal (K69A, K72A, K102A and K103A) of the cysteine cluster, as well as wt-SNAP25 *(+3)* for reference. **(b)** Confocal micrographs of the respective constructs from live PC12 cells.

(c) Intensity traces of cells (n=21-31) were normalized and values are given as mean ± s.e.m. **(d)** Periphery / cytosol ratios are averaged from several days (mean ± s.e.m.; n=3; t-test *p<0.05, **p<0.01, ***p<0.001) (modified from Weber et al., 2017).

The overall effect of reduced membrane targeting, as seen for SNAP25-*5,* seems to be less prominent for both SNAP25 -*1 distal* and SNAP25-*1 proximal*, when only four of the eight available lysines are exchanged (Figure 23b/c). This is already clearly visible for both mutant phenotypes since a membrane fraction is easily visible in comparison to the phenotype of the SNAP25-*5* mutant. The periphery / cytosol ratio shows for wt-SNAP25 *(+3)*, a ratio of 3.12 which is consistent with the value previously observed. For SNAP25-*1 distal* the ratio is 2.02 and for SNAP25-*1 proximal* the ratio is slightly further reduced to 1.81 (Figure 23d). However a student's t-test shows no significant difference between these two constructs. So a difference in proximity of the deleted charges to the palmitoylation sites leads to no clear difference in the effect of diminished membrane association.

In conclusion this observation fits an underlying electrostatic anchoring mechanism rather than a direct influence of the deleted lysines on the palmitoylation itself. In addition a correlation can be seen between the amount of reduced positive charges and the effect on the membrane localization, as it is considerably less prominent with only four of the eight replaced lysines.

5.1.3 Decreased membrane targeting of SNAP25 by substitution of negatively charged residues in the linker region

To clarify if the acidic neighbors of the lysines might play an equally important role for membrane targeting and in order to further test if indeed solely electrostatic forces are the dominant factor behind the crucial lysine cluster, mutations were implemented aiming for an increase in the overall net charge of the CRR.

At first a construct termed SNAP25+*7* was tested which contains substitutions of the negatively charged amino acids Asp70, Glu73, Glu75 and Asp80 with alanine, resulting in an excess of seven positive charges in the CRR (Figure 24a).

This higher net charge however was not accompanied by an increase in plasma membrane targeting efficiency (Figure 24b;c), but shows even a reduced binding to the plasma membrane as the periphery / cytosol ratio is reduced to 1.89 (Figure 24d).

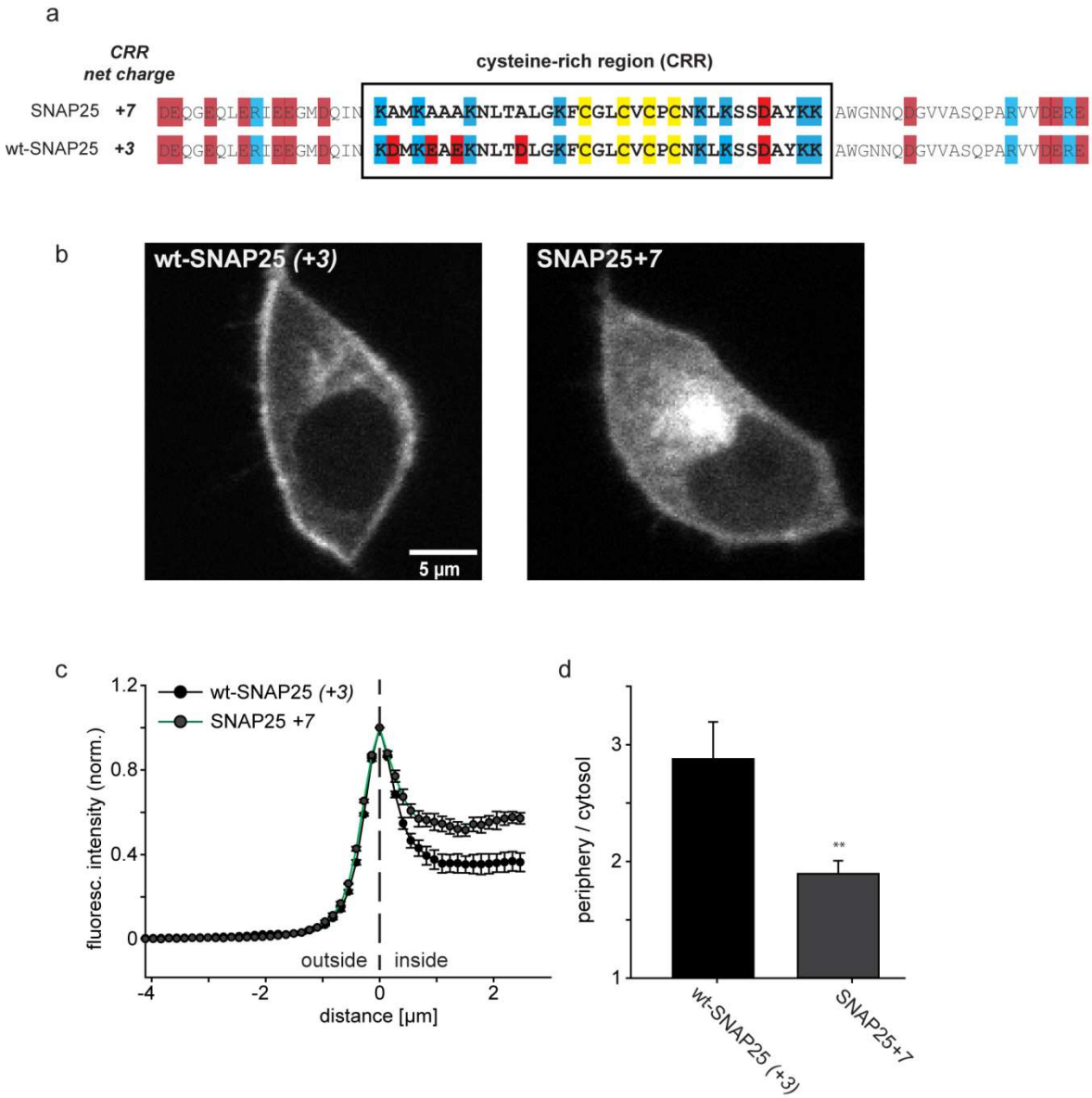

Figure 24: Decreased plasma membrane targeting of SNAP25+*7*

(a) Comparison of the CRR for wt-SNAP25 *(+3)* and SNAP25+*7*, in which negatively charged amino acids Asp70, Glu73, Glu75 and Asp80 are replaced by alanine. **(b)** Confocal micrographs from live PC12 cells expressing wt-SNAP25 *(+3)* and SNAP25+*7*. **(c)** Intensity traces of cells (n=23-31) were normalized and values are given as mean ± s.e.m. **(d)** Periphery / cytosol ratios are given as mean ± s.e.m. (n=3; t-test *p<0.05, **p<0.01, ***p<0.001) (modified from Weber et al., 2017).

5.1.4 Increased membrane targeting of SNAP25 by introduction of additional lysines in the linker region

Since the SNAP25+*7* mutant did not show an increase in membrane localization the next step was to further increase the overall positive net charge. In addition some of the positions where mutations were introduced in the CRR were changed.

Therefore another construct termed SNAP25+*10* was designed in which two of the previously mutated negatively charged amino acids (Glu73, Asp80), in addition to one different negatively charged (Asp99) and one neutral amino acid (Asn77) are replaced by lysines. Here the additional lysines present in the CRR indeed help and promote the targeting efficiency of SNAP25, with a further increased net charge resulting in a higher periphery / cytosol ratio of 4.64 in comparison to wt-SNAP25(+*3*) (Figure 25).

In conclusion the removal of positive charges is always accompanied by diminished targeting, while an increase of positive charges can lead to an increase (Figure 25) but also a decrease (Figure 24) in membrane targeting.

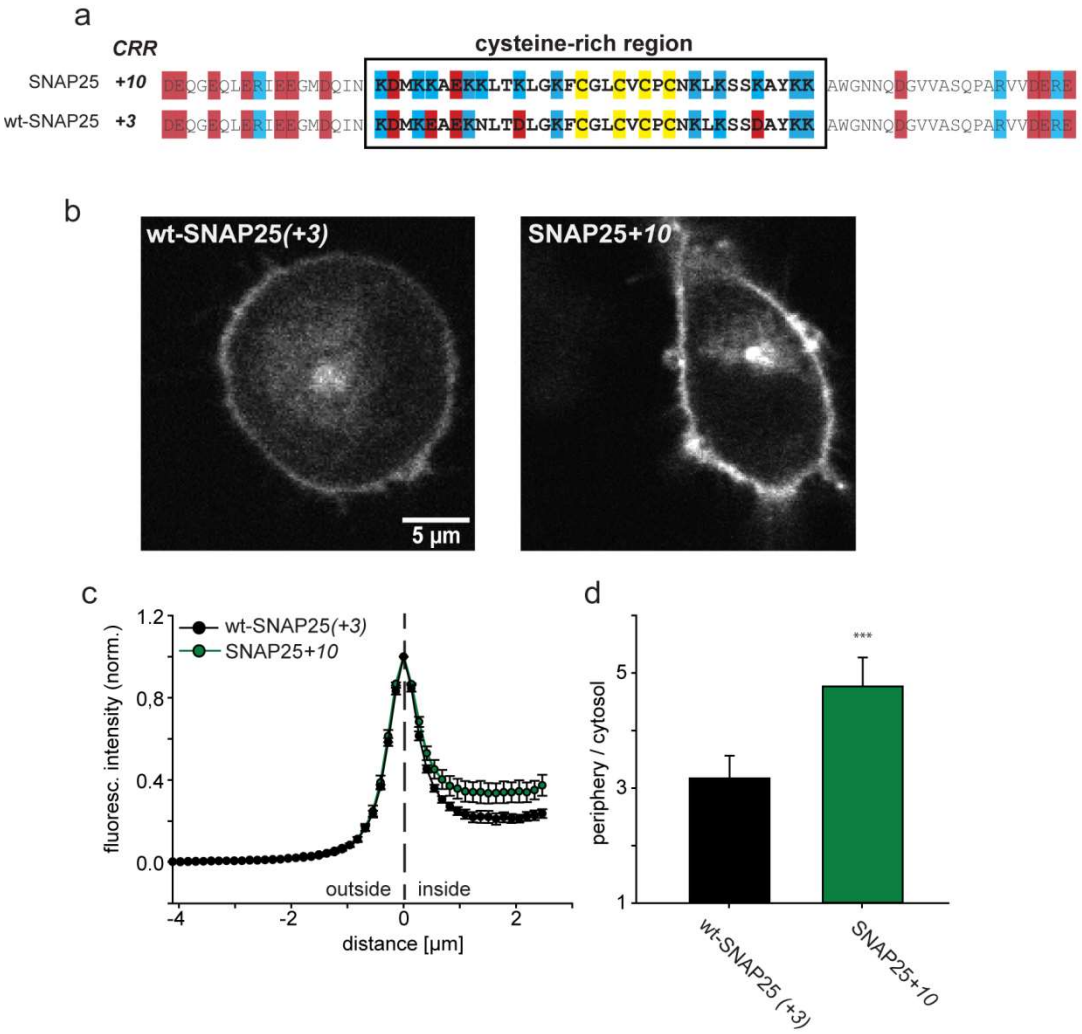

Figure 25: Increased plasma membrane targeting of SNAP25+*10*

(a) Comparison of the cysteine rich region for wt-SNAP25 *(+3)* and SNAP25+*10*, which has four additional lysines (E73K, N77K, D80K, D99K) added into the CRR. **(b)** Confocal micrographs from live PC12 cells expressing wt-SNAP25 *(+3)* and SNAP25+*10*. **(c)** Intensity traces of cells (n=15-36) were normalized and values are given as mean ± s.e.m. **(d)** Periphery / cytosol ratios are given as mean ± s.e.m. (n=6; t-test *p<0.05, **p<0.01, ***p<0.001) (modified from Weber et al., 2017).

Since the SNAP25+*10* mutant construct further increases the amount of bound SNAP25 at the plasma membrane, it could be possible, especially at higher expression levels, that the membrane localization reaches a limit due to saturation of the plasma membrane.

To exclude that higher expression levels might cause a saturation of membrane binding, the fluorescence peak intensity values were plotted versus the periphery / cytosol ratios of individual cells for the SNAP25-*5* and SNAP25+*10* constructs in comparison to wt-SNAP25 *(+3)* (**Figure** 26).

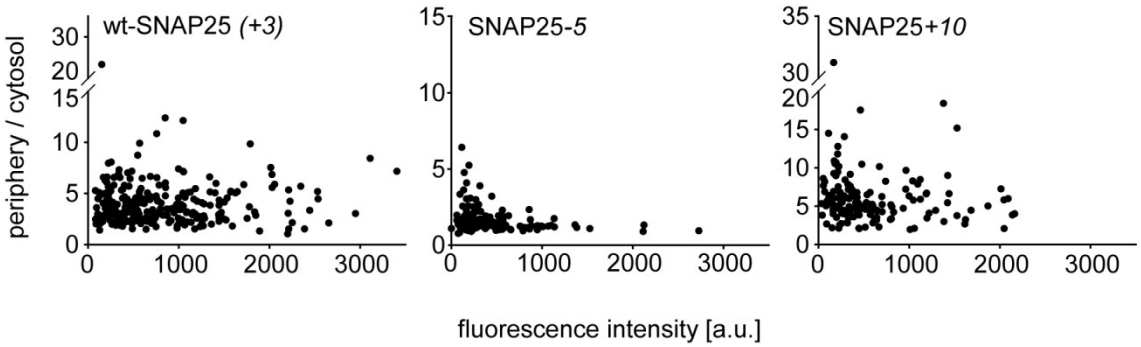

Figure 26: Periphery / cytosol ratio versus fluorescence peak intensity
Scatter plot from individual cells the periphery / cytosol-ratio is plotted versus the fluorescence peak intensity values for wt-SNAP25 *(+3)* (n=259), SNAP25-*5* (n=146) and SNAP25+*10* (n=149). The data for each construct is pooled from all available experiments. Note the different scaling of the individual scatter plots for each construct and the interrupted y-axes for better visibility of the individual data points (Weber et al., 2017).

There is no decrease of the periphery / cytosol ratio with increased fluorescence intensities; therefore a saturation of the plasma membrane is not observed.

5.1.5 Increased hydrophobicity decreases membrane targeting of SNAP25 construct

As described in the introduction, previous studies report a possible role for hydrophobic domains on initial membrane association (Greaves et al., 2009). The difference in retention times in comparison to glycine, determined on reversed phase columns, can be taken as a measurement for hydrophobicity (Monera et al., 1995). Lysines have a retention time (Δt_R) relative to glycine ($\Delta t_R = 0$) of $\Delta t_R = -23$ whereas the hydrophobic phenylalanine has a Δt_R of 100.

To answer the question if replacing the lysine residues with highly hydrophobic residues would preserve membrane targeting, a construct termed SNAP25-$5_{hydrophob}$ was designed in which the eight lysines of the CRR were not replaced by alanines but instead by even more hydrophobic leucines. Leucines are strongly hydrophobic with a Δt_R of 97.

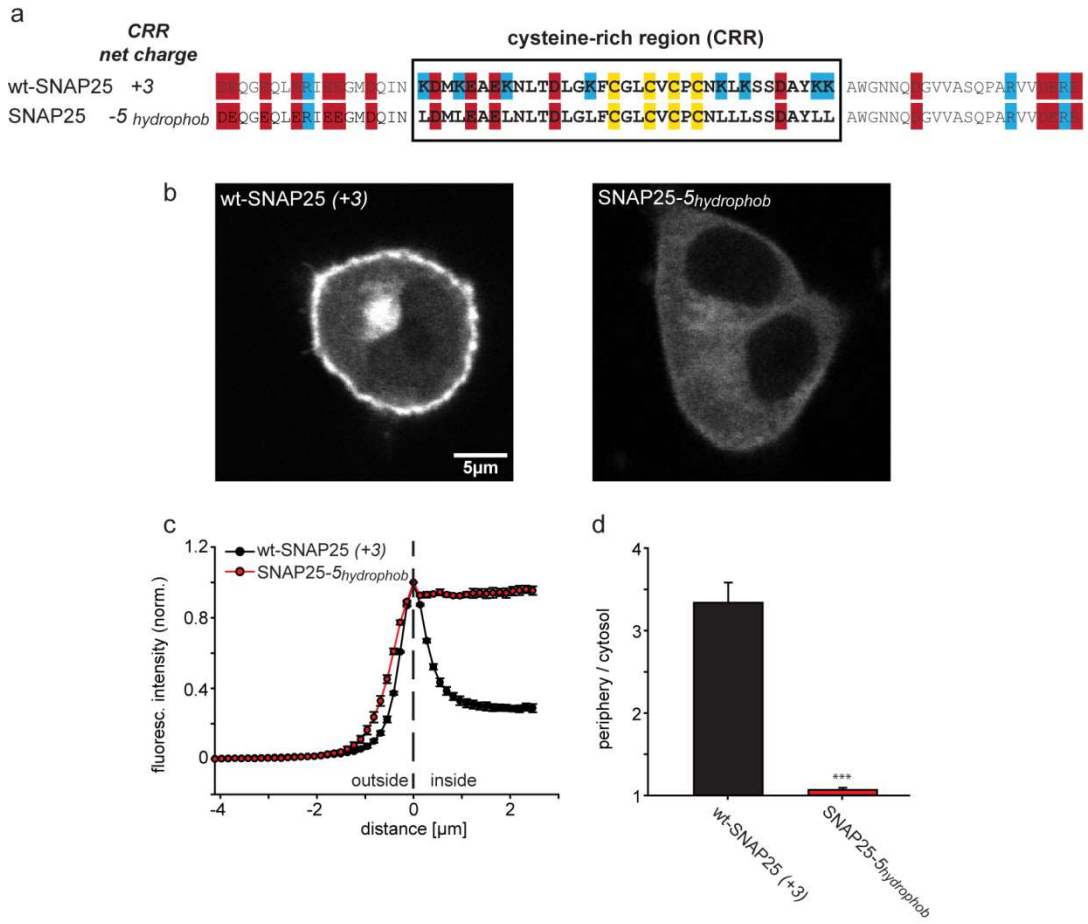

Figure 27: SNAP25 membrane targeting further reduced by replacing lysines with hydrophobic leucines

(a) Comparison of the CRR of wt-SNAP25 *(+3)* and SNAP25-$5_{hydrophob}$, in which all eight lysines (K; marked blue) present in the CRR were replaced by leucines (L). **(b)** Confocal micrographs from live PC12 cells expressing wt-SNAP25 *(+3)* and SNAP25–$5_{hydrophob}$. **(c)** Intensity traces of Cells (n=30-34) were normalized and values are given as mean ± s.e.m. **(d)** Periphery / cytosol ratios are averaged from several days and given as mean ± s.e.m. (n=3; t-test *p<0.05, **p<0.01, ***p<0.001) (modified from Weber et al., 2017).

The replacement with more hydrophobic leucines results in a crucial loss of targeting and the membrane fraction was hardly visible (Figure 27). The periphery / cytosol ratios are 3.34 for wt-SNAP25 *(+3)* and 1.07 for SNAP25-$5_{hydrophob}$, which is reduced, in comparison with SNAP25-*5,* even further. The data suggests that the increased hydrophobicity within the SNAP25-$5_{hydrophob}$ cannot target the protein to the membrane

independent of electrostatic anchoring and the positively charged lysines remain critical for efficient membrane targeting.

5.1.6 SNAP25 plasma membrane targeting is independent of c-terminal positive charges

Another smaller polybasic cluster of positively charged amino acids is located at the c-terminal part of SNAP25 and may also contribute to plasma membrane localization. To clarify whether this charge accumulation far from the CRR is necessary for initial binding, another construct with mutations in the c-terminal part of SNAP25 was investigated (Figure 28).

Elimination of these c-terminal charges by introducing the mutations R191A, R198A and K201A has no effect on membrane targeting as the periphery / cytosol ratios show no significant difference between wt-SNAP25(+3) with 3.4 and $SNAP25_{R191A/R198A/K201A}$ with 3.7 (Figure 28c). Although the overall net charge of the whole SNAP25 protein was reduced by 3 charges, no influence can be seen on the predominant localization at the plasma membrane.

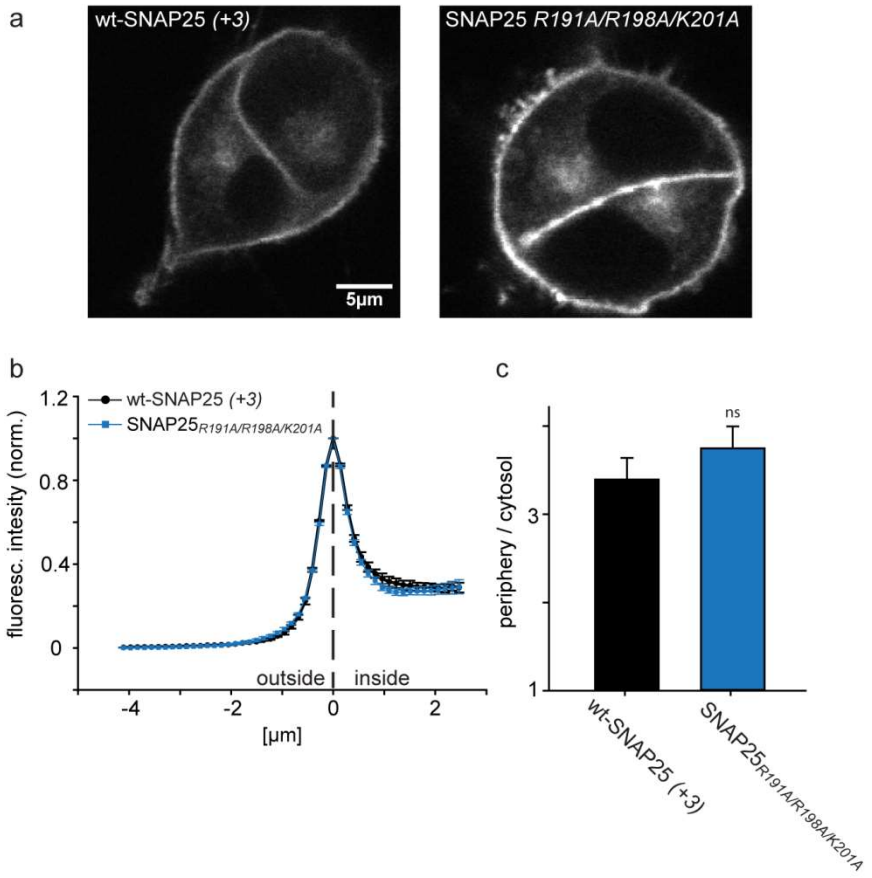

Figure 28: SNAP25 plasma membrane targeting independent of c-terminal positive charges

(a) Confocal micrographs from live PC12 cells expressing wt-SNAP25 *(+3)* (left) and SNAP25 *R191A/R198A/K201A* (right). **(b)** Intensity traces of individual cells were normalized to the membrane and averages (n=27-37 ± s.e.m.) for wt-SNAP25 *(+3)* (black circles) and SNAP25 *R191A/R198A/K201A* (blue circles) are shown. **(c)** Periphery / cytosol ratios from three experiments are given as mean ± s.e.m. (n=3; t-test *p<0.05, **p<0.01, ***p<0.001, ns = not significant) (modified from Weber et al., 2017).

5.1.7 Correlation between SNAP23 targeting and the net charge of the CRR

The ubiquitously expressed homologue SNAP23 also has a surplus of three positive charges in the otherwise only slightly altered CRR. As seen for SNAP25, confocal microscopy and linescan analysis show that an exchange of lysines and therefore the reduction of the positive charges reduce membrane association (Figure 29).

The periphery to cytosol ratio of 2.67 of wt-SNAP23 *(+3)* is lower when compared to wt-SNAP25 *(+3)*. The mutant construct lacking four lysines (SNAP23-*3*) has decreased membrane localization with a periphery to cytosol ratio of 1.86. A construct termed SNAP23+*10* and the construct SNAP23+*16* with the indicated increased overall net charge both promote membrane targeting. The increase of additional six positive charges is accompanied by a significant increase in membrane targeting. Two other constructs termed SNAP23+*11a* and SNAP23*11b* failed to increase the membrane targeting. Finally, as was the case for $SNAP25_{(C\text{-}to\text{-}G)}$ the $SNAP23_{(C\text{-}to\text{-}G)}$ construct showed a predominantly cytosolic phenotype.

In summary similar observations were made for SNAP23 and SNAP25. Therefore, a similar involvement of an electrostatic anchoring mechanism to the PM via the polybasic cluster of lysine residues can be concluded.

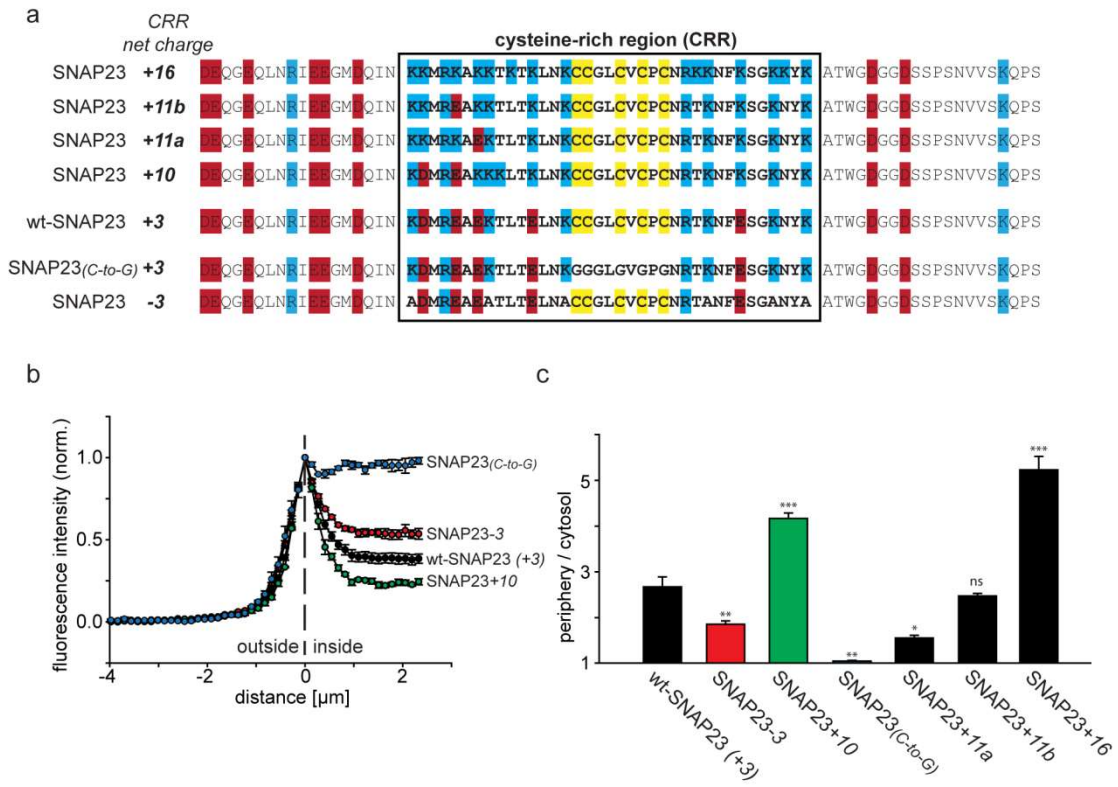

Figure 29: SNAP23 localization dependent on charge-distribution in the CRR

(a) Amino acid sequences of rat SNAP23 from position 45 to 119 for wt-SNAP23 *(+3)*, SNAP23$_{(C\text{-}to\text{-}G)}$ and several constructs carrying different charges in the CRR (from 64 to 100, box). The net charge in this region is given by the numbers associated with the constructs' names. Cysteines for palmitoylation are highlighted in yellow, negatively and positively charged amino acids in red and blue, respectively. **(b)** Intensity traces of cells (n=15-36) were normalized and values are given as mean ± s.e.m. **(c)** Periphery / cytosol-ratios for wt-SNAP23 *(+3)* and the SNAP23 mutants. Values are given as means ± s.e.m. (n = 3 – 8; t-test * p <0.05, ** p <0.01, *** p <0.001). I would like to thank Stefan Dahlhoff for his help with the experiments regarding SNAP23 constructs (modified from Weber et al., 2017).

5.2 Analysis of the palmitoylation-dependent membrane targeting

To confirm past reports showing that palmitoylation of the cysteine residues present in the CRR is crucial to anchoring SNAP25 to the plasma membrane, a mutant construct of SNAP25 was used. For this construct the four cysteins (C85, C88, C90 and C92) were substituted by glycine. In addition, the replacement of cysteine was also implemented in the SNAP25+*10* construct. The reason for this was to check for a conceivable rescue of its plasma membrane targeting with the help of its enhanced electrostatic potential, despite its lack of any possible anchoring by palmitoyl chains. Besides linescan analysis using microscopy, further analysis of a selection of the most relevant mutants included western blot analysis of cell fractions and microscopy of membrane sheets.

5.2.1 Cysteines critical for SNAP25 membrane targeting

Confocal microscopy shows a dominant cytosolic appearance for both the SNAP25$_{(C\text{-}to\text{-}G)}$ and the SNAP25+*10*$_{(C\text{-}to\text{-}G)}$ constructs (Figure 30b). A linescan analysis also reflects the dominant cytosolic fraction with no distinguishable membrane fraction (Figure 30c) and the periphery / cytosol ratios have a value of 1 (Figure 30d). Since the thickness of the membrane is only about 5 nm, which is not resolved by the confocal microscopy set up, the value obtained for the cell periphery is the sum of the membrane and cytosol signals. In the case of both SNAP25$_{(C\text{-}to\text{-}G)}$ and SNAP25+*10*$_{(C\text{-}to\text{-}G)}$ the dominant cytosolic fraction outshines any possibly existent membrane fraction and therefore results in a periphery / cytosol ratio of approximately 1.

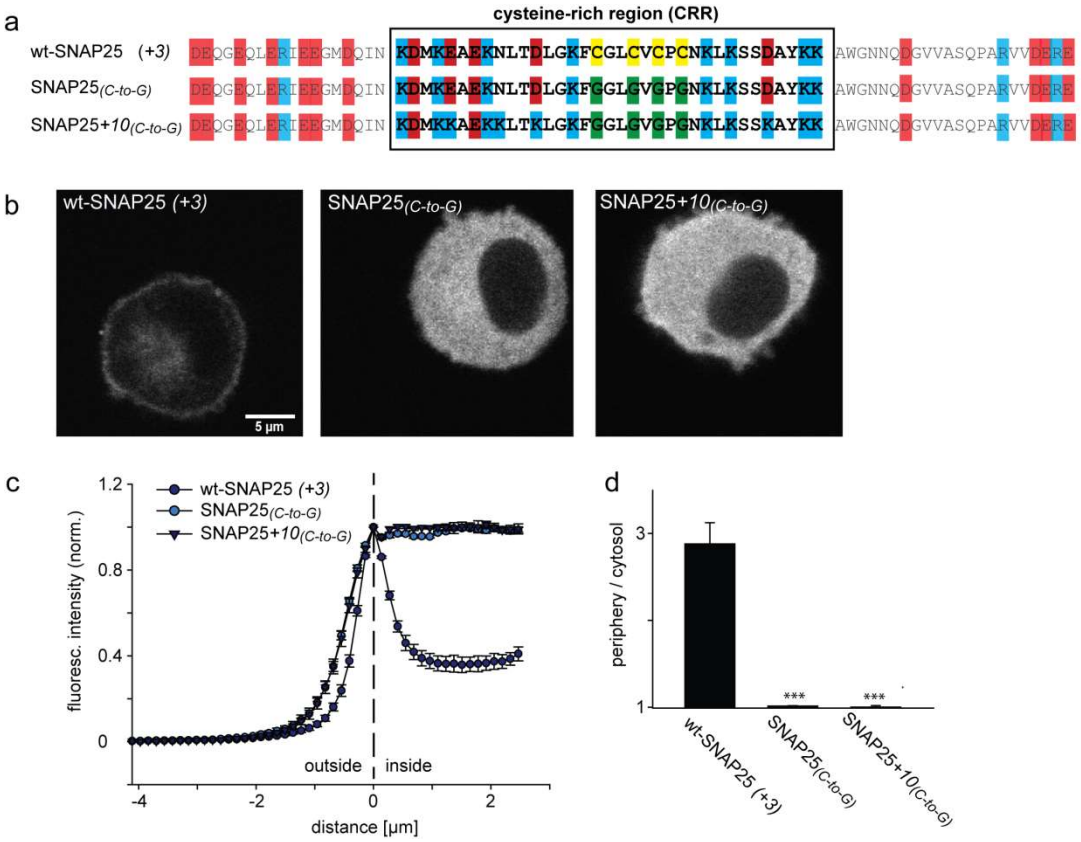

Figure 30: SNAP25 plasma membrane targeting is eliminated without a functional palmitoyl anchoring site

(a) The CRR for SNAP25$_{(C\text{-}to\text{-}G)}$ and SNAP25+*10*$_{(C\text{-}to\text{-}G)}$, for which the cysteins (C85, C88, C90, C92) were replaced by glycine (G). **(b)** Confocal micrographs of the respective constructs from live PC12 cells. **(c)** Intensity traces of cells (n=12-27) were normalized and values are given as mean ± s.e.m. **(d)** Periphery / cytosol ratios are given as mean ± s.e.m. (n=6; t-test *p<0.05, **p<0.01, ***p<0.001) (modified after Weber et al., 2017).

In conclusion the results confirm the crucial importance of the palmitoylation of SNAP25 for its proper plasma membrane localization.

5.2.2 Subcellular distribution of SNAP25 constructs analysed by cell fractionation and microscopy of membrane sheets

Since the linescan analysis applied in confocal microscopy cannot distinguish a membrane associated fraction when the cytosolic fraction is very dominant, an additional method was used in order to be able to relate absolute values from both membranous and cytosolic SNAP25. To reveal a possible existence of a membrane-associated SNAP25 fraction, both SNAP25$_{(C\text{-}to\text{-}G)}$ and SNAP25+*10*$_{(C\text{-}to\text{-}G)}$ constructs were analysed by subcellular fractionation using western blot. Additionally the most prominent mutants (SNAP25-*5* and SNAP25+*10*) and wt-SNAP25 *(+3)* were included in the analysis to further support the results of the preceding linescans.

Therefore a subcellular fractionation assay was applied to transfected cells enabling the separation of the cytosolic and membrane fractions of cell lysates by centrifugation. The lysates were analysed via western blot (Figure 31a) using antibodies against the GFP tag, membrane and cytosolic fractions were calculated in a similar way to the periphery / cytosol ratios in linescans.

The trends of decreased membrane targeting for SNAP25-*5* and an increased membrane fraction for SNAP25+*10* were again shown by the respective membrane / cytosol ratios of the western blot analysis (Figure 31b). While the overall expression levels were very variable between different experiments (Figure 31c), the principal outcome of the linescan analysis was confirmed. For SNAP25$_{(C\text{-}to\text{-}G)}$, no significant membrane-associated fraction was detectable in the western blot analysis. In contrast, the SNAP25+*10*$_{(C\text{-}to\text{-}G)}$ mutant indeed showed a small membranous fraction, possibly reflecting the underlying increased electrostatic potential.

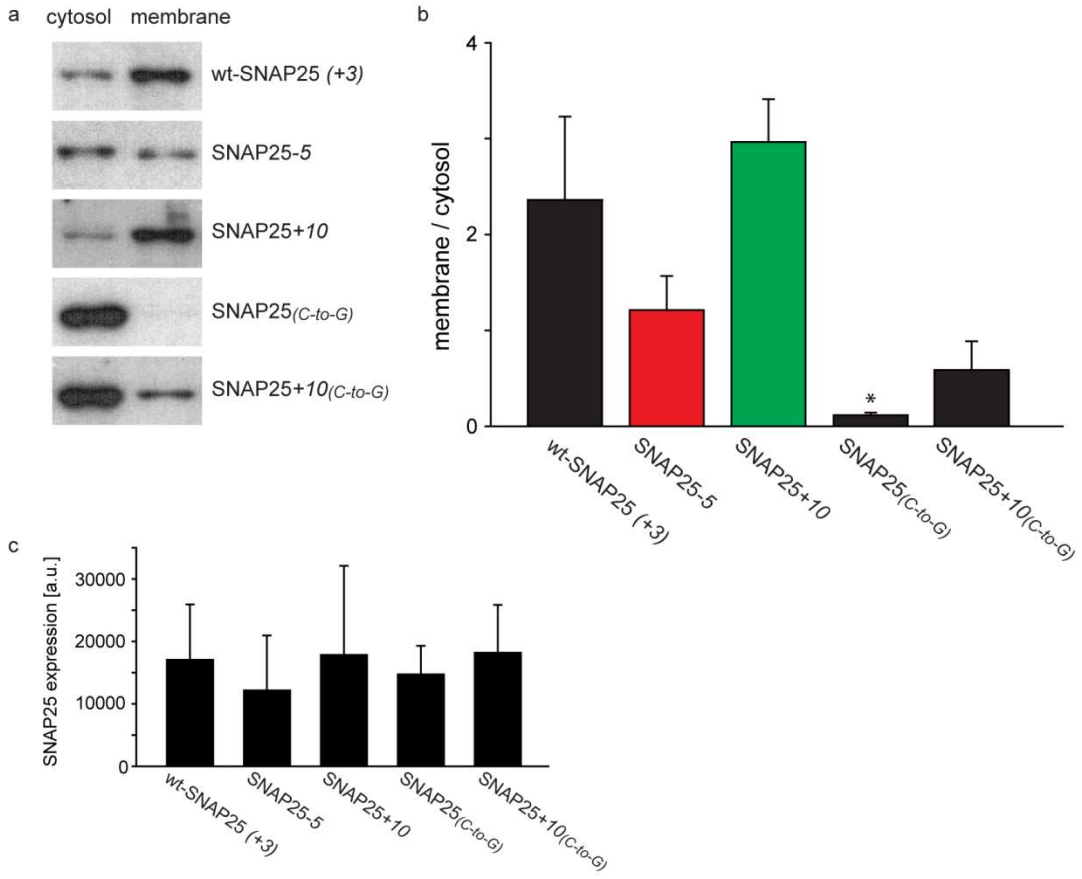

Figure 31: Cell fractionation analysis of SNAP25 constructs

(a) Immunoblots of one representative experiment showing the respective cytosol and membrane fractions at arbitrary scaling for better visibility for each construct. PC12 cells were transfected with wt-SNAP25 *(+3)*, SNAP25-*5*, SNAP25+*10*, SNAP25$_{(C\text{-}to\text{-}G)}$ or SNAP25+*10*$_{(C\text{-}to\text{-}G)}$ and collected 48 h after transfection, followed by a mechanical homogenization. After centrifugation of the cell lysate a pellet and supernatant are collected that are enriched in membrane and cytosolic fraction, respectively. Using an antibody against GFP the respective fractions were analysed by western blotting. The entire blot is depicted in Supplementary Figure 1. **(b)** Membrane / cytosol ratios were quantified from the band intensities and are given as mean ± s.e.m. (n=4; t-test *p<0.05, **p<0.01, ***p<0.001) **(c)** The average expression levels for each construct. Values are given as means ± S.E.M. (n = 4; t-test * p <0.05, ** p <0.01, *** p <0.001) (modified after Weber et al., 2017).

A second method to help visualize the membrane-associated fraction of SNAP25 is the microscopy of membrane sheets. With the help of a short sonication pulse transfected cells were unroofed, leaving only the basal plasma membrane. These membrane sheets are completely void of any cytosolic SNAP25 and a comparison of the absolute membrane fractions between different mutant constructs is possible. Again, compared to wt-SNAP25 *(+3),* the mutant constructs SNAP25-*5* and SNAP25+*10* show a decreased or increased membrane targeting respectively (Figure 32).

For SNAP25$_{(C\text{-}to\text{-}G)}$ no GFP signal was detectable, indicating the requirement of palmitoylation for a stable membrane association of SNAP25. These results were confirmed by screening the membrane sheets for any SNAP25 expression, but none was found.

In the case of SNAP25+*10*$_{(C\text{-}to\text{-}G)}$ a small fraction of cells showed a signal reflecting the observed membranous fraction in the western blot analysis. It seems that the SNAP25+*10*$_{(C\text{-}to\text{-}G)}$ construct with its increased electrostatic potential may allow a stable enough electrostatic anchoring of SNAP25 to the plasma membrane without any palmitoyl chains present.

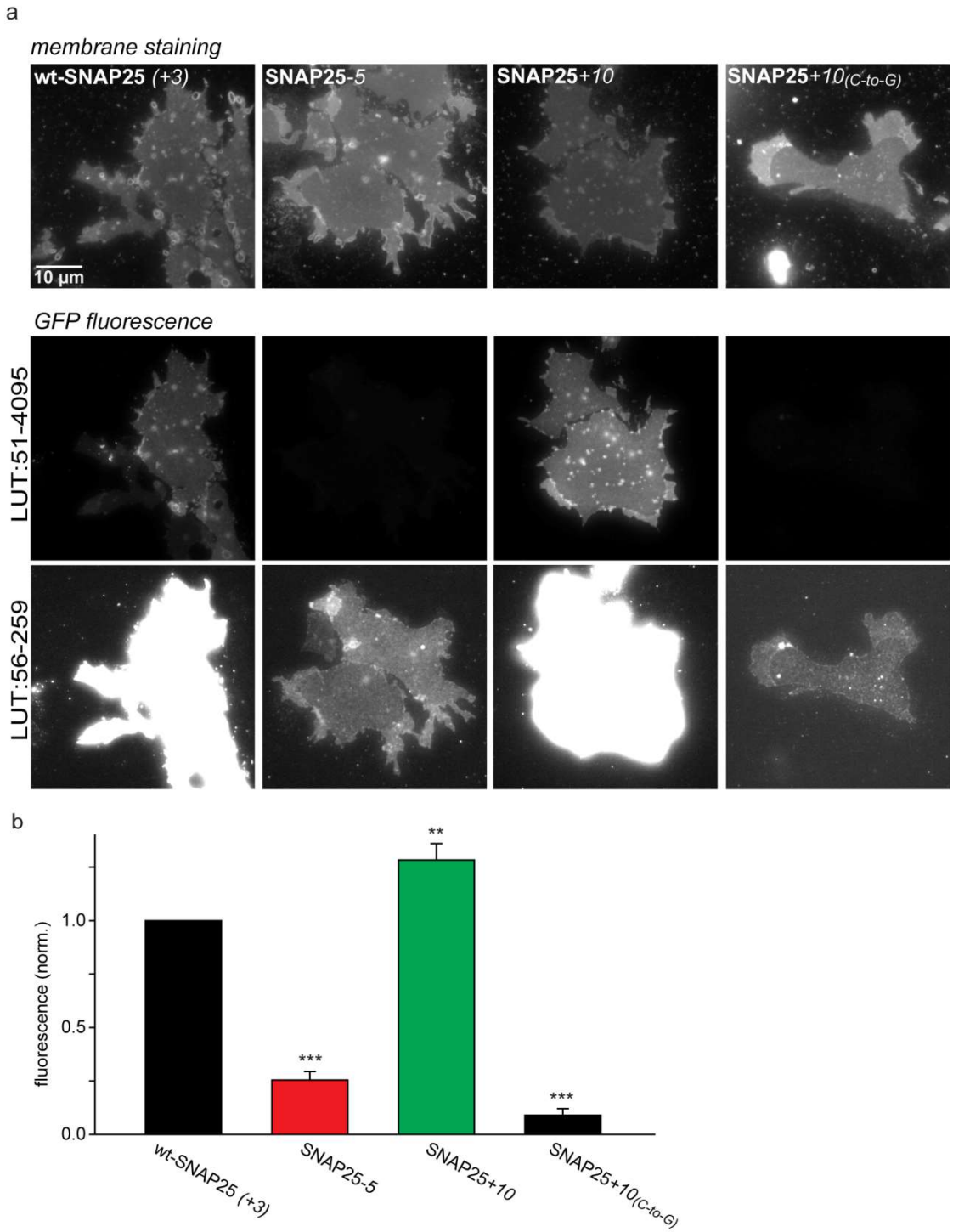

Figure 32: Quantification of SNAP25-GFP-fluorescence on membrane sheets
(a) From cells expressing the indicated GFP-SNAP25 constructs plasma membrane sheets were generated by mechanical shearing forces through a sonication pulse.

Directly after membrane sheet generation the samples were screened for green fluorescence and all membranes exhibiting green fluorescence were recorded in the green (GFP fluorescence) followed by the blue channel (TMA-DPH for membrane staining). $SNAP25_{(C\text{-}to\text{-}G)}$ (not shown) was also included in the experiment but showed no visually detectable green fluorescence during the screening process. The top panel shows fluorescence of TMA-DPH visualizing the membrane sheets. Bottom panels show the respective GFP-fluorescence for each construct with two different lookup tables (LUT) for better visibility of the lower fluorescence signals. **(b)** The quantification of the GFP-fluorescence of each construct were normalized to wt-SNAP25 *(+3)* and the values are given as means of individual days ± S.E.M. (n = 3 – 7; t-test * $p < 0.05$, ** $p < 0.01$, *** $p < 0.001$) (modified after Weber et al., 2017).

The analysis of the cell fractionation and the membrane sheets together show, even in the absence of any palmitoylation, that an artificial increase in positive net charge can result in an increased membrane association.

5.2.3 Assessment of SNAP25 palmitoylation

The palmitoylation status was examined to test whether the extent of membrane association observed for SNAP25+*10* and SNAP2-*5* correlates with the palmitoylation degree. A reduced membrane targeting of SNAP25-*5* should result in a reduced degree of palmitoylation. Including both constructs and as a negative control $SNAP25_{(C\text{-}to\text{-}G)}$, which has no palmitoylation sites, a comparison was made with the palmitoylation degree of wt-SNAP25 by click labeling of palmitate followed by western blot analysis.

PC12 cells were transfected and incubated over night with clickable palmitate which was taken up and metabolized by the cells. After cell lysis the constructs were immunoprecipitated via their GFP tag and the palmitate was labeled with a Cy5-fluorophore by click chemistry. Finally the western blot analysis allowed the visualization of both palmitate and the immunostained GFP tag of the respective SNAP25 construct (Figure 33). Relating the palmitate signal to the SNAP25 signal, the ratios correlate as expected with increased or decreased membrane association.

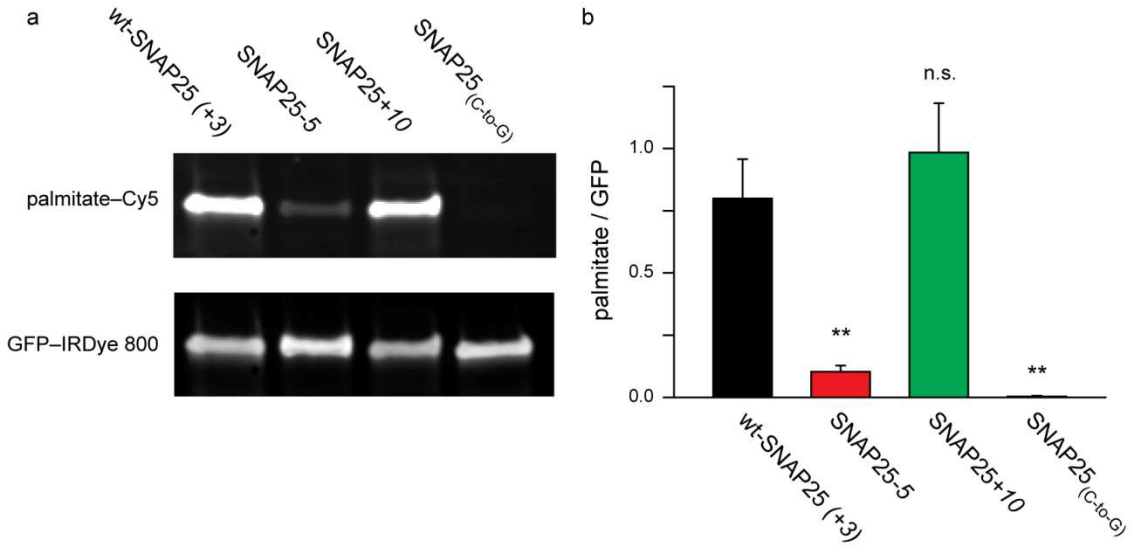

Figure 33: Palmitoylation of SNAP25-GFP constructs analysed by western blot.

(a) Representative immunoblot of the Cy5-labelled palmitate (top) and the IRDye 800-labelled, GFP-tagged SNAP25 constructs (bottom). After transfection with wt-SNAP25 *(+3)*, SNAP25-*5*, SNAP25+*10*, or $SNAP25_{(C\text{-}to\text{-}G)}$, PC12 cells were fed with alkyne-palmitate overnight. Cell lysation was followed by an immunoprecipitation of the GFP-tagged constructs. With the help of a click reaction the incorporated palmitate was labeled with Cy5-azide and the samples were subjected to SDS-PAGE and western blotting. **(b)** Palmitate/GFP ratios were quantified from the band intensities and are given as mean ± s.e.m. (n=5; t-test *p<0.05, **p<0.01, ***p<0.001, n.s. = not significant). Protein quantification by immunolabelling (anti-GFP antibody/IRDye-labelled secondary antibody) allowed a normalization of the palmitate-Cy5 signal, yielding the palmitate / GFP ratios (modified after Weber et al., 2017; I would like to thank Kerstin Pinkwart and Helena Batoulis for help with the palmitoylation assessment).

The negative control in the form of $SNAP25_{(CtoG)}$ indeed showed no detectable fluorescence for palmitate-Cy5. The decreased membrane association of SNAP25-*5* is accompanied by a reduced degree of palmitoylation and SNAP25+*10* showed only a slight trend towards a higher degree of palmitoylation. Since the difference between SNAP25+*10* and wt-SNAP25 *(+3)* palmitoylation is not significant, the data hints toward a possible anchoring solely by electrostatic interactions, in addition to the stable attachment of palmitoylated SNAP25+*10*.

5.3 Syntaxins interaction with mutated SNAP25

As mentioned in the introduction, it is reported that syntaxin could help SNAP25 in membrane association by binding to it and thereby guiding it to the plasma membrane (Vogel et al, 2000; Washbourne et al, 2001). The binding of GFP-tagged SNAP25 to Syntaxin 1A was probed with a FRAP experiment (Halemani et al., 2010) using PC12 membrane sheets in order to verify that the introduction of mutations next to or even inside the SNARE domain of SNAP25 would not simply influence or disrupt a possible interaction with syntaxin. The FRAP measurements show that SNAP25 is slowed down significantly (Figure 34) when it can interact with the additional co-transfected Syntaxin 1A (RFP), resulting in strongly increased halftimes accompanied by a reduction in the maximal recovery. For wt-SNAP25 *(+3)* the average halftime of 3.3 s is increased to 9.8 s, for SNAP25-*5* the increase is from 3.7 s to 10.2 s and for SNAP25+*10* it is increased from 4 s to 8.5 s. For both mutants with decreased (SNAP25-*5*) or increased (SNAP25+*10*) net charges, no significant alterations in halftimes in comparison to wildtype SNAP25 are observed (Figure 34d).

In conclusion, a possible disturbed syntaxin binding as an explanation for reduced membrane association of the SNAP25-*5* construct can be excluded.

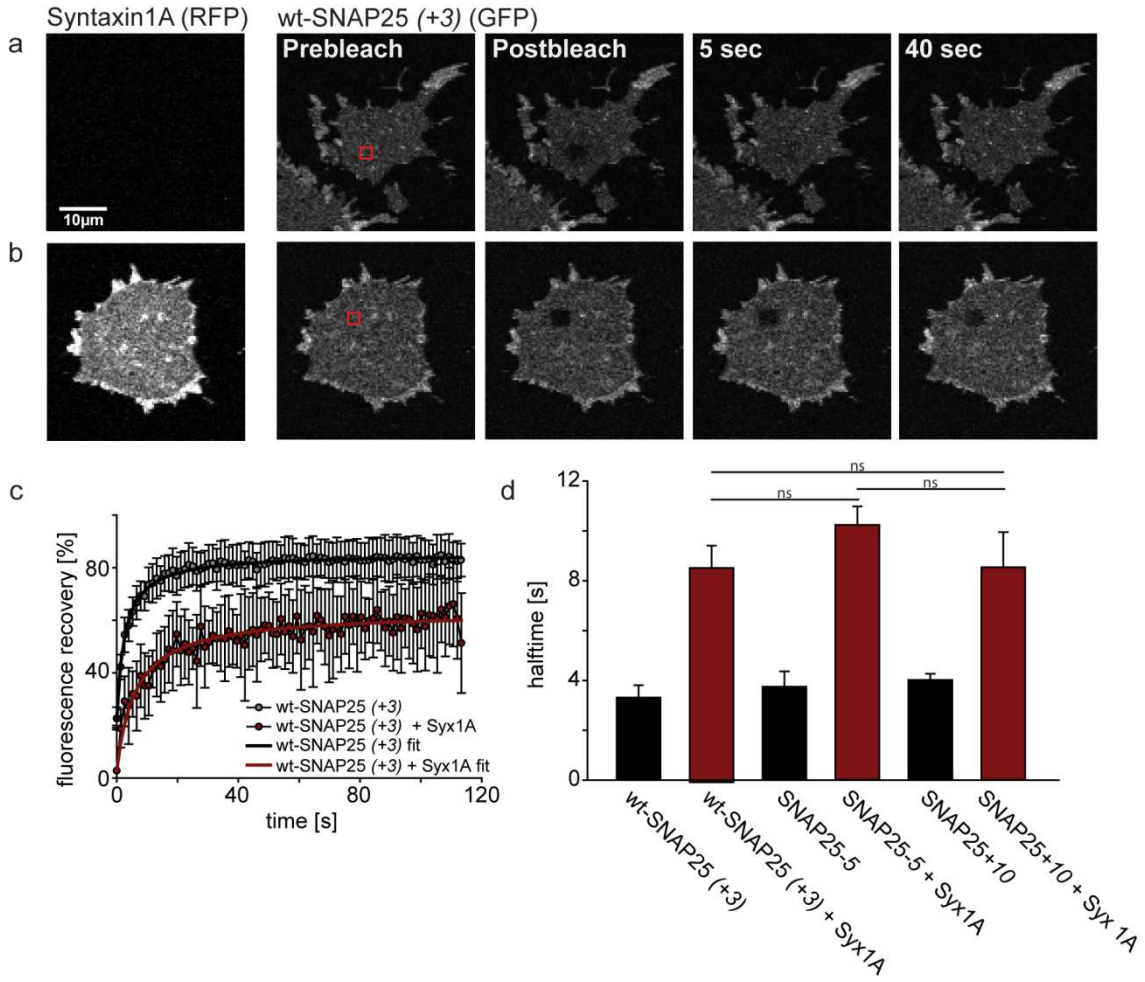

Figure 34: Syntaxin interaction conserved in SNAP25 mutant constructs
Confocal micrographs monitoring the basal plasma membrane of a PC12 cell expressing either solely **(a)** GFP-labeled wt-SNAP25 *(+3)* or **(b)** a co-expression with RFP-labeled Syntaxin 1A (Syx1A). Syntaxin expression is depicted on the left images respectively, followed by an arrangement of images portraying a fluorescence recovery after photobleaching (FRAP) experiment. From left to right: membrane sheets before bleaching of a squared ROI (red box), followed by the first postbleach image and images for 5 and 40 s after bleaching. Image sequences were taken at 1.2 Hz for a total of 113 s. **(c)** Example fluorescence recovery traces from one experiment, in the absence (grey) or presence (red) of syntaxin 1A-RFP. Values are given as mean ± s.d. (n = 7 – 12 membrane sheets). A hyperbolic function is fitted to the averaged traces yielding **(d)** the halftime of recovery for wt-SNAP25 *(+3)*, SNAP25-*5* and SNAP25+*10*, in the absence (black bar) and presence (red bar) of co-expressed Syntaxin 1A. Values are given as means ± s.e.m. (n = 3 – 4; t-test * p <0.05, ** p <0.01, *** p <0.001, ns = not significant) (modified after Weber et al., 2017).

To probe whether a diminished membrane targeting would also occur in the complete absence of Syntaxin 1A, the SNAP25-*5* mutant was over-expressed in BHK cells which are void of endogenous syntaxin. The typical phenotype of the predominant membrane association was readily observed in wt-SNAP25 *(+3).* The SNAP-*5* construct again showed a reduced association with the membrane and a dominant cytosolic fraction (Figure 35).

These results together with the FRAP experiments confirm the independence of SNAP25's electrostatic anchoring mechanism from Syntaxin 1A.

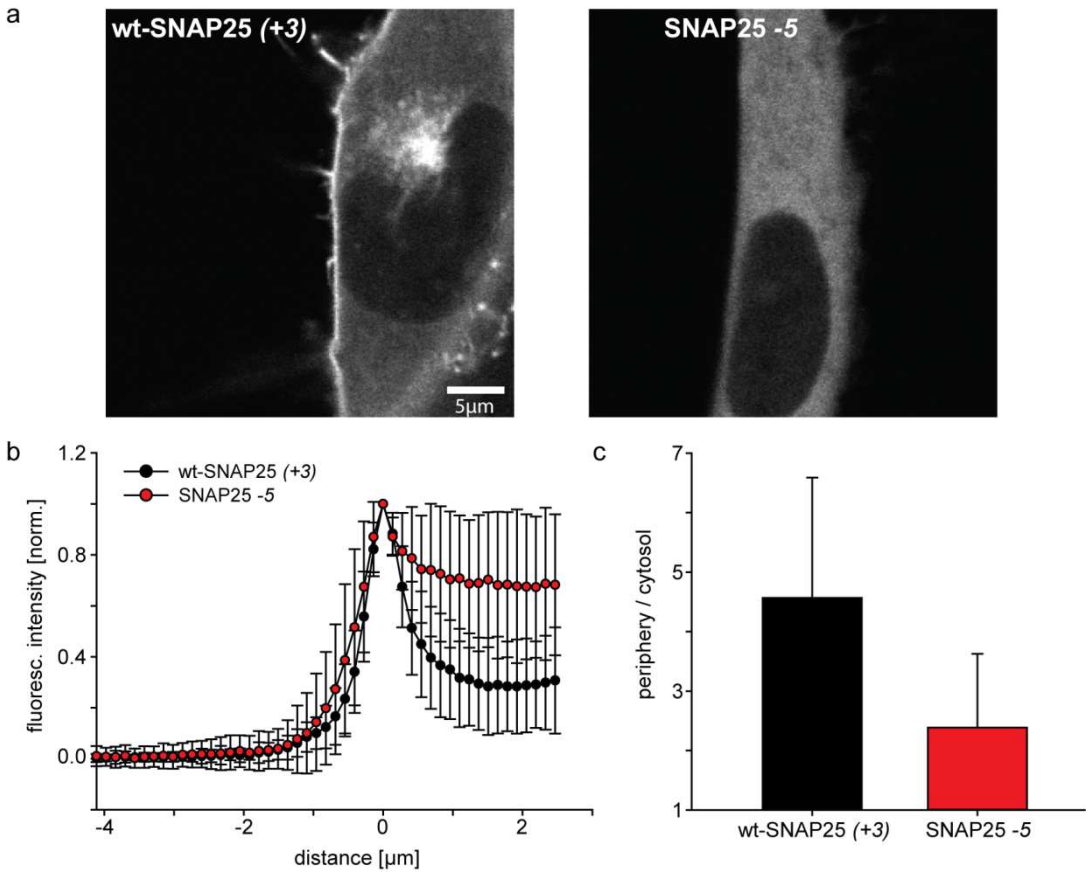

Figure 35: SNAP25 plasma membrane targeting in BHK cells
(a) Confocal micrographs from live BHK cells expressing wt-SNAP25 *(+3)* (left) and SNAP25-*5* (right) 24 hours after transfection. **(b)** Intensity traces of individual cells were normalized to the membrane and averages for wt-SNAP25 *(+3)* (black circles) and SNAP25-*5* (red circles) are shown. **(c)** Ratios of periphery and cytosol were averaged from individual cells (n= 32-35 ± s.e.m).

5.4 Role of negatively charged membrane lipids

The next step is to investigate the role of negatively charged lipids in the electrostatic anchoring process of SNAP25. First hints were given by a molecular dynamic simulation (personal correspondence Thomas H. Schmidt; Supplementary Figure 2) showing the SNAP25 binding behavior for small peptides of wt-SNAP25 *(+3)*, SNAP25-*5* and SNAP25+*10,* which generally confirm the binding behavior of the corresponding mutant constructs observed via linescan analysis in living cells. A look at the preferred lipid species to which the SNAP25 peptides bind during the MD simulations reveals the most promising binding partner at the plasma membrane (personal correspondence Thomas H. Schmidt; Supplementary Figure 3). Barely any interactions take place with SNAP25-*5* for all lipid species. Most prominent are the three PIPs (PIP, PIP_2, PIP_3) with a modest number of interactions for wt-SNAP25 *(+3)*, increased interactions with SNAP25+*10*, but no or hardly any interactions with SNAP25-*5*.

5.4.1 Binding of purified SNAP25 constructs to reconstituted liposomes

To reconstruct the results of the molecular dynamics simulations, with a membrane separated from the rest of a cell's machinery and free of any other proteins, a study of binding purified SNAP25 proteins to liposomes was conducted. The wt-SNAP25 *(+3)* and mutant constructs SNAP25-*5* and SNAP25+*10* were modified with a GST-tag enabling purification of the proteins. Since expression of the constructs was performed in bacteria the possible modifications with palmitoyl are absent, meaning the electrostatic anchoring can be studied isolated from any palmitoylation-dependent anchoring.

The GST-tagged constructs were bound to glutathione beads and incubated with Atto647N-PE labelled liposomes composed of either PC/PS or PC/PS/PE/PI/cholesterol in the absence or presence of distinct phosphoinositides. Readout of the Atto657N-PE fluorescence of liposomes bound to SNAP25 constructs allowed for quantification while

unspecific binding of liposomes to GST beads was accounted for. No binding of either construct was observed for liposomes consisting of solely PC with 16% PS, excluding a major role for PS in SNAP25 membrane association. The replacement of 16% PS with 4% PIP_2 however allowed for binding of SNAP25 to the liposomes. Similar to the binding behavior in live cells, decreased and increased interactions of SNAP25-*5* and SNAP25+*10* in comparison to wt-SNAP25 *(+3)* was observed (Figure 36). The same picture unfolded in the complex liposome mixtures where SNAP25 binding could only be establish with 4% PIP_2 present. The characteristic differences between the constructs persisted despite the lack of a palmitoylation machinery, confirming the results of the previous studies in living cells. Interestingly a complex liposome mixture with 4% PIP_3 shows the strongest binding but removes the differences between the SNAP25 constructs because wt-SNAP25 *(+3)* and SNAP25-*5* binding are strongly increased. Additional negative charges available for binding seem to compensate for any differences in the CRR. When lowering the concentration of PIP_3 to 2.8% to adapt the available negative charges to a comparable level provided by 4% PIP_2, the membrane binding of both wt-SNAP25 *(+3)* and SNAP25-*5* are reduced, whereas SNAP25+*10* retains its very high binding capacity.

In conclusion the lack of positively charged lysines in the SNAP25-*5* construct again results in a diminished binding in comparison to wt-SNAP25 *(+3)*. Accordingly the increase of the net charge is accompanied by an increase in membrane targeting. Since the experiments were conducted without the possibility of interactions with other proteins, nor a possible influence of the palmitoylation machinery, the results obtained strongly confirm the existence of an electrostatic anchoring mechanism that is independently responsible for an initial membrane contact.

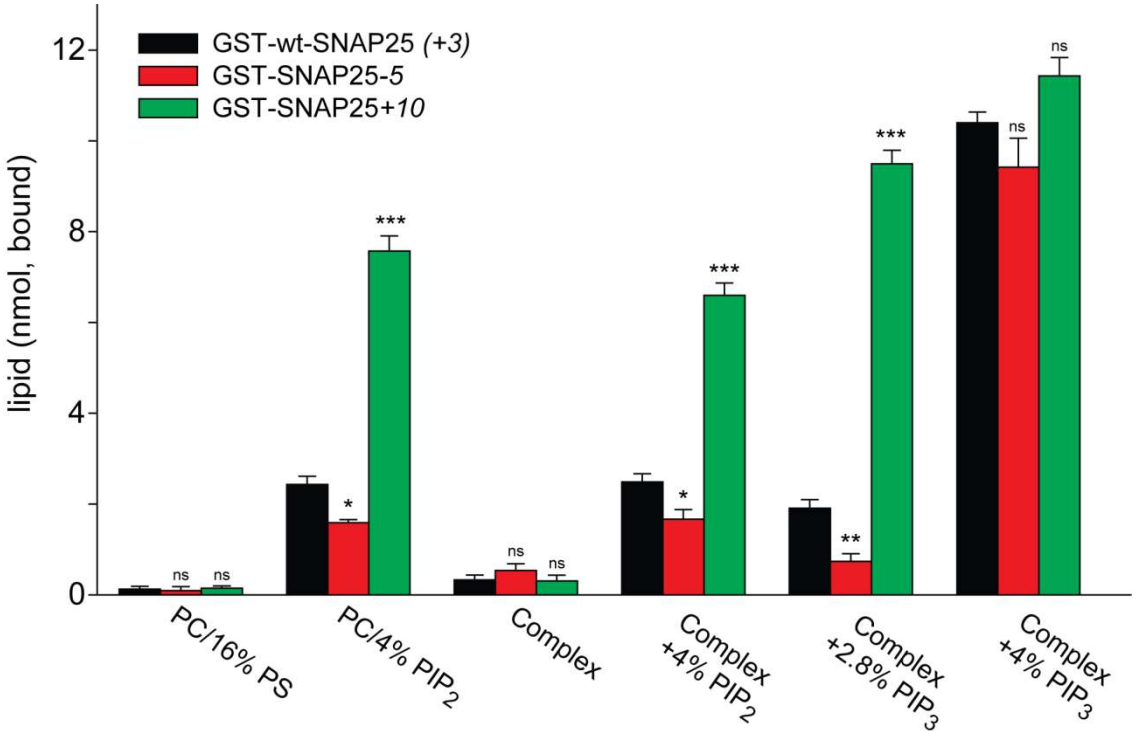

Figure 36: Membrane association of SNAP25 mediated by negatively charged lipids

Reconstituted liposomes containing lipid compositions in distinct concentrations of either PS, PI(4,5)P2, or PI(3,4,5)P3, but lacking any proteins, were incubated for one hour at 4°C with immobilized and GST (glutathione S-transferase)-tagged wtSNAP25 *(+3)*, GST-SNAP25-*5* or GST-SNAP25+*10*. The bound amount (lipid (nmol, bound)) of Atto647N-labeled liposomes was quantified by fluorescence (excitation: 639 nm, emission: 669 nm) measurements with a fluorometer. The values were corrected for non-specific binding by subtracting GST control values. Values are given as means ± s.e.m. (n = 3; t-test * p <0.05, ** p <0.01, *** p <0.001) (modified after Weber et al., 2017; I would like to thank Kerstin M. Rink and Thomas H. Söllner for the collaboration and help with the liposome binding studies).

5.4.2 Competition of SNAP25 and a PH domain for binding of PIP_2

To demonstrate the importance of negatively charged lipids like PIP_2 for SNAP25 binding in live conditions, a competition study was carried out. The PH domain of phospholipase Cδ marked with mCherry (PLC-δPH) was co-expressed with GFP tagged wt-SNAP25 *(+3)* to test whether both compete for binding of PIP_2 resulting in reduced membrane association with the plasma membrane. Quantification of the fluorescence of both constructs was performed on membrane sheets of PC12 cells after 48 hours of co-transfection. The $SNAP25_{(C\text{-}to\text{-}G)}$ construct was included as a negative control which will not associate with the plasma membrane and therefore should have no influence on PIP_2 binding by the PH domain.

When comparing the co-transfection of GFP-wt-SNAP25 *(+3)* and PLC-δPH to their respective single transfections a reduction in membrane association can be observed for both competing proteins (Figure 37). The co-transfection itself seems to have no influence on the amount of membrane association since $SNAP25_{C\text{-}to\text{-}G}$ expression does not reduce the level of PH domain binding (Figure 37b; left panel). So a reduced availability of PIP_2 does indeed reduce the effectiveness of SNAP25 membrane targeting.

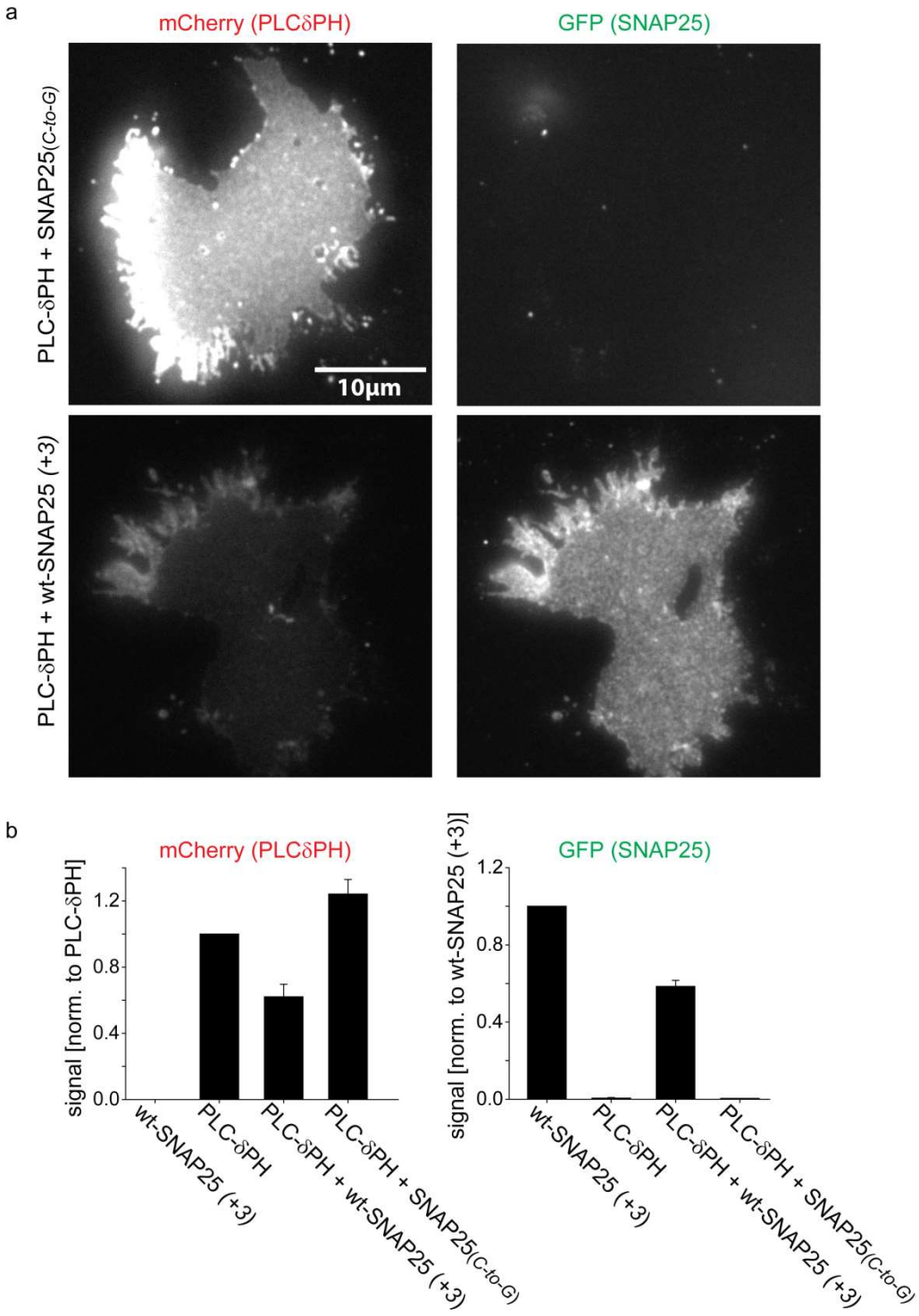

Figure 37: Competition of SNAP25 and the PH domain of PLC-delta for PIP_2
(a) Membrane sheets from PC12 cells expressing the mCherry tagged PH domain of phospholipase C-δ (PLC-δPH) together with either GFP tagged SNAP25*(C-to-G)* (top) or GFP tagged wt-SNAP25 *(+3)*(bottom). Left pictures show the mCherry fluorescence in the red channel and the right pictures show GFP fluorescence in the green channel. **(b)** Quantification of the mCherry fluorescence (left) and GFP fluorescence (right). Values in

the respective channels are normalized to single transfections controls of PLC-δPH and wt-SNAP25 *(+3)*. The wt-SNAP25 *(+3)* competes with PLC-δPH for membrane association, resulting in a reduced fluorescence in both channels. With SNAP25$_{(C\text{-}to\text{-}G)}$ the PLC-δPH association is not reduced and even slightly exceeds the level of PLC-δPH single transfections. Values are given as means ± s.e.m. (n = 3 - 4).

To further exclude that a reduced expression level of SNAP25 upon co-transfection could be responsible for a diminished membrane association in comparison to single transfections, further experiments were conducted.

Therefore a PH-PLCδ domain carrying the mutations K32A, W36N and R38K (PLC-δPH$_{mut}$) resulting in impaired binding to PIP_2 was used as a baseline control (Flesch et al., 2005). This enables a direct comparison of the competing wt-SNAP25 *(+3)* and PLC-δPH (PLC-δPH) with one condition in which one of the competitors is disabled (PLC-δPH$_{mut}$). Additionally the expression levels were monitored by western blot analysis of the same batch of co-transfected cells used for microscopy (Supplementary Figure 4) and the co-transfection efficiency was assessed by plotting the m-cherry and GFP fluorescence (Supplementary Figure 5). This enables a correction for a possible difference in expression levels. In addition, using Hepg2 cells, which lack endogenous SNAP25, excludes any influence of the non-monitored endogenous SNAP25 in the competition for PIP_2 binding.

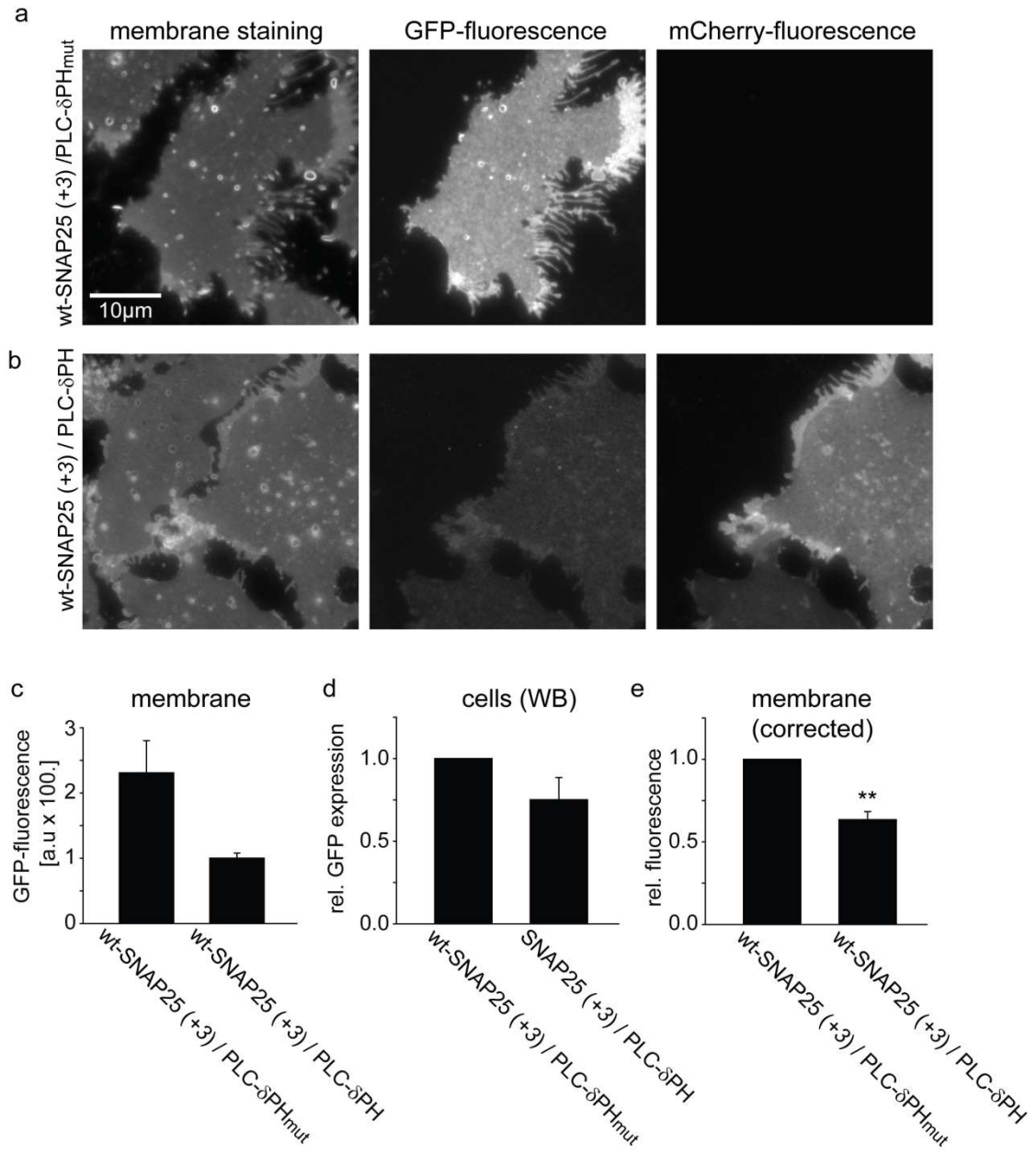

Figure 38: Co-expression of the PH domain of phospholipase C-delta reduces SNAP25 targeting

(a) Membrane sheets from HepG2 cells, which lack endogenous SNAP25, expressing, in addition to GFP tagged wt-SNAP25 *(+3,)* either an mCherry-tagged mutated PH domain of phospholipase C (PLC-δPH_{mut}) with disabled binding capabilities or **(b)** an intact mCherry-labelled PH domain of PLC (PLC-δPH). Membrane sheets were imaged in the blue channel (TMA-DPH; membrane stain; left), green channel (membrane-associated SNAP25 tagged with GFP; middle) and red channel (membrane-associated PH domain

tagged with mCherry; right). PLC-δPH_{mut} shows, as expected, no fluorescence in the mCherry channel (a; right panel). **(c)** The GFP fluorescence of membrane-associated wt-SNAP25 *(+3)* co-expressed with either PLC-δPH or PLC-δPH_{mut} was quantified. From the same transfections, intact cells were imaged showing that all GFP-SNAP25 expressing cells co-express the mCherry-labelled PH or PH_{mut} (Supplementary Figure 5). **(d)** Additionally the SNAP25 expression level was analysed by western blot (see Supplementary Figure 4), showing that a co-expression with the wt-PH domain causes lower GFP-SNAP25 expression levels compared to co-expression with PLC-δPH_{mut}. **(e)** Therefore values shown in c) were corrected for the lower expression levels as determined in (d). Values are given as means ± s.e.m. (n = 3 independent experiments; t-test * p <0.05, ** p <0.01, *** p <0.001).

The absolute GFP fluorescence levels already show a decreased SNAP25 binding to the membrane when wt-SNAP25 *(+3)* has to compete with the mCherry-labelled PH domain of PLC-δPH (Figure 38c). Even when taking the difference in expression levels (Figure 38d) into account, the corrected fluorescence levels show a significant difference in SNAP25 membrane targeting (Figure 38e). The PH domain of PLCδ (PH) is indeed able to compete with SNAP25 for available PIP_2 in the plasma membrane. A reduction of available PIP_2 is followed by a reduced SNAP25 binding to the membrane.

In conclusion, the competition experiments confirm the previous experiment with liposomes and emphasize the importance of PIP_2 for the electrostatic anchoring of SNAP25 to the plasma membrane.

6 Discussion

This study identifies an electrostatic anchoring mechanism that underlies the initial plasma membrane contact of SNAP25. The first part of this study focuses on the characterization of the cysteine-rich region and the importance of the inherent polybasic amino acid residues forming an electrostatic anchor prior to the stable attachment of SNAP25 by palmitoylation. Mutagenesis experiments in live PC12 cells revealed the critical importance of the polybasic cluster for plasma membrane targeting of SNAP25 as well as SNAP23. Subsequently, unhindered interactions between SNAP25 and Syntaxin 1A showed no dependency on syntaxin for the different plasma membrane localization patterns of the SNAP25 mutant variants. Additionally the palmitoylation status of the SNAP25 variants was examined, showing indeed a decreased palmitoylation status for the construct with decreased membrane association.
Finally, the role of negatively charged lipids present in the plasma membrane was addressed, demonstrating that PIP_2 is essential for the membrane association and serves as the counterpart to the electrostatic anchor, the polybasic cluster of SNAP25. These findings draw attention to an aspect of SNARE proteins that has not yet been extensively studied. The electrostatic anchoring by the use of a rather small and finely tuned polybasic cluster as a determinant for membrane association can have strong effects for cellular mechanisms and this previously underestimated mechanism may have potential generality for different types of cells and proteins

6.1 Electrostatic anchoring of SNAP25 to the plasma membrane

As mentioned in the introduction, it is established that SNAP25 is not stably bound to the plasma membrane until the addition of hydrophobic palmitoyl chains to its cysteines. This is achieved through palmitoylation via palmitoyl transferases (DHHC proteins), which are firmly integrated in the plasma membrane (see chapter 2.3.4). However neither intrinsic membrane binding domains, nor any other post-translational modifications are present for the overall negatively charged SNAP25, which could help drive its initial approach and attachment to the also negatively charged cytosolic leaflet of the plasma membrane. This initial requirement of localization of SNAP25 to the plasma membrane in order to get palmitoylated by the membrane-bound palmitoyl transferases therefore needs to be achieved by other means. Previous studies (see chapter 2.3.3) on several other proteins showed that interactions between larger polybasic domains and anionic lipids play a role in, or are even the main driving force for, membrane targeting.

So, as described for other peripheral proteins like K-Ras (Cadwallader et al., 1994; Wright and Philips, 2006), electrostatic interactions could play a pivotal role in the initial SNAP25 membrane targeting mechanism. The main focus and first aim (see chapter 3.1) of this study was to test whether a relatively small excess charge present in the CRR is responsible for electrostatic anchoring of SNAP25 to the plasma membrane, despite SNAP25 having an overall negative net charge.

6.1.1 SNAP25 plasma membrane targeting is dependent on the electrostatic potential of a polybasic cluster in the CRR

Conserved cysteine-rich region of SNAP25

The evaluation of the highly conserved cystein rich region found in all mammalian species shows only a small amount of eight positively charged lysines present in the vicinity of the palmitoylation sites and in addition negatively charged glutamic acid and aspartic acid residues which might, in part, counteract the lysines. So an excess of three positive charges after offsetting positive against negative charges is present in the CRR. Highly conserved regions or specific amino acids indicate that natural selection has continually eliminated forms with mutations, emphasizing the importance of the exact sequence of amino acids in order to carry out its specific functions.

This supports the idea of a fine-tuned electrostatic anchor provided by the polybasic lysine cluster. In comparison to other proposed electrostatic anchoring mechanisms mentioned in the introduction, like the polybasic clusters of K-Ras used in combination with myristoylation (Cadwallader et al., 1994; Wright & Philips, 2006, Heo et al., 2006) or the basic effector domain consistent of thirteen basic residues present in MARCKS (Gambhir et al., 2004), having only a small excess charge of three is very low. But particularly in the presence of multivalent lipids present in the membrane such as PIP_2, this limited number of charged residues may be sufficient for facilitating an initial membrane contact and to electrostatically anchor SNAP25 to the plasma membrane until being thoroughly bound via palmitoylation.

SNAP25 plasma membrane targeting dependent on the polybasic cluster of the CRR

To address the main question of this study and support the existence of such an electrostatic anchoring mechanism for SNAP25, a disruption of the cluster of lysines should prove to be crucial for membrane targeting. The first analyzed mutant SNAP25-*5* has therefore no lysines left in the CRR, which were replaced by alanines, resulting in an overall net charge of negative five (*-5*).

The linescan analysis of the SNAP25-*5* distribution indeed clearly showed a cessation of the predominant localization at the plasma membrane when compared to wt-SNAP25 (*+3*) (see chapter 5.1.2), confirming the importance of the polybasic cluster for membrane association. This was confirmed by further experiments using cell fractionations analyzed by western blot and the microscopy of membrane sheets. The results reflect the expected outcome of strongly decreased membrane localization when the polybasic cluster is removed. These outcomes are well in line with the results of previous studies when the minimal domain necessary for SNAP25 plasma membrane targeting was mapped to amino acids 85–120 (Gonzalo et al., 1999), which contains the CRR.

Interestingly the deletion of all eight positive charges in the SNAP25-*5* mutant leads to a strongly diminished membrane association of SNAP25 but it is not completely absent, as a small fraction can still be detected at the membrane. Since the cysteines were not subject to mutations, SNAP25-*5* should still be viable for palmitoylation and therefore still be stably bound to the membrane. Therefore the observed membrane-bound fraction represents the palmitoylated fraction of SNAP25, which shows that palmitoylation of SNAP25 via palmitoyl transferases is indeed still intact and SNAP25 slowly enriches in the plasma membrane over time. This notion is supported by the observation that the critical difference between wt-SNAP25 and SNAP25-*5* seems to increase over time since an analysis after a shorter time period of only a few hours after

transfection shows a diminished but still visible and measurable difference between the two constructs.

In conclusion, the initial contact to the membrane achieved through electrostatic anchoring seems to be rate-limiting for the process of attachment via palmitoylation to the plasma membrane, as the strong difference between wildtype and the SNAP25-*5* mutant phenotype suggests.

To get further insight into the importance of the charge distribution and to evaluate the polybasic cluster, two additional mutation variants (SNAP25-$1_{proximal}$ and SNAP25-1_{distal}) were tested. The question addressed was whether the charges in close proximity to the cysteins were of more importance, and deletion of the nearest positive charges would suffice to reduce membrane targeting. A direct influence of the amino acid substitutions on the palmitoylation of the cysteines, as is described for alterations in hydrophobicity in the CRR (Greaves et al., 2009), might also be possible and must be excluded. Since the substitutions of the closest lysines are more likely to show an influence on the palmitoylation status of cysteins, possibly leading on this account to a decreased membrane association, a difference between the two constructs would reflect this. Furthermore, now only four lysines are replaced by alanines in each construct, resulting in an only a reduced, instead of a completely absent, electrostatic potential of the polybasic cluster. This should be reflected in the comparison of the phenotypes of both mutants versus the wildtype SNAP25 and the previously tested SNAP25-*5* mutant.

When compared to wt-SNAP25 *(+3)* both constructs (SNAP25-$1_{proximal}$ and SNAP25-1_{distal}) still show a strong reduction in membrane localization. Interestingly this effect is indeed less prominent and reflects the higher excess of positive charges in both mutants compared to the SNAP25-*5* mutant. Together the reduced membrane association for all three mutants (SNAP25-$1_{proximal}$, SNAP25-1_{distal} and SNAP25-*5*) speaks for the dependency on the charges provided by the polybasic cluster. Since there is no

significant difference between SNAP25-*1*$_{proximal}$ and SNAP25-1$_{distal}$ constructs an influence of solely the closest lysines to the palmitoylation sites can be excluded.

The charge-dependency observed here, rather than dependency on lysine mutations in specific places, supports the hypothesis of an underlying electrostatic mechanism for initial membrane association rather than any direct influence on the following palmitoylation. Since the for palmitoyl transferases important QPARV motif (Greaves et al., 2010) is located further distal to the introduced mutations, a disturbed interaction with the palmitoyl transferases is unlikely. Despite these promising results, the important question remains if the introduced mutations of the lysines hinder at least partially the palmitoylation of the cysteines and therefore lead to a reduced membrane targeting. This critical question was addressed in several separate experiments and the cumulative results will be discussed in further detail (see section 6.2).

C-terminal polybasic cluster has no influence on SNAP25 membrane targeting

A small polybasic cluster of positively charged arginines and a lysine can be found at the c-terminal part of SNAP25. A mutation analysis showed no influence on membrane targeting and confirmed that the electrostatic anchor needs to be established close to the cysteines. This result is in agreement with previous studies showing that, the critical region for correct membrane targeting relies on the linker region of SNAP25 (Gonzalo et al., 1999).

Increased hydrophobicity cannot compensate for the polybasic cluster

Since a previous study suggested that the hydrophobicity of the CRR plays a role in SNAP25 membrane targeting (Greaves et al., 2009), an experiment was conducted to clarify if increased hydrophobicity can compensate for the loss of the electrostatic anchor.

Compared to SNAP25-*5* the mutant construct SNAP25-*5hydrophob* with increased hydrophobicity showed no increase in targeting, nor could it compensate for the loss of

the polybasic cluster. Instead, the targeting was further reduced and hardly detectable. This result must be interpreted with caution and a clear answer cannot be stated since alterations in the CRR showed, it is a fine-tuned highly conserved region and alterations in the amino acid sequence can have drastic effects on targeting. Prior studies that have suggested the importance of palmitoylation for the stable binding of SNAP25 to the plasma membrane (Gonzalo & Linder, 1998, Salaün et al., 2004), together with the fact that protein palmitoylation enhances the hydrophobicity of proteins, speak for the importance of the hydrophobicity provided by the modification of the protein itself.

A recent study (Salaun et al., 2020) claims that amino acids 93–111 in SNAP25 act solely as a molecular spacer, which ensures efficient coupling to the palmitoyl transferase responsible for stable membrane attachment. However, the mutant investigated by this study showed a partial loss of *S*-acylation mediated by zDHHC7, which as the study states, might reflect a difference in membrane affinity. Since four lysines (K69, K72, K76, K83) remain outside the flexible linker (93-111) this reflects the results obtained for the partial substitutions of the polybasic cluster done for SNAP25-1_{proximal} and SNAP25-1_{distal} constructs. Interestingly the described loss in membrane association (Salaun et al., 2020) can be compensated for by *S*-acylation mediated by the co-expressed palmitoyl transferase zDHHC17. These observations show that alterations in the CRR and a partial loss of the polybasic cluster are not hindering the availability of the cysteines for palmitoylation.

Altogether this further speaks for an electrostatic anchoring that is responsible for the initial contact to the plasma membrane preceding the stable membrane attachment by palmitoylation which is of course reliant on hydrophobicity.

6.1.2 Bipolar nature of the electrostatic anchoring mechanism

So far the results confirm the crucial importance of the polybasic cluster of lysines present in the CRR for efficient membrane targeting of SNAP25. Fitting to an underlying electrostatic mechanism, a correlation between the amount of charge reduction and the effect of membrane targeting disruption was observed (SNAP25-$1_{proximal}$ and SNAP25-1_{distal}). The bipolar nature of electrostatics however would suggest that increased electrostatic potential could be translated to an increased membrane targeting.

Although physiologically not relevant, two different mutant constructs (SNAP25+*7* and SNAP25+*10*) were designed to test this proof of concept hypothesis. Contrary to expectations the increased overall net charge to +7 introduced by replacing the negatively charged amino acids neighboring the lysines with alanines, did not lead to an increase in membrane targeting but, surprisingly, even reduced the targeting. A possible explanation might be that the mutations introduced lead to effects that change the orientation and helical structure of SNAP25, which might disfavor an effective binding to the plasma membrane, despite an increased positive net charge. Nevertheless in line with the above stated hypothesis are the observations with the SNAP25+*10* mutant, which showed significantly increased membrane targeting, speaking for the influence of an electrostatic anchor.

Although having a strong influence on the SNAP25 membrane targeting, it is not solely the overall net charge that seems responsible. Possibly, the exact positions and thereby orientation of the charged residues towards the plasma membrane are important for the formation of the electrostatic anchor, responsible for initial contact of SNAP25 to the plasma membrane. However the overall net charge of the CRR, whether it is overall positive or negative, can indeed have an opposite influence on the membrane targeting, reflecting, in principle, the bipolar nature of electrostatic effects.

Further research questions that could be asked include the interesting question why the highly conserved CRR of SNAP25 has exactly an excess charge of just three which is, as previously discussed, very low in comparison to other proposed electrostatic anchoring mechanisms. One study on plasma membrane-localized small GTPases, concludes that association results from the additive binding energies of individual subclusters (Heo et al.,2006). For SNAP25 the small polybasic cluster seems sufficient for the electrostatic anchoring to the PM, thereby increasing its dwell time, promoting the stable binding to and integration into the PM via palmitoylation. Since SNAP25 palmitoylation is a reversible modification (Resh, 2006) the relatively small electrostatic force with only an excess of three positive charges might also be optimal to allow SNAP25 to dissociate from the PM after depalmitoylation. A further study could try to resolve this question.

6.1.3 Electrostatic anchoring of SNAP23

Since SNAP23 is a homologue to the neuronal SNAP25, it is interesting to see if similar mutations in SNAP23 produce comparable results to SNAP25. Indeed the decrease of the electrostatic potential of the polybasic lysine cluster by substitution of four of the eight lysines present, again results in decreased membrane targeting. But the contrary picture of increased and decreased plasma membrane targeting, when increasing the positive net charge in several mutants of SNAP23, can also be seen. Whereas a construct (SNAP23+*10*) similar to the SNAP25+*10* promotes membrane targeting, the construct SNAP23+*11b* has no positive effect on targeting, even with an additional positive charge. Interestingly a small change in the position of substituted amino acids, as applied in SNAP23+*11a,* leads to an even further reduced targeting, despite having the same net charge. These mutations might interfere with palmitoylation of the nearby cysteines or change the folding and orientation of the protein, prohibiting a stable membrane binding. This illustrates the importance of orientation and accessibility of the amino acids as was already observed for the SNAP25-*7* mutant construct.

To take it to the extreme, a construct was designed with a surplus of sixteen positive charges (SNAP23+*16*), which indeed was even further enriched at the plasma membrane, showing the progressive effect of the further increased overall net charge, speaking further for an electrostatic anchoring mechanism.
In conclusion the analysis shows that charge-dependent membrane localization is also at work for SNAP23. This speaks also for an electrostatic anchoring mechanism providing the initial membrane contact. However a second factor, most likely the palmitoylation of cysteines, plays also a critical role for the final localization of the protein.

6.1.4 Syntaxin's role in SNAP25 membrane targeting

Previous studies evaluating syntaxin's role in the targeting of SNAP25 to the plasma membrane found inconsistent results on whether syntaxin has an influence or not. As mentioned in the introduction, early studies (Vogel et al., 2000; Washbourne et al., 2001) suggested that Syntaxin 1A ("syntaxin") serves to direct newly synthesized SNAP25 through the Golgi transport pathway to the plasma membrane, while subsequent studies (Loranger & Linder, 2002) suggested a syntaxin-independent targeting mechanism reliant on a neuronal co-factor.

Although it appears unlikely that syntaxin serves as a chaperone for SNAP25 plasma membrane targeting (Salaün et al., 2004), the mutations introduced during this study might disable possible interactions between SNAP25 and syntaxin. This could result in a reduced targeting of SNAP25 to the plasma membrane. Since some of the mutations are also located in the N-terminal SNARE motif responsible for interactions with syntaxin, the interaction status with syntaxin was investigated.

A FRAP assay probing the interaction of SNAP25 with syntaxin showed no influence of the mutations introduced on the capability of complex formation with syntaxin (see chapter 5.3). Further, the diminished targeting seen when deleting the polybasic cluster of SNAP25 can also be observed in BHK cells, which have no endogenous Syntaxin 1A.

Therefore an influence of syntaxin on the SNAP25 membrane targeting of the mutation constructs used in the previous experiments is entirely excluded.

Whether Syntaxin 1A is indeed capable to act as a chaperone for SNAP25 under certain circumstances and in addition to other targeting mechanisms of SNAP25 is not addressed by these experiments. But the present study shows that syntaxin cannot compensate for the loss of SNAP25's electrostatic anchoring. Nevertheless Syntaxin 1A plays a pivotal role in SNAP25's further remaining at the plasma membrane. As mentioned in the introduction Syntaxin 1A and PIP_2 are thought to function as a molecular docking site for the complete SNARE fusion machinery (Jahn & Scheller, 2006; Aoyagi et al., 2005; van den Bogaart et al., 2011), the complex ensures the remainder of SNAP25 at the fusion site.

Additionally the liposome binding studies, which eliminated a possible role of potential SNAP25 binding partners such as Syntaxin 1A, confirm the independency of the electrostatic anchoring. The distinct binding behaviors are solely dependent on the available polybasic cluster.

Altogether the results confirm clearly that the effects of diminished plasma membrane targeting of mutated SNAP25 observed during this study cannot be attributed to diminished Syntaxin1A interactions. While syntaxins participation cannot be fully excluded, the proposed electrostatic anchoring mechanism of SNAP25 at least provides a syntaxin-independent plasma membrane targeting mechanism.

6.2 Palmitoylation-dependent membrane targeting

As mentioned in the literature review, palmitoylation is mainly responsible for the stable binding of SNAP25 to the plasma membrane (Gonzalo & Linder, 1998, Salaün et al., 2004), which was confirmed by this study as the cysteines proved to be critical for SNAP25 membrane targeting (see chapter 5.2).

An assessment of the palmitoylation status of the mutant constructs with the most distinct phenotypes confirms that the construct lacking the polybasic cluster (SNAP25-*5*) is less targeted to the membrane and therefore accordingly less palmitoylated than wildtype SNAP25 (wt-SNAP25+*3*). The assessment of the palmitoylation status of the SNAP25+*10* construct shows only an inconclusive trend towards an increased membrane targeting. Nonetheless, together with the results from the linescans, the membrane sheet analysis and, most convincingly, the liposome binding studies, an increased membrane targeting solely by the electrostatic anchoring can be assumed.

Increased positive charges (SNAP25+$10_{(C\text{-}to\text{-}G)}$) could not fully compensate for the lack of a functional palmitoylation. Nevertheless, interestingly a membrane-associated fraction of SNAP25+$10_{(C\text{-}to\text{-}G)}$ was detectable at the membrane shown by both cell fractionation analysis and microscopy of membrane sheets. This construct represents the initial electrostatic anchoring of SNAP25 to the plasma membrane without any palmitoylation present.

Liposome binding studies provide a view on the electrostatic anchoring of SNAP25 isolated from any possible interference of palmitoylation. The results obtained from these experiments strongly support the independence of the electrostatic anchoring mechanism for initial contact establishment from the palmitoylation status. This is further supported by one interesting finding, which showed the equalization of the

differences between the constructs examined when the negative potential present in the targeting membrane is artificially increased (see Figure 34; chapter 5.4.1).

As already mentioned in the introduction, palmitoylation often follows a myristoylation or a prenylation as a second step but nonetheless, can also occur without any other premodification, as is the case with SNAP25 (Veit et al., 1996), SNAP23 (Chen et al., 1999) or G-alpha subunits (Linder et al, 1993). The electrostatic anchoring therefore replaces the premodification as an initial contact preceding the stable attachment to the PM via palmitoylation of SNAP25.

6.3 PIPs - the match for SNAP25's electrostatic anchoring to the PM

First hints towards the role of negatively charged lipids in the electrostatic anchoring process of SNAP25 stem from a molecular dynamic simulation (personal correspondence Thomas H. Schmidt). With the help of a MARTINI CG coarse grain model (Marrink & Tieleman, 2013) the SNAP25 binding behavior and establishment of the first contact to the plasma membrane was retraced. Peptides of wt-SNAP25 *(+3)*, SNAP25-*5* and SNAP25+*10* were located at a distance of about 2.7 nm above a plasma membrane (Ingólfsson et al, 2014) composed of 63 different lipid species (Supplementary Figure 2).

The simulation run comprises 2 µs in which all 36 (12 for each construct) of the placed peptides were finally associated to the membrane in about 750 ns. The average time the peptides establish a first contact shows only a slight delay for SNAP25+*10* and a more distinct delay for SNAP25-*5*. As an influence of the charge over a greater distance is implausible, the time until the differently charged peptides establish its first contact is not strongly influenced by charge alterations. But a distinctive behaviour of numerous cycles of binding, unbinding and rebinding was observed for SNAP25-*5* which elongates the time until the final stable association with the membrane is formed. This "on/off" cycling is less prominent for wt-SNAP25 (*+3)* and especially less pronounced for the SNAP25+*10* construct. Therefore the final association time, which is defined as the time point where the peptides are finally stably associated to the membrane, is elongated for SNAP25-*5* and shortened for SNAP25+*10*.

These simulations fit to the experimental data of this study, showing that the absence of lysines accompanied by a lack of positive charges leads to SNAP25 having trouble in association with the membrane. The opposite can be seen for SNAP25+*10* where additional lysines seem to help the in the stable initial association with the membrane, most likely by binding to negatively charged lipid counterparts.

Monitoring the contact establishment of the peptides in the MD simulations with negatively charged lipids like PA, PS, PI and PIP, PIP_2 and PIP_3 confirmed this assumption (Supplementary Figure 3).
While taking account for the large differences in lipid concentrations, the interactions of the three peptide constructs are shown for different lipid species. PS and PA show little interactions and no significant differences in the binding behaviour of the three peptides. Barely any interactions are taking place with SNAP25-*5* for all lipid species. For PI the interactions are increased for the SNAP25+*10* in comparison to wt-SNAP25 *(+3)*. Most prominent are the three PIPs with modest number of interactions for wt-SNAP25 *(+3)*, elevated interactions with SNAP25+*10* and still no or barely any interactions with SNAP25-*5*. Interestingly the number of interactions increases even after stable association with the membrane representing a continuous recruitment of peptides. This may prohibit the on/off cycling behaviour enabling a stable association with the plasma membrane and finally anchoring by palmitoylation.

These observations were confirmed by the experimental data of this study (see section 5.4). The binding of SNAP25 constructs to liposomes showed the possible binding partners for SNAP25's electrostatic anchor. Phosphatidylserine can be excluded as a major binding partner since no binding of either construct was observed. Only the multivalent phosphoinositides produce observations similar to the linescan analysis in living cells. The presence of both PIP_2 and PIP_3 significantly enhance the binding of wildtype SNAP25 (GST-wt-SNAP25 *(+3)*) as well as the mutant constructs (GST-SNAP25-*5* and GST-SNAP25+*10*). The most critical finding of the previous experiments of reduction or addition of positive charges being accompanied by reduced or increased SNAP25 interaction was confirmed. When the liposome composition includes PIP_3 at high concentrations the binding of the GST-SNAP25 constructs are

strongly elevated and differences between the constructs are diminished. This reflects the bipolar nature of the electrostatic anchor similar to the mutant constructs with further elevated net charges (SNAP23+*16*) leading to an even increased membrane binding, only in this case the increased electrostatic potential is on the side of the membrane. Presumably this increase is due to additional contacts of PIP_3 to positively charged residues outside the CRR of SNAP25. Interestingly when the amount of PIP_3 was reduced to match the level of negative charges provided by PIP_2 the difference between the GST-constructs was re-established.

In conclusion the results confirm the previous experiments in PC12 cells. Since the liposome binding studies exclude any possibility of palmitoylation or any other external binding partner acting as a chaperone for SNAP25, the observations clearly speak for an electrostatic anchoring of SNAP25 preceding its palmitoylation. Both PIP_2 and PIP_3 seem to be likely anchoring partners to SNAP25 and membrane microdomains enriched with PIP_2 or PIP_3 might act as molecular docking sites.

Although PIP_3 has a very prominent effect on SNAP25's liposome binding capabilities it is significantly less abundant in the PM in comparison to PIP_2 (Balla, 2013). PIP_3 is also enriched in endosomal compartments (Wang and Richards, 2012) which might be reflected by the highly increased signals for SNAP25-GFP observed in PC12 cells, presumably reflecting such compartments.

As mentioned in the introduction Syntaxin 1A and PIP_2 interactions facilitate membrane sequestering and microdomain formation (van den Bogaart et al 2011). The enrichment of SNAP25 at PIP_2 microdomains by electrostatic interactions therefore has clear advantages since accumulation of SNAP25 together with Syntaxin 1A may facilitate SNARE interactions and thereby increase of the membrane fusion efficiency.

The critical importance of PIP_2 is demonstrated further by experiments using PC12 and HepG2 cells, where readily available PIP_2 as a binding partner for the electrostatic

anchor of SNAP25 was reduced by competition with a PH domain with high affinity towards PIP_2. A reduction of available PIP_2 was followed by a reduced SNAP25 binding to the membrane.

In conclusion PIP_2 is the most likely candidate to fulfill the role as an electrostatic anchoring partner for the polybasic lysine cluster of SNAP25, increasing its dwell time at the PM, thereby ensuring the palmitoylation by the membrane-bound palmitoyl transferases, which finally establishes a stable membrane binding (see Figure 39).

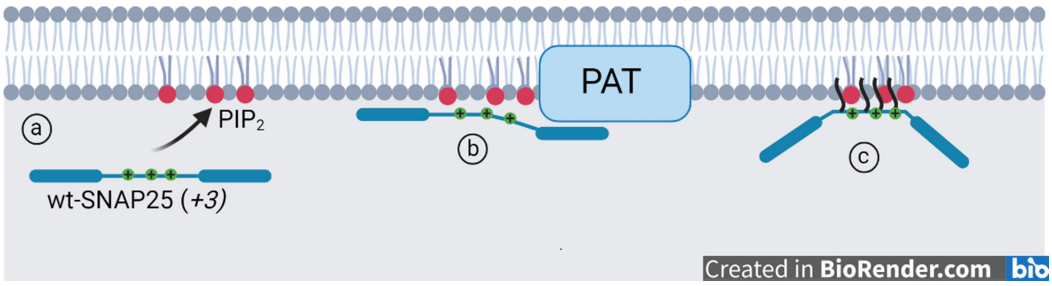

Figure 39: Electrostatic anchoring of SNAP25 precedes stable membrane attachment

(a) Initially cytosolic and not yet palmitoylated SNAP25 establishes with the help of a small polybasic cluster (net charge: +3; green +) in the CRR an initial contact via the phosphoinositide PIP_2 present at the inner leaflet of the PM. **(b)** The dwell time is increased through the transiently electrostatic anchoring of SNAP25 so that membrane-bound palmitoyl transferases (PAT) can efficiently modify the cysteines by adding palmitoyl chains. **(c)** The hydrophobic palmitoyl chains insert into the lipid bilayer and stably bind SNAP25 to the PM (created by Pascal Weber in biorender.com).

6.4 Main Conclusions

This study shows clear evidence for the existence of an electrostatic anchoring mechanism establishing initial contact preceding the stable membrane attachment of SNAP25 to the plasma membrane. The investigation of the electrostatic anchoring mechanism of SNAP25 reveals the critical dependency of SNAP25 membrane targeting on a small polybasic cluster of lysine residues present in the CRR.

Although previous studies suggested similar electrostatic anchoring mechanisms, the characterization of the CRR shows that a surprisingly small cluster is sufficient to facilitate initial membrane contact in the case of SNAP25. The mechanism described represents an extension of previous theories of plasma membrane targeting via electrostatics and could have potential generality as other proteins might use a similar electrostatic anchor. As mentioned in the introduction one example for this would be critical lysine residues, potentially important for interactions with negatively charged phospholipids, like in the case of Osh4 mediated sterol transfer (Schulz et al., 2009).

The principal findings could also be reproduced in SNAP23, the ubiquitously expressed analogue of the neuronal SNAP25, meaning an electrostatic anchoring mechanism is also present in the CRR of SNAP23 and utilized for initial membrane contact.

A potential influence of Syntaxin1A on the electrostatic anchoring of SNAP25 was excluded and any involvement is unlikely.

While the existence of an electrostatic anchoring mechanism could also be confirmed in liposomes, an environment lacking any palmitoylation, when experiments were conducted in cells the palmitoylation was still intact. These results further support the existence of the electrostatic anchoring for initial membrane attachment prior to the stable binding of SNAP25 to the plasma membrane.

Extensive efforts to identify the initial potential lipid binding partner for SNAP25's electrostatic anchor revealed PIP_2 as the most likely candidate. It may act as a molecular docking site similar to the previously described lipid-protein interactions between PIP_2 and Syntaxin 1A.

In conclusion, this study identifies an electrostatic anchoring mechanism, which relies on only a very small polybasic cluster, serving as a determinant for membrane association, which may have potential generality for different types of other cellular mechanisms. This shows that finely-tuned protein electrostatics can have a large influence on a proteins task and localization.

7 Bibliography

Aikawa, Y., Lynch, K.L., Boswell, K.L., and Martin, T.F.J. (2006). A Second SNARE Role for Exocytic SNAP25 in Endosome Fusion. Mol Biol Cell 17, 2113–2124.

Alberts, B., Wilson, J.H., and Hunt, T. Alberts, B., Wilson, J. H. & Hunt, T. (2008). Molecular biology of the cell, 5th edn. New York, N.Y., Abingdon: Garland Science.

Alland, L., Peseckis, S.M., Atherton, R.E., Berthiaume, L., and Resh, M.D. (1994). Dual myristylation and palmitylation of Src family member p59fyn affects subcellular localization. J. Biol. Chem. 269, 16701–16705.

Antonucci, F., Corradini, I., Fossati, G., Tomasoni, R., Menna, E., and Matteoli, M. (2016). SNAP-25, a Known Presynaptic Protein with Emerging Postsynaptic Functions. Front. Synaptic Neurosci. 8.

Aoyagi, K., Sugaya, T., Umeda, M., Yamamoto, S., Terakawa, S., and Takahashi, M. (2005). The activation of exocytotic sites by the formation of phosphatidylinositol 4,5-bisphosphate microdomains at syntaxin clusters. J Biol Chem 280, 17346–17352.

Augustine, G.J., Burns, M.E., DeBello, W.M., Hilfiker, S., Morgan, J.R., Schweizer, F.E., Tokumaru, H., and Umayahara, K. (1999). Proteins involved in synaptic vesicle trafficking. J Physiol 520, 33–41.

Avery, J., Ellis, D.J., Lang, T., Holroyd, P., Riedel, D., Henderson, R.M., Edwardson, J.M., and Jahn, R. (2000). A Cell-Free System for Regulated Exocytosis in Pc12 Cells. J Cell Biol 148, 317–324.

Aveyard, R., Aveyard, R., and Haydon, D.A. (1973). An Introduction to the Principles of Surface Chemistry (CUP Archive).

Balla, T. (2013). Phosphoinositides: Tiny Lipids With Giant Impact on Cell Regulation. Physiological Reviews 93, 1019–1137.

Bark, I.C., and Wilson, M.C. (1994). Human cDNA clones encoding two different isoforms of the nerve terminal protein SNAP-25. Gene 139, 291–292.

Batoulis, H., Schmidt, T.H., Weber, P., Schloetel, J.-G., Kandt, C., and Lang, T. (2016). Concentration Dependent Ion-Protein Interaction Patterns Underlying Protein Oligomerization Behaviours. Sci Rep 6, 24131.

Baumann, N.A., and Menon, A.K. (2002). Chapter 2 Lipid modifications of proteins. In New Comprehensive Biochemistry, (Elsevier), pp. 37–54.

Berger, M., and Schmidt, M.F. (1985). Protein fatty acyltransferase is located in the rough endoplasmic reticulum. FEBS Lett. 187, 289–294.

Berridge, M.J. (1984). Inositol trisphosphate and diacylglycerol as second messengers. Biochem. J. 220, 345–360.

Berridge, M.J., and Irvine, R.F. (1984). Inositol trisphosphate, a novel second messenger in cellular signal transduction. Nature 312, 315–321.

Bhalla, A., Chicka, M.C., Tucker, W.C., and Chapman, E.R. (2006). Ca(2+)-synaptotagmin directly regulates t-SNARE function during reconstituted membrane fusion. Nat Struct Mol Biol 13, 323–330.

Bhatnagar, R.S., and Gordon, J.I. (1997). Understanding covalent modifications of proteins by lipids: where cell biology and biophysics mingle. Trends Cell Biol. 7, 14–20.

Bijlmakers, M.-J., and Marsh, M. (2003). The on-off story of protein palmitoylation. Trends Cell Biol. 13, 32–42.

van den Bogaart, G., and Jahn, R. (2011). Counting the SNAREs needed for membrane fusion. J Mol Cell Biol 3, 204–205.

van den Bogaart, G., Meyenberg, K., Risselada, H.J., Amin, H., Willig, K.I., Hubrich, B.E., Dier, M., Hell, S.W., Grubmüller, H., Diederichsen, U., et al. (2011). Membrane protein sequestering by ionic protein–lipid interactions. Nature 479, 552–555.

Bottomley, M.J., Salim, K., and Panayotou, G. (1998). Phospholipid-binding protein domains. Biochim. Biophys. Acta 1436, 165–183.

Brunger, A.T. (2001). Structure of proteins involved in synaptic vesicle fusion in neurons. Annu Rev Biophys Biomol Struct 30, 157–171.

Brunger, A.T., Weninger, K., Bowen, M., and Chu, S. (2009). Single-molecule studies of the neuronal SNARE fusion machinery. Annu. Rev. Biochem. 78, 903–928.

Cadwallader, K.A., Paterson, H., Macdonald, S.G., and Hancock, J.F. (1994). N-terminally myristoylated Ras proteins require palmitoylation or a polybasic domain for plasma membrane localization. Mol. Cell. Biol. 14, 4722–4730.

Campbell, R.E., Tour, O., Palmer, A.E., Steinbach, P.A., Baird, G.S., Zacharias, D.A., and Tsien, R.Y. (2002). A monomeric red fluorescent protein. PNAS 99, 7877–7882.

Chapman, E.R. (2008). How does synaptotagmin trigger neurotransmitter release? Annu. Rev. Biochem. 77, 615–641.

Chen, Y.A., and Scheller, R.H. (2001). SNARE-mediated membrane fusion. Nat. Rev. Mol. Cell Biol. 2, 98–106.

Chen, D., Minger, S.L., Honer, W.G., and Whiteheart, S.W. (1999). Organization of the secretory machinery in the rodent brain: distribution of the t-SNAREs, SNAP-25 and SNAP-23. Brain Res. 831, 11–24.

Cockcroft, S., and De Matteis, M.A. (2001). Inositol lipids as spatial regulators of membrane traffic. J. Membr. Biol. 180, 187–194.

Coskun, U., and Simons, K. (2011). Cell membranes: the lipid perspective. Structure 19, 1543–1548.

Cremona, O., and De Camilli, P. (2001). Phosphoinositides in membrane traffic at the synapse. J. Cell. Sci. 114, 1041–1052.

Czech, M.P. (2000). PIP2 and PIP3: complex roles at the cell surface. Cell 100, 603–606.

De Matteis, M.A., and Godi, A. (2004). Protein-lipid interactions in membrane trafficking at the Golgi complex. Biochim. Biophys. Acta 1666, 264–274.

Deschenes, R.J. (2013). Protein Palmitoylation. In Encyclopedia of Biological Chemistry (Second Edition), W.J. Lennarz, and M.D. Lane, eds. (Waltham: Academic Press), pp. 645–647.

Dey, P., Su, W.-M., Han, G.-S., and Carman, G.M. (2017). Phosphorylation of lipid metabolic enzymes by yeast protein kinase C requires phosphatidylserine and diacylglycerol. J Lipid Res 58, 742–751.

Dunphy, J.T., and Linder, M.E. (1998). Signalling functions of protein palmitoylation. Biochim. Biophys. Acta 1436, 245–261.

Dunphy, W.G., Fries, E., Urbani, L.J., and Rothman, J.E. (1981). Early and late functions associated with the Golgi apparatus reside in distinct compartments. Proc. Natl. Acad. Sci. U.S.A. 78, 7453–7457.

Engelman, D.M. (2005). Membranes are more mosaic than fluid. Nature 438, 578–580.

Escribá, P.V., González-Ros, J.M., Goñi, F.M., Kinnunen, P.K.J., Vigh, L., Sánchez-Magraner, L., Fernández, A.M., Busquets, X., Horváth, I., and Barceló-Coblijn, G.

(2008). Membranes: a meeting point for lipids, proteins and therapies. J Cell Mol Med 12, 829–875.

Fahy, E., Subramaniam, S., Brown, H.A., Glass, C.K., Merrill, A.H., Murphy, R.C., Raetz, C.R.H., Russell, D.W., Seyama, Y., Shaw, W., et al. (2005). A comprehensive classification system for lipids. J. Lipid Res. 46, 839–862.

Fahy, E., Subramaniam, S., Murphy, R.C., Nishijima, M., Raetz, C.R.H., Shimizu, T., Spener, F., van Meer, G., Wakelam, M.J.O., and Dennis, E.A. (2009). Update of the LIPID MAPS comprehensive classification system for lipids. J. Lipid Res. 50 Suppl, S9-14.

Fahy, E., Cotter, D., Sud, M., and Subramaniam, S. (2011). Lipid classification, structures and tools. Biochim Biophys Acta 1811, 637–647.

Flesch, F.M., Yu, J.W., Lemmon, M.A., and Burger, K.N.J. (2005). Membrane activity of the phospholipase C-δ1 pleckstrin homology (PH) domain. Biochemical Journal 389, 435–441.

Frye, L.D., and Edidin, M. (1970). The Rapid Intermixing of Cell Surface Antigens After Formation of Mouse-Human Heterokaryons. Journal of Cell Science 7, 319–335.

Fujimoto, T., and Parmryd, I. (2017). Interleaflet Coupling, Pinning, and Leaflet Asymmetry—Major Players in Plasma Membrane Nanodomain Formation. Front Cell Dev Biol 4.

Fukata, M., Fukata, Y., Adesnik, H., Nicoll, R.A., and Bredt, D.S. (2004). Identification of PSD-95 palmitoylating enzymes. Neuron 44, 987–996.

Gambhir, A., Hangyás-Mihályné, G., Zaitseva, I., Cafiso, D.S., Wang, J., Murray, D., Pentyala, S.N., Smith, S.O., and McLaughlin, S. (2004). Electrostatic Sequestration of

PIP2 on Phospholipid Membranes by Basic/Aromatic Regions of Proteins. Biophys J 86, 2188–2207.

García-Cañaveras, J.C., Peris-Díaz, M.D., Alcoriza-Balaguer, M.I., Cerdán-Calero, M., Donato, M.T., and Lahoz, A. (2017). A lipidomic cell-based assay for studying drug-induced phospholipidosis and steatosis. Electrophoresis 38, 2331–2340.

Gelb, M.H. (1997). Protein prenylation, et cetera: signal transduction in two dimensions. Science 275, 1750–1751.

Gianoli, F., Risler, T., and Kozlov, A.S. (2017). Lipid bilayer mediates ion-channel cooperativity in a model of hair-cell mechanotransduction. Proc Natl Acad Sci U S A 114, E11010–E11019.

Gonzalo, S., and Linder, M.E. (1998). SNAP-25 Palmitoylation and Plasma Membrane Targeting Require a Functional Secretory Pathway. Mol Biol Cell 9, 585–597.

Gonzalo, S., Greentree, W.K., and Linder, M.E. (1999). SNAP-25 is targeted to the plasma membrane through a novel membrane-binding domain. J. Biol. Chem. 274, 21313–21318.

Gorter, E., and Grendel, F. (1925). On Bimolecular Layers of Lipoids on the Chromocytes of the Blood. Journal of Experimental Medicine 41, 439–443.

Greaves, J., and Chamberlain, L.H. (2011). Differential palmitoylation regulates intracellular patterning of SNAP25. J. Cell. Sci. 124, 1351–1360.

Greaves, J., Prescott, G.R., Fukata, Y., Fukata, M., Salaun, C., and Chamberlain, L.H. (2009). The hydrophobic cysteine-rich domain of SNAP25 couples with downstream residues to mediate membrane interactions and recognition by DHHC palmitoyl transferases. Mol. Biol. Cell 20, 1845–1854.

Greaves, J., Gorleku, O.A., Salaun, C., and Chamberlain, L.H. (2010). Palmitoylation of the SNAP25 protein family: specificity and regulation by DHHC palmitoyl transferases. J. Biol. Chem. 285, 24629–24638.

Gubbens, J., and de Kroon, A.I.P.M. (2010). Proteome-wide detection of phospholipid-protein interactions in mitochondria by photocrosslinking and click chemistry. Mol Biosyst 6, 1751–1759.

Halemani, N.D., Bethani, I., Rizzoli, S.O., and Lang, T. (2010). Structure and dynamics of a two-helix SNARE complex in live cells. Traffic 11, 394–404.

Hancock, J.F., Paterson, H., and Marshall, C.J. (1990). A polybasic domain or palmitoylation is required in addition to the CAAX motif to localize p21ras to the plasma membrane. Cell 63, 133–139.

Heo, W.D., Inoue, T., Park, W.S., Kim, M.L., Park, B.O., Wandless, T.J., and Meyer, T. (2006). PI(3,4,5)P3 and PI(4,5)P2 lipids target proteins with polybasic clusters to the plasma membrane. Science 314, 1458–1461.

Hess, D.T., Slater, T.M., Wilson, M.C., and Skene, J.H. (1992). The 25 kDa synaptosomal-associated protein SNAP-25 is the major methionine-rich polypeptide in rapid axonal transport and a major substrate for palmitoylation in adult CNS. J. Neurosci. 12, 4634–4641.

Heumann, R., Kachel, V., and Thoenen, H. (1983). Relationship between NGF-mediated volume increase and "priming effect" in fast and slow reacting clones of PC12 pheochromocytoma cells: Role of cAMP. Experimental Cell Research 145, 179–190.

Heuser, J. (2000). The Production of 'Cell Cortices' for Light and Electron Microscopy. Traffic 1, 545–552.

Hilgemann, D.W., Feng, S., and Nasuhoglu, C. (2001). The complex and intriguing lives of PIP2 with ion channels and transporters. Sci. STKE 2001, re19.

van't Hof, W., and Resh, M.D. (1997). Rapid plasma membrane anchoring of newly synthesized p59fyn: selective requirement for NH2-terminal myristoylation and palmitoylation at cysteine-3. J. Cell Biol. 136, 1023–1035.

Holz, R.W., Hlubek, M.D., Sorensen, S.D., Fisher, S.K., Balla, T., Ozaki, S., Prestwich, G.D., Stuenkel, E.L., and Bittner, M.A. (2000). A pleckstrin homology domain specific for phosphatidylinositol 4, 5-bisphosphate (PtdIns-4,5-P2) and fused to green fluorescent protein identifies plasma membrane PtdIns-4,5-P2 as being important in exocytosis. J. Biol. Chem. 275, 17878–17885.

Honigmann, A., van den Bogaart, G., Iraheta, E., Risselada, H.J., Milovanovic, D., Mueller, V., Müllar, S., Diederichsen, U., Fasshauer, D., Grubmüller, H., et al. (2013). Phosphatidylinositol 4,5-bisphosphate clusters act as molecular beacons for vesicle recruitment. Nat Struct Mol Biol 20, 679–686.

Höning, S., Ricotta, D., Krauss, M., Späte, K., Spolaore, B., Motley, A., Robinson, M., Robinson, C., Haucke, V., and Owen, D.J. (2005). Phosphatidylinositol-(4,5)-bisphosphate regulates sorting signal recognition by the clathrin-associated adaptor complex AP2. Mol. Cell 18, 519–531.

Hooke, R. (1665). Micrographia : or, Some physiological descriptions of minute bodies made by magnifying glasses. With observations and inquiries thereupon (London, England: J. Allestry).

Huang, C.L., Feng, S., and Hilgemann, D.W. (1998). Direct activation of inward rectifier potassium channels by PIP2 and its stabilization by Gbetagamma. Nature 391, 803–806.

Hurley, J.H., and Meyer, T. (2001). Subcellular targeting by membrane lipids. Curr. Opin. Cell Biol. 13, 146–152.

Hurley, J.H., and Misra, S. (2000). Signaling and subcellular targeting by membrane-binding domains. Annu Rev Biophys Biomol Struct 29, 49–79.

Hurley, J.H., Newton, A.C., Parker, P.J., Blumberg, P.M., and Nishizuka, Y. (1997). Taxonomy and function of C1 protein kinase C homology domains. Protein Sci. 6, 477–480.

Hurst, J.H. (2013). Richard Scheller and Thomas Südhof receive the 2013 Albert Lasker Basic Medical Research Award. J Clin Invest 123, 4095–4101.

Ingólfsson, H.I., Melo, M.N., van Eerden, F.J., Arnarez, C., Lopez, C.A., Wassenaar, T.A., Periole, X., de Vries, A.H., Tieleman, D.P., and Marrink, S.J. (2014). Lipid organization of the plasma membrane. J Am Chem Soc 136, 14554–14559.

Irvine, R.F., and Schell, M.J. (2001). Back in the water: the return of the inositol phosphates. Nat. Rev. Mol. Cell Biol. 2, 327–338.

Jacobson, K., Mouritsen, O.G., and Anderson, R.G.W. (2007). Lipid rafts: at a crossroad between cell biology and physics. Nat. Cell Biol. 9, 7–14.

Jahn, R., and Fasshauer, D. (2012). Molecular machines governing exocytosis of synaptic vesicles. Nature 490, 201–207.

Jahn, R., and Scheller, R.H. (2006). SNAREs--engines for membrane fusion. Nat. Rev. Mol. Cell Biol. 7, 631–643.

James, D.J., Khodthong, C., Kowalchyk, J.A., and Martin, T.F.J. (2008). Phosphatidylinositol 4,5-bisphosphate regulates SNARE-dependent membrane fusion. J Cell Biol 182, 355–366.

J.F., S., and Russell, D. (2001). Molecular Cloning: A Laboratory Manual (3-Volume Set).

Jurado, S., Goswami, D., Zhang, Y., Molina, A.J.M., Südhof, T.C., and Malenka, R.C. (2013). LTP requires a unique postsynaptic SNARE fusion machinery. Neuron 77, 542–558.

Kanaani, J., Patterson, G., Schaufele, F., Lippincott-Schwartz, J., and Baekkeskov, S. (2008). A palmitoylation cycle dynamically regulates partitioning of the GABA-synthesizing enzyme GAD65 between ER-Golgi and post-Golgi membranes. J. Cell. Sci. 121, 437–449.

Kavran, J.M., Klein, D.E., Lee, A., Falasca, M., Isakoff, S.J., Skolnik, E.Y., and Lemmon, M.A. (1998). Specificity and promiscuity in phosphoinositide binding by pleckstrin homology domains. J. Biol. Chem. 273, 30497–30508.

Khoury, G.A., Baliban, R.C., and Floudas, C.A. (2011). Proteome-wide post-translational modification statistics: frequency analysis and curation of the swiss-prot database. Sci Rep 1.

Kleinzeller, A. (1999). Chapter 1 Charles Ernest Overton's Concept of a Cell Membrane. In Current Topics in Membranes, D.W. Deamer, A. Kleinzeller, and D.M. Fambrough, eds. (Academic Press), pp. 1–22.

Knowles, M.K., Barg, S., Wan, L., Midorikawa, M., Chen, X., and Almers, W. (2010). Single secretory granules of live cells recruit syntaxin-1 and synaptosomal associated protein 25 (SNAP-25) in large copy numbers. Proc. Natl. Acad. Sci. U.S.A. 107, 20810–20815.

Kusumi, A., Sako, Y., and Yamamoto, M. (1993). Confined lateral diffusion of membrane receptors as studied by single particle tracking (nanovid microscopy). Effects of calcium-induced differentiation in cultured epithelial cells. Biophys. J. 65, 2021–2040.

Kusumi, A., Nakada, C., Ritchie, K., Murase, K., Suzuki, K., Murakoshi, H., Kasai, R.S., Kondo, J., and Fujiwara, T. (2005). Paradigm shift of the plasma membrane concept from the two-dimensional continuum fluid to the partitioned fluid: high-speed single-molecule tracking of membrane molecules. Annu Rev Biophys Biomol Struct 34, 351–378.

Kusumi, A., Suzuki, K.G.N., Kasai, R.S., Ritchie, K., and Fujiwara, T.K. (2011). Hierarchical mesoscale domain organization of the plasma membrane. Trends in Biochemical Sciences 36, 604–615.

Kwiatkowska, K. (2010). One lipid, multiple functions: how various pools of PI(4,5)P(2) are created in the plasma membrane. Cell Mol Life Sci 67, 3927–3946.

Kyhse-Andersen, J. (1984). Electroblotting of multiple gels: a simple apparatus without buffer tank for rapid transfer of proteins from polyacrylamide to nitrocellulose. J Biochem Biophys Methods 10, 203–209.

Laemmli, U.K. (1970). Cleavage of Structural Proteins during the Assembly of the Head of Bacteriophage T4. Nature 227, 680–685.

Lane, S.R., and Liu, Y. (1997). Characterization of the palmitoylation domain of SNAP-25. J. Neurochem. 69, 1864–1869.

Lang, T., Bruns, D., Wenzel, D., Riedel, D., Holroyd, P., Thiele, C., and Jahn, R. (2001). SNAREs are concentrated in cholesterol-dependent clusters that define docking and fusion sites for exocytosis. EMBO J 20, 2202–2213.

Laude, A.J., and Prior, I.A. (2004). Plasma membrane microdomains: organization, function and trafficking. Mol. Membr. Biol. 21, 193–205.

Lecuit, M., Dramsi, S., Gottardi, C., Fedor-Chaiken, M., Gumbiner, B., and Cossart, P. (1999). A single amino acid in E-cadherin responsible for host specificity towards the human pathogen Listeria monocytogenes. EMBO J. 18, 3956–3963.

Legrain, P., Aebersold, R., Archakov, A., Bairoch, A., Bala, K., Beretta, L., Bergeron, J., Borchers, C.H., Corthals, G.L., Costello, C.E., et al. (2011). The Human Proteome Project: Current State and Future Direction. Mol Cell Proteomics 10.

Lemmon, M.A. (2003). Phosphoinositide Recognition Domains. Traffic 4, 201–213.

Liang, L., and Astruc, D. (2011). The copper(I)-catalyzed alkyne-azide cycloaddition (CuAAC) "click" reaction and its applications. An overview. Coordination Chemistry Reviews 255, 2933–2945.

Linder, M.E., and Deschenes, R.J. (2003). New insights into the mechanisms of protein palmitoylation. Biochemistry 42, 4311–4320.

Linder, M.E., Middleton, P., Hepler, J.R., Taussig, R., Gilman, A.G., and Mumby, S.M. (1993). Lipid modifications of G proteins: alpha subunits are palmitoylated. PNAS 90, 3675–3679.

Lingwood, D., and Simons, K. (2010). Lipid rafts as a membrane-organizing principle. Science 327, 46–50.

Lomasney, J.W., Cheng, H.F., Wang, L.P., Kuan, Y., Liu, S., Fesik, S.W., and King, K. (1996). Phosphatidylinositol 4,5-bisphosphate binding to the pleckstrin homology domain of phospholipase C-delta1 enhances enzyme activity. J Biol Chem 271, 25316–25326.

Loranger, S.S., and Linder, M.E. (2002). SNAP-25 traffics to the plasma membrane by a syntaxin-independent mechanism. J. Biol. Chem. 277, 34303–34309.

Lydic, T.A., and Goo, Y.-H. (2018). Lipidomics unveils the complexity of the lipidome in metabolic diseases. Clin Transl Med 7, 4.

Magee, A.I., and Courtneidge, S.A. (1985a). Two classes of fatty acid acylated proteins exist in eukaryotic cells. EMBO J 4, 1137–1144.

Magee, A.I., and Courtneidge, S.A. (1985b). Two classes of fatty acid acylated proteins exist in eukaryotic cells. EMBO J 4, 1137–1144.

Marrink, S.J., and Tieleman, D.P. (2013). Perspective on the Martini model. Chem. Soc. Rev. 42, 6801–6822.

Martens, S., Kozlov, M.M., and McMahon, H.T. (2007). How synaptotagmin promotes membrane fusion. Science 316, 1205–1208.

Martin, T.F. (2001). PI(4,5)P(2) regulation of surface membrane traffic. Curr. Opin. Cell Biol. 13, 493–499.

Martin, B.R., and Cravatt, B.F. (2009). Large-scale profiling of protein palmitoylation in mammalian cells. Nat Methods 6, 135–138.

Martin, D.D.O., Vilas, G.L., Prescher, J.A., Rajaiah, G., Falck, J.R., Bertozzi, C.R., and Berthiaume, L.G. (2008). Rapid detection, discovery, and identification of post-translationally myristoylated proteins during apoptosis using a bio-orthogonal azidomyristate analog. FASEB J 22, 797–806.

McLaughlin, S., and Murray, D. (2005). Plasma membrane phosphoinositide organization by protein electrostatics. Nature 438, 605–611.

McLaughlin, S., Wang, J., Gambhir, A., and Murray, D. (2002). PIP(2) and proteins: interactions, organization, and information flow. Annu Rev Biophys Biomol Struct 31, 151–175.

McNew, J.A. (2008). Regulation of SNARE-mediated membrane fusion during exocytosis. Chem. Rev. 108, 1669–1686.

van Meer, G. (2011). Dynamic transbilayer lipid asymmetry. Cold Spring Harb Perspect Biol 3.

van Meer, G., and de Kroon, A.I.P.M. (2011). Lipid map of the mammalian cell. J. Cell. Sci. 124, 5–8.

van Meer, G., Gahmberg, C.G., Op den Kamp, J.A., and van Deenen, L.L. (1981). Phospholipid distribution in human En(a-) red cell membranes which lack the major sialoglycoprotein, glycophorin A. FEBS Lett. 135, 53–55.

van Meer, G., Voelker, D.R., and Feigenson, G.W. (2008). Membrane lipids: where they are and how they behave. Nat. Rev. Mol. Cell Biol. 9, 112–124.

Monera, O.D., Sereda, T.J., Zhou, N.E., Kay, C.M., and Hodges, R.S. (1995). Relationship of sidechain hydrophobicity and alpha-helical propensity on the stability of the single-stranded amphipathic alpha-helix. J Pept Sci 1, 319–329.

Mumby, S.M. (1997). Reversible palmitoylation of signaling proteins. Curr. Opin. Cell Biol. 9, 148–154.

Nalefski, E.A., and Falke, J.J. (1996). The C2 domain calcium-binding motif: structural and functional diversity. Protein Sci 5, 2375–2390.

Nao, N., Kajihara, M., Manzoor, R., Maruyama, J., Yoshida, R., Muramatsu, M., Miyamoto, H., Igarashi, M., Eguchi, N., Sato, M., et al. (2015). A Single Amino Acid in

the M1 Protein Responsible for the Different Pathogenic Potentials of H5N1 Highly Pathogenic Avian Influenza Virus Strains. PLoS ONE 10, e0137989.

Nicolson, G.L. (2014). The Fluid-Mosaic Model of Membrane Structure: still relevant to understanding the structure, function and dynamics of biological membranes after more than 40 years. Biochim. Biophys. Acta 1838, 1451–1466.

Nyathi, Y., Wilkinson, B.M., and Pool, M.R. (2013). Co-translational targeting and translocation of proteins to the endoplasmic reticulum. Biochim. Biophys. Acta 1833, 2392–2402.

Odorizzi, G., Babst, M., and Emr, S.D. (2000). Phosphoinositide signaling and the regulation of membrane trafficking in yeast. Trends Biochem. Sci. 25, 229–235.

Olson, E.N., and Spizz, G. (1986). Fatty acylation of cellular proteins. Temporal and subcellular differences between palmitate and myristate acylation. J. Biol. Chem. 261, 2458–2466.

Papayannopoulos, V., Co, C., Prehoda, K.E., Snapper, S., Taunton, J., and Lim, W.A. (2005). A polybasic motif allows N-WASP to act as a sensor of PIP(2) density. Mol. Cell 17, 181–191.

van Paridon, P.A., de Kruijff, B., Ouwerkerk, R., and Wirtz, K.W. (1986). Polyphosphoinositides undergo charge neutralization in the physiological pH range: a 31P-NMR study. Biochim. Biophys. Acta 877, 216–219.

Payrastre, B., Missy, K., Giuriato, S., Bodin, S., Plantavid, M., and Gratacap, M. (2001). Phosphoinositides: key players in cell signalling, in time and space. Cell. Signal. 13, 377–387.

Pertsinidis, A., Mukherjee, K., Sharma, M., Pang, Z.P., Park, S.R., Zhang, Y., Brunger, A.T., Südhof, T.C., and Chu, S. (2013). Ultrahigh-resolution imaging reveals formation

of neuronal SNARE/Munc18 complexes in situ. Proc. Natl. Acad. Sci. U.S.A. 110, E2812-2820.

Politis, E.G., Roth, A.F., and Davis, N.G. (2005). Transmembrane topology of the protein palmitoyl transferase Akr1. J. Biol. Chem. 280, 10156–10163.

Puffer, E.B., Lomneth, R.B., Sarkar, H.K., and Singh, B.R. (2001). Differential roles of developmentally distinct SNAP-25 isoforms in the neurotransmitter release process. Biochemistry 40, 9374–9378.

Quinn, P., Griffiths, G., and Warren, G. (1983). Dissection of the Golgi complex. II. Density separation of specific Golgi functions in virally infected cells treated with monensin. J. Cell Biol. 96, 851–856.

Raucher, D., Stauffer, T., Chen, W., Shen, K., Guo, S., York, J.D., Sheetz, M.P., and Meyer, T. (2000). Phosphatidylinositol 4,5-bisphosphate functions as a second messenger that regulates cytoskeleton-plasma membrane adhesion. Cell 100, 221–228.

Rebecchi, M.J., and Pentyala, S.N. (2000). Structure, function, and control of phosphoinositide-specific phospholipase C. Physiol. Rev. 80, 1291–1335.

Rehm, H., and Letzel, T. (2016). Der Experimentator: Proteinbiochemie/Proteomics (Springer Spektrum).

Resh, M.D. (2006). Trafficking and signaling by fatty-acylated and prenylated proteins. Nat Chem Biol 2, 584–590.

Rizo, J., and Südhof, T.C. (1998). Mechanics of membrane fusion. Nat. Struct. Biol. 5, 839–842.

Rizzolo, L.J., and Kornfeld, R. (1988). Post-translational protein modification in the endoplasmic reticulum. Demonstration of fatty acylase and deoxymannojirimycin-sensitive alpha-mannosidase activities. J Biol Chem 263, 9520–9525.

Rocks, O., Gerauer, M., Vartak, N., Koch, S., Huang, Z.-P., Pechlivanis, M., Kuhlmann, J., Brunsveld, L., Chandra, A., Ellinger, B., et al. (2010). The palmitoylation machinery is a spatially organizing system for peripheral membrane proteins. Cell 141, 458–471.

Rothman, J.E. (1994). Mechanisms of intracellular protein transport. Nature 372, 55–63.

Salaün, C., James, D.J., Greaves, J., and Chamberlain, L.H. (2004). Plasma membrane targeting of exocytic SNARE proteins. Biochim Biophys Acta 1693, 81–89.

Salaun, C., Greaves, J., and Chamberlain, L.H. (2010). The intracellular dynamic of protein palmitoylation. J Cell Biol 191, 1229–1238.

Salaun, C., Greaves, J., Tomkinson, N.C.O., and Chamberlain, L.H. (2020). The linker domain of the SNARE protein SNAP25 acts as a flexible molecular spacer that ensures efficient S-acylation. J Biol Chem 295, 7501–7515.

Sambrook, J., and Russell, D.W. (2006). Purification of nucleic acids by extraction with phenol:chloroform. CSH Protoc 2006.

Schaub, J.R., Lu, X., Doneske, B., Shin, Y.-K., and McNew, J.A. (2006). Hemifusion arrest by complexin is relieved by Ca2+-synaptotagmin I. Nat Struct Mol Biol 13, 748–750.

Schlesinger, M.J., and Magee, A.I. (1982). Fatty Acid Acylation of Membrane Proteins. Biophys J 37, 126–127.

Schmidt, M.F., and Schlesinger, M.J. (1979). Fatty acid binding to vesicular stomatitis virus glycoprotein: a new type of post-translational modification of the viral glycoprotein. Cell 17, 813–819.

Schmidt, M., Schmidt, M.F., and Rott, R. (1988). Chemical identification of cysteine as palmitoylation site in a transmembrane protein (Semliki Forest virus E1). J. Biol. Chem. 263, 18635–18639.

Schulz, T.A., Choi, M.-G., Raychaudhuri, S., Mears, J.A., Ghirlando, R., Hinshaw, J.E., and Prinz, W.A. (2009). Lipid-regulated sterol transfer between closely apposed membranes by oxysterol-binding protein homologues. Journal of Cell Biology 187, 889–903.

Schwann, T. (1839). Mikroskopische Untersuchungen über die Uebereinstimmung in der Struktur und dem Wachsthum der Thiere und Pflanzen (Berlin: Sander).

Shahinian, S., and Silvius, J.R. (1995). Doubly-lipid-modified protein sequence motifs exhibit long-lived anchorage to lipid bilayer membranes. Biochemistry 34, 3813–3822.

Sheetz, M.P., Turney, S., Qian, H., and Elson, E.L. (1989). Nanometre-level analysis demonstrates that lipid flow does not drive membrane glycoprotein movements. Nature 340, 284–288.

Shen, J., Tareste, D.C., Paumet, F., Rothman, J.E., and Melia, T.J. (2007). Selective activation of cognate SNAREpins by Sec1/Munc18 proteins. Cell 128, 183–195.

Shevchenko, A., and Simons, K. (2010). Lipidomics: coming to grips with lipid diversity. Nat. Rev. Mol. Cell Biol. 11, 593–598.

Sieber, J.J., Willig, K.I., Heintzmann, R., Hell, S.W., and Lang, T. (2006). The SNARE motif is essential for the formation of syntaxin clusters in the plasma membrane. Biophys J 90, 2843–2851.

Sieber, J.J., Willig, K.I., Kutzner, C., Gerding-Reimers, C., Harke, B., Donnert, G., Rammner, B., Eggeling, C., Hell, S.W., Grubmüller, H., et al. (2007). Anatomy and dynamics of a supramolecular membrane protein cluster. Science 317, 1072–1076.

Sievers, F., Wilm, A., Dineen, D., Gibson, T.J., Karplus, K., Li, W., Lopez, R., McWilliam, H., Remmert, M., Söding, J., et al. (2011). Fast, scalable generation of high-quality protein multiple sequence alignments using Clustal Omega. Mol Syst Biol 7, 539.

Simons, K., and Gerl, M.J. (2010). Revitalizing membrane rafts: new tools and insights. Nat. Rev. Mol. Cell Biol. 11, 688–699.

Simons, K., and Ikonen, E. (1997). Functional rafts in cell membranes. Nature 387, 569–572.

Simonsen, A., Wurmser, A.E., Emr, S.D., and Stenmark, H. (2001). The role of phosphoinositides in membrane transport. Curr. Opin. Cell Biol. 13, 485–492.

Singer, S.J., and Nicolson, G.L. (1972). The fluid mosaic model of the structure of cell membranes. Science 175, 720–731.

Smotrys, J.E., and Linder, M.E. (2004). Palmitoylation of intracellular signaling proteins: regulation and function. Annu. Rev. Biochem. 73, 559–587.

Söllner, T., Whiteheart, S.W., Brunner, M., Erdjument-Bromage, H., Geromanos, S., Tempst, P., and Rothman, J.E. (1993). SNAP receptors implicated in vesicle targeting and fusion. Nature 362, 318–324.

Stauffer, T.P., Ahn, S., and Meyer, T. (1998). Receptor-induced transient reduction in plasma membrane PtdIns(4,5)P2 concentration monitored in living cells. Curr. Biol. 8, 343–346.

Stein, A., Weber, G., Wahl, M.C., and Jahn, R. (2009). Helical extension of the neuronal SNARE complex into the membrane. Nature 460, 525–528.

Strickfaden, S.C., Winters, M.J., Ben-Ari, G., Lamson, R.E., Tyers, M., and Pryciak, P.M. (2007). A mechanism for cell-cycle regulation of MAP kinase signaling in a yeast differentiation pathway. Cell 128, 519–531.

Subramaniam, S., Fahy, E., Gupta, S., Sud, M., Byrnes, R.W., Cotter, D., Dinasarapu, A.R., and Maurya, M.R. (2011). Bioinformatics and systems biology of the lipidome. Chem. Rev. 111, 6452–6490.

Südhof, T.C., and Rothman, J.E. (2009). Membrane fusion: grappling with SNARE and SM proteins. Science 323, 474–477.

Suh, B.-C., and Hille, B. (2005). Regulation of ion channels by phosphatidylinositol 4,5-bisphosphate. Curr. Opin. Neurobiol. 15, 370–378.

Sutton, R.B., Fasshauer, D., Jahn, R., and Brunger, A.T. (1998). Crystal structure of a SNARE complex involved in synaptic exocytosis at 2.4 A resolution. Nature 395, 347–353.

Thiele, C., Papan, C., Hoelper, D., Kusserow, K., Gaebler, A., Schoene, M., Piotrowitz, K., Lohmann, D., Spandl, J., Stevanovic, A., et al. (2012). Tracing Fatty Acid Metabolism by Click Chemistry. ACS Chem. Biol. 7, 2004–2011.

Toker, A. (1998). The synthesis and cellular roles of phosphatidylinositol 4,5-bisphosphate. Curr. Opin. Cell Biol. 10, 254–261.

Toner, M., Vaio, G., McLaughlin, A., and McLaughlin, S. (1988). Adsorption of cations to phosphatidylinositol 4,5-bisphosphate. Biochemistry 27, 7435–7443.

Towbin, H., Staehelin, T., and Gordon, J. (1979). Electrophoretic transfer of proteins from polyacrylamide gels to nitrocellulose sheets: procedure and some applications. Proc Natl Acad Sci U S A 76, 4350–4354.

Towler, D.A., Gordon, J.I., Adams, S.P., and Glaser, L. (1988). The biology and enzymology of eukaryotic protein acylation. Annu. Rev. Biochem. 57, 69–99.

Turner, K.M., Burgoyne, R.D., and Morgan, A. (1999). Protein phosphorylation and the regulation of synaptic membrane traffic. Trends Neurosci. 22, 459–464.

Vance, J.E. (2015). Phospholipid Synthesis and Transport in Mammalian Cells. Traffic 16, 1–18.

Vanhaesebroeck, B., Leevers, S.J., Ahmadi, K., Timms, J., Katso, R., Driscoll, P.C., Woscholski, R., Parker, P.J., and Waterfield, M.D. (2001). Synthesis and function of 3-phosphorylated inositol lipids. Annu. Rev. Biochem. 70, 535–602.

Várnai, P., and Balla, T. (1998). Visualization of phosphoinositides that bind pleckstrin homology domains: calcium- and agonist-induced dynamic changes and relationship to myo-[3H]inositol-labeled phosphoinositide pools. J. Cell Biol. 143, 501–510.

Varner, A.S., Ducker, C.E., Xia, Z., Zhuang, Y., Vos, M.L.D., and Smith, C.D. (2003). Characterization of human palmitoyl-acyl transferase activity using peptides that mimic distinct palmitoylation motifs. 9.

Veit, M., Söllner, T.H., and Rothman, J.E. (1996). Multiple palmitoylation of synaptotagmin and the t-SNARE SNAP-25. FEBS Lett. 385, 119–123.

Verkleij, A.J., Zwaal, R.F., Roelofsen, B., Comfurius, P., Kastelijn, D., and van Deenen, L.L. (1973). The asymmetric distribution of phospholipids in the human red cell membrane. A combined study using phospholipases and freeze-etch electron microscopy. Biochim. Biophys. Acta 323, 178–193.

Vogel, K., and Roche, P.A. (1999). SNAP-23 and SNAP-25 are palmitoylated in vivo. Biochem. Biophys. Res. Commun. 258, 407–410.

Vogel, K., Cabaniols, J.P., and Roche, P.A. (2000). Targeting of SNAP-25 to membranes is mediated by its association with the target SNARE syntaxin. J. Biol. Chem. 275, 2959–2965.

Wang, J., and Richards, D.A. (2012). Segregation of PIP2 and PIP3 into distinct nanoscale regions within the plasma membrane. Biol Open 1, 857–862.

Wang, J., Gambhir, A., Hangyás-Mihályneá, G., Murray, D., Golebiewska, U., and McLaughlin, S. (2002). Lateral Sequestration of Phosphatidylinositol 4,5-Bisphosphate by the Basic Effector Domain of Myristoylated Alanine-rich C Kinase Substrate Is Due to Nonspecific Electrostatic Interactions*. Journal of Biological Chemistry 277, 34401–34412.

Washbourne, P., Cansino, V., Mathews, J.R., Graham, M., Burgoyne, R.D., and Wilson, M.C. (2001). Cysteine residues of SNAP-25 are required for SNARE disassembly and exocytosis, but not for membrane targeting. Biochem J 357, 625–634.

Watt, S.A., Kular, G., Fleming, I.N., Downes, C.P., and Lucocq, J.M. (2002). Subcellular localization of phosphatidylinositol 4,5-bisphosphate using the pleckstrin homology domain of phospholipase C delta1. Biochem J 363, 657–666.

Weber, P., Batoulis, H., Rink, K.M., Dahlhoff, S., Pinkwart, K., Söllner, T.H., and Lang, T. (2017). Electrostatic anchoring precedes stable membrane attachment of SNAP25/SNAP23 to the plasma membrane. ELife 6, e19394.

Weber, T., Zemelman, B.V., McNew, J.A., Westermann, B., Gmachl, M., Parlati, F., Söllner, T.H., and Rothman, J.E. (1998). SNAREpins: minimal machinery for membrane fusion. Cell 92, 759–772.

Wen, P.J., Osborne, S.L., and Meunier, F.A. (2011). Dynamic control of neuroexocytosis by phosphoinositides in health and disease. Prog Lipid Res 50, 52–61.

Wenk, M.R. (2010). Lipidomics: new tools and applications. Cell 143, 888–895.

Wenk, M.R., and Camilli, P.D. (2004). Protein-lipid interactions and phosphoinositide metabolism in membrane traffic: Insights from vesicle recycling in nerve terminals. PNAS 101, 8262–8269.

Wilhelm, B.G., Mandad, S., Truckenbrodt, S., Kröhnert, K., Schäfer, C., Rammner, B., Koo, S.J., Claßen, G.A., Krauss, M., Haucke, V., et al. (2014). Composition of isolated synaptic boutons reveals the amounts of vesicle trafficking proteins. Science 344, 1023–1028.

Wright, L.P., and Philips, M.R. (2006). Thematic review series: lipid posttranslational modifications. CAAX modification and membrane targeting of Ras. J. Lipid Res. 47, 883–891.

Wu, C.-S., Lin, J.-T., Chien, C.-L., Chang, W.-C., Lai, H.-L., Chang, C.-P., and Chern, Y. (2011). Type VI Adenylyl Cyclase Regulates Neurite Extension by Binding to Snapin and Snap25. Molecular and Cellular Biology 31, 4874–4886.

Yeung, T., Gilbert, G.E., Shi, J., Silvius, J., Kapus, A., and Grinstein, S. (2008). Membrane phosphatidylserine regulates surface charge and protein localization. Science 319, 210–213.

Yount, J.S., Moltedo, B., Yang, Y.-Y., Charron, G., Moran, T.M., López, C.B., and Hang, H.C. (2010). Palmitoylome profiling reveals S-palmitoylation-dependent antiviral activity of IFITM3. Nat Chem Biol 6, 610–614.

Zhang, F.L., and Casey, P.J. (1996). Protein prenylation: molecular mechanisms and functional consequences. Annu. Rev. Biochem. 65, 241–269.

Zilly, F.E., Halemani, N.D., Walrafen, D., Spitta, L., Schreiber, A., Jahn, R., and Lang, T. (2011). Ca2+ induces clustering of membrane proteins in the plasma membrane via electrostatic interactions. EMBO J 30, 1209–1220.

8 Acknowledgements

First and foremost I would like to express my sincere gratitude to my research supervisor Prof. Dr. Thorsten Lang for providing me with the opportunity to do research work in his group and for providing invaluable guidance throughout the process. I have greatly benefited from his support, his supervision and his dedication.

Furthermore I would like to thank the thesis committee for the support and evaluation of this thesis. In addition, special thanks go to Prof. Dr. Christoph Thiele for providing important *"click"* tools and for his helpful advice.

I am also very thankful for the interesting collaboration with Prof. Dr. Thomas H. Söllner and Dr. Kerstin M. Rink.

Further I am very thankful for, Dr. Thomas Quast, for his help and support with confocal microscopy at Prof. Dr. Waldemar Kolanus lab. I would like to thank Stephan Dahlhoff for his work and contributions regarding experiments on SNAP23. Many thanks also go to Kerstin Pinkwart and Helena Batoulis for their work and contributions for the palmitoylation assessment and for the general support and work during the review process of the publication accompanying this thesis.

I would also like to offer my special thanks to all other current and former members of the Lang group, especially Thomas Schmidt,.Elisa Merklinger, Dennis de Coninck, Jan-Gero Schlötel and Nora Karnowski, for the unlimited support, helpful discussions and suggestions and the great team work and team spirit at work. A special thank you to Yahya Homsi for his proofreading and general support and advice during my time at the Lang lab.

My appreciation also goes out to the Porcas family, especially Richard, for the support and proofreading and to all my friends for the continuous cheers, backing and offerings.

I would like to give a very special thank you to my family (Brigitte, Rudolf, Sandra and Patrick), who with their continuous support, encouragement and advice all helped me in a tremendous way to finalize this work.

Last but not least I want to thank Julia Porcas – for her invaluable help, untiring support, love and patience (and impatience).

9 Supplementary Figures

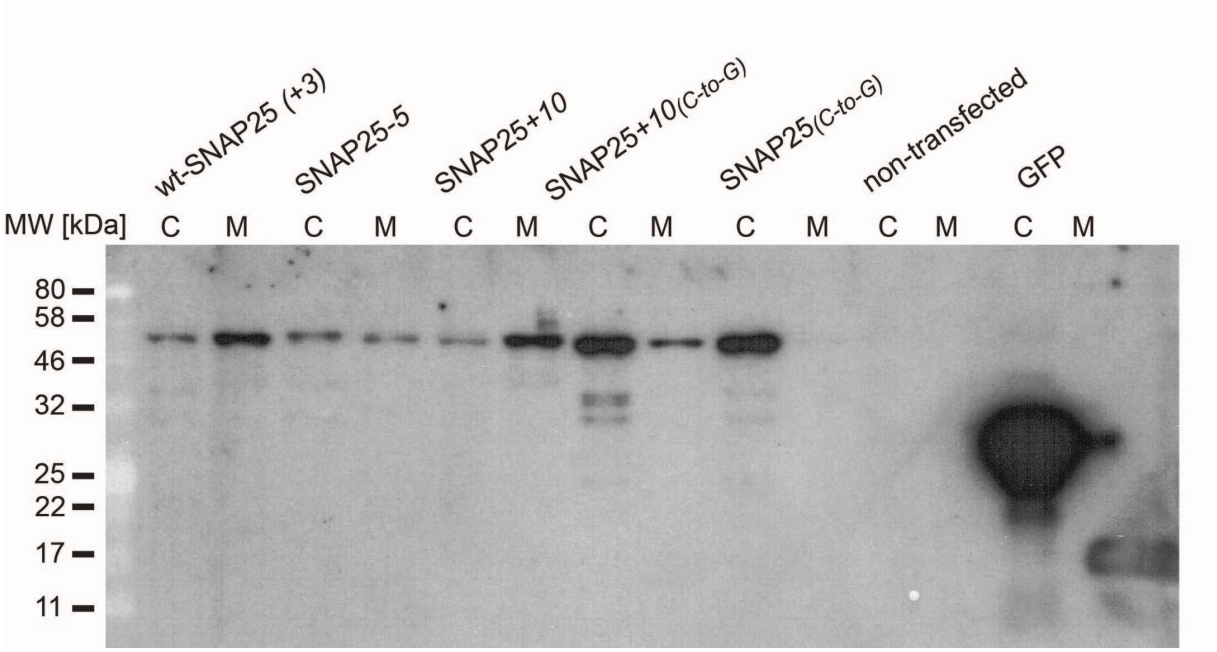

Supplementary Figure 1: Subcellular distribution of SNAP25 constructs
Western Blot used for Figure 31 with fraction for cytosol (**C**) and membrane (**M**). Equal amounts of proteins were loaded, measured via a BCA assay. In this experiment SNAP25$_{(C\text{-}to\text{-}G)}$ and SNAP25+*10*$_{(C\text{-}to\text{-}G)}$ showed a higher expression level. On average, expression levels of the constructs were similar (see Figure 31 c) (modified after Weber et al., 2017)

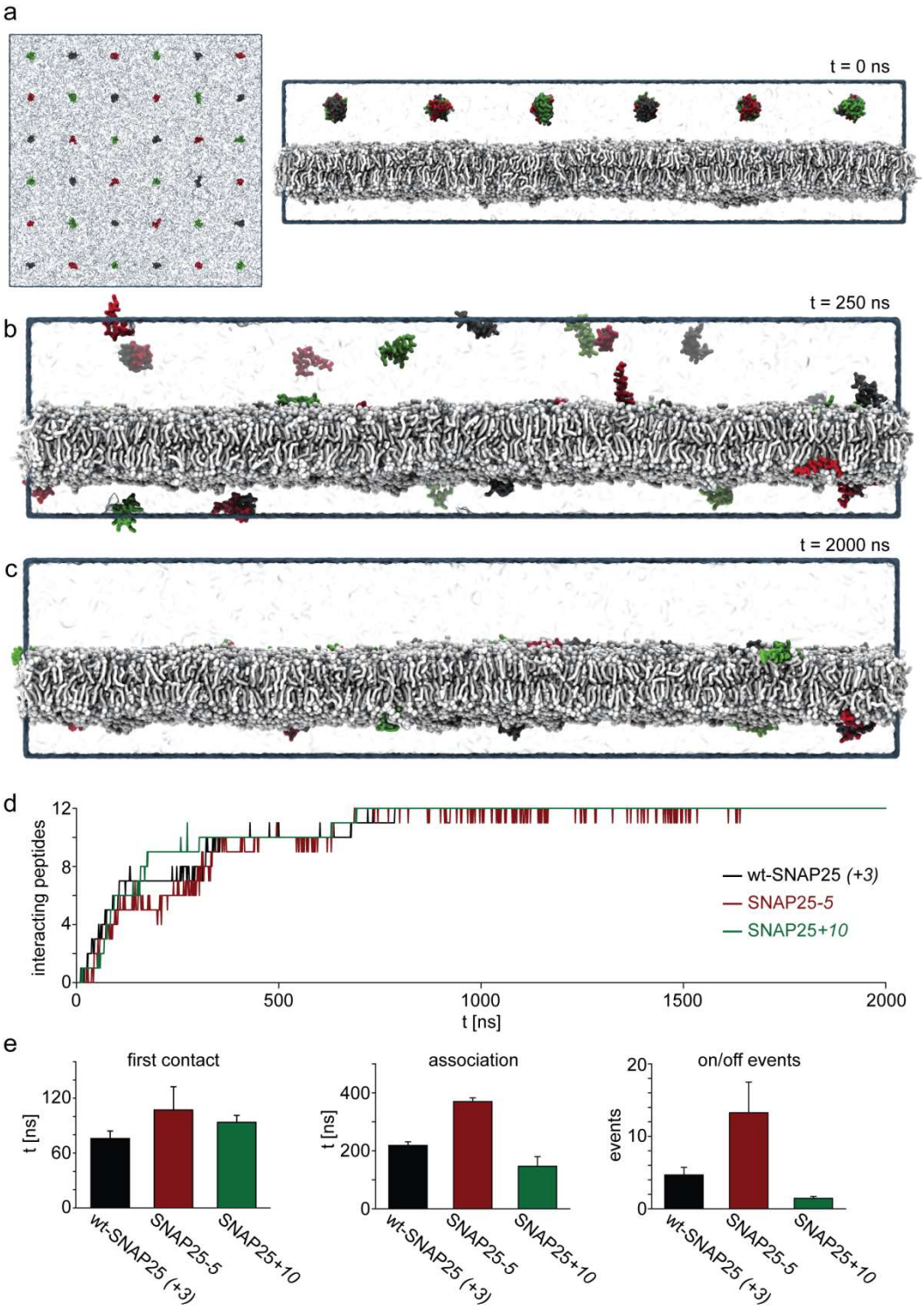

Supplementary Figure 2: MD simulation of peptide-membrane binding
(a) top and side view of the MD initial configuration (t = 0 ns). Peptides of wt-SNAP25 *(+3)* (grey), SNAP25-*5* (red) and SNAP25+*10* (green) were located into the aqueous phase on a 6 x 6 grid with a distance of 2.7 nm to the intracellular surface of a plasma membrane model (70 x 70 nm, see also text) in a 150 mM NaCl solution. **(b)** System configurations after 250 ns and **(c)** 2000 ns MD simulation.**(d)** Peptide association with the plasma membrane over time. Peptide lipid distances ≤ 0.6 nm were rated as contacts.

Note that before peptides associate (establish a stable contact), "on/off"-events (vertical lines in the traces) can occur that reflect a transient contact. **(e)** Peptide interaction behavior averaged from three runs. Shown are the time of the first contact with the membrane (left), the time after which peptides stably associate with the membrane (middle) and the number of "on/off" events before association (average of all peptides per variant). Bar charts indicate means ± s.e.m. (n = 3 runs) (Images in shown in **(a)**, **(b)** and **(c)** from personal correspondence with Thomas H. Schmidt; Graph and Bar diagrams in **(d)** and **(e)** are based on data from personal correspondence with Thomas H. Schmidt)**.**

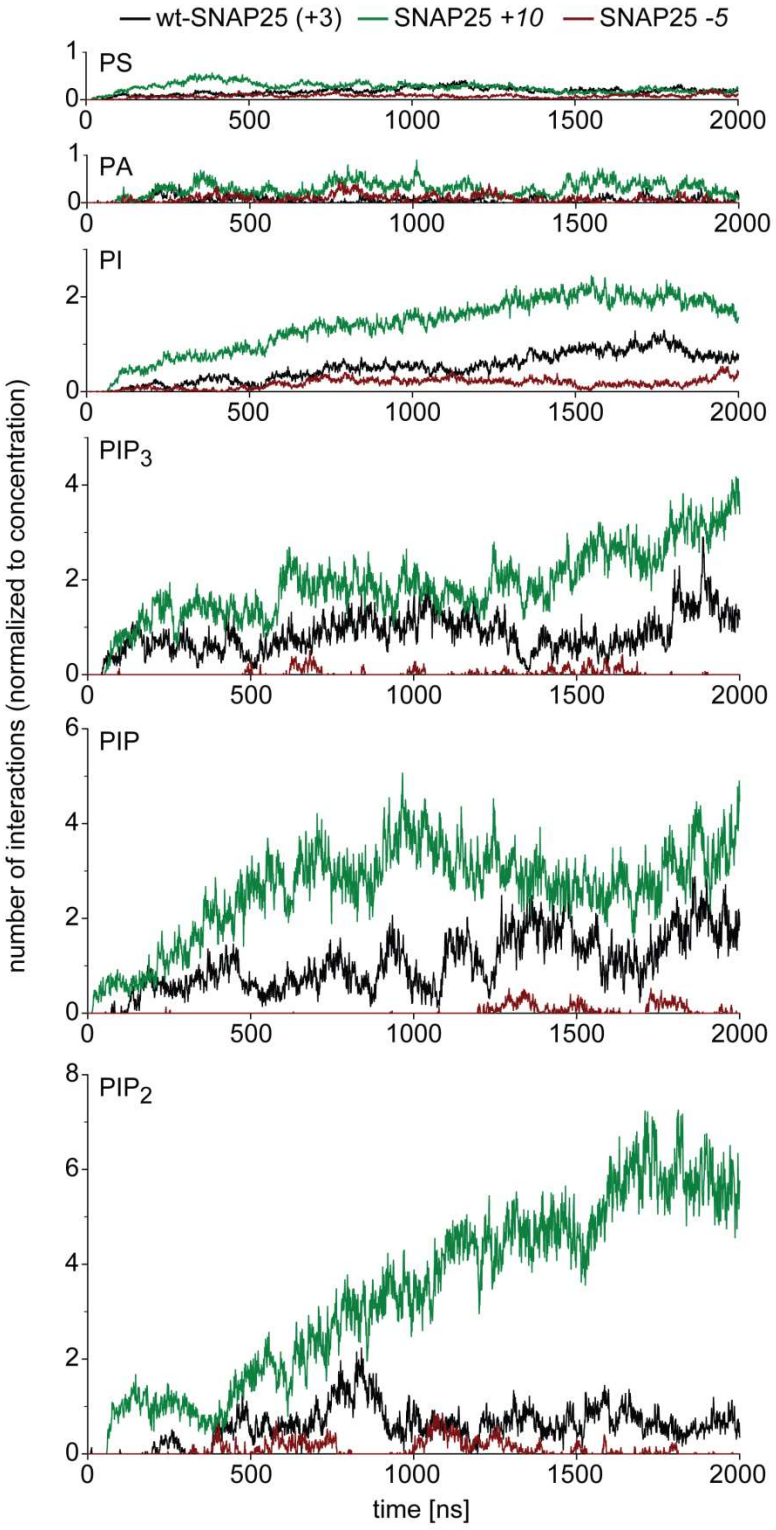

Supplementary Figure 3: Contacts with negatively charged lipids
Referring to the negatively charged lipids present in the inner leaflet of the plasma membrane, contacts with phosphatidylserine (PS), phosphatidic acid (PA), phosphatidylinositol (PI) and phosphatidylinositol (mono-/bis-/tris-)phosphate ($PIP/PIP_2/PIP_3$) were monitored over time for the run shown in Supplementary Figure 2)

PS, PA and PI are available as variable species that differ in their fatty acid tails. Contacts of PS, PA and PI are the sum of contacts involving all species. Concentrations are normalized to the lipid concentration (Graphs are based on data from personal correspondence with Thomas H. Schmidt).

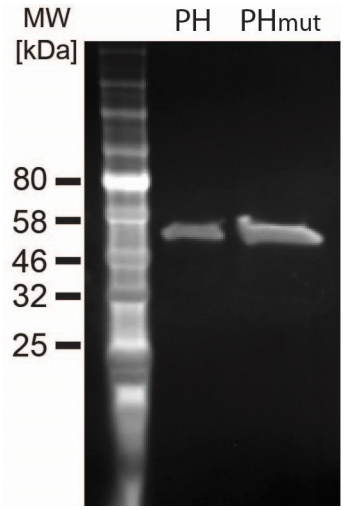

Supplementary Figure 4: Quantification of GFP-SNAP25 expression levels
From HepG2 cells co-expressing GFP-labelled SNAP25 and the mCherry-labelled PH domain (PLC-δPH) or the PH domain mutant (PLC-δPH_{mut}) equal amounts of lysates were analysed by western blot. The GFP was detected by an anti GFP antibody. Band signal intensities were corrected for the amount of the lysate protein concentration determined with a BCA assay. The SNAP25 level in cells co-expressing PH was normalized to the SNAP25 level in cells co-expressing the PLC-δPH_{mut}. For averages see Figure 38.

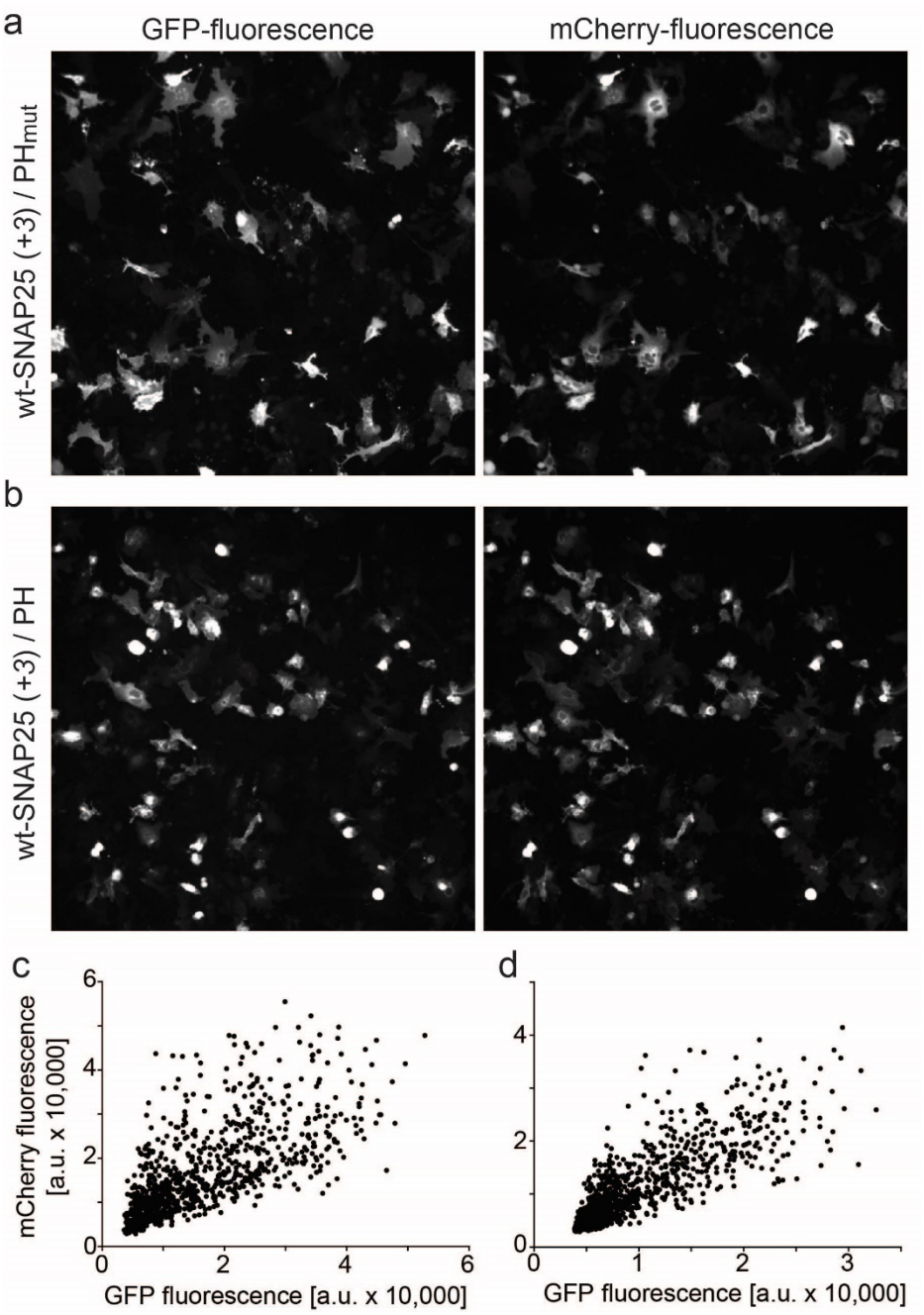

Supplementary Figure 5: Co-transfection efficiency of intact HepG2 cells
HepG2 cells co-expressing GFP-labelled SNAP25 and the mCherry-labelled PH domain (PLC-δPH) **(a)** or the PH domain mutant (PLC-δPHmut) **(b)**. Cells were fixed with PFA and analysed via microscopy and outlined via ImageJ software to quantify the fluorescence in the green (GFP fluorescence; left panels) and the red channel (mCherry fluorescence; right panels). Plotting green against red fluorescence shows that all green cells co-express the mCherry construct for both PLC-δPH **(c)** and PLC-δPH$_{mut}$ **(d)** (data from three independent experiments are pooled in one graph).